Variations in Mediterranean Outflow Water and its salt discharge versus Pliocene changes in North Atlantic thermohaline circulation prior and during the onset of major Northern Hemisphere Glaciation, 3.7 – 2.6 Ma

Dissertation

zur Erlangung des Doktorgrades

der Mathematisch-Naturwissenschaftlichen Fakultät

der Christian-Albrechts-Universität

zu Kiel

Vorgelegt von

Nabil Khélifi

Kiel 2010

Referent:	Prof. Dr. Emer. Michael Sarnthein
Korreferent:	Prof. Dr. Martin Frank
Tag der Disputation:	12 Mai 2010
Zum Druck genehmigt:	Kiel, den
Der Dekan:	

Gedruckt mit Unterstützung des Deutschen Akademischen Austauschdienstes (DAAD).

Printed with support from the German Academic Exchange Service (DAAD).

Eidesstattliche Erklärung

Hiermit erkläre ich, daß die Abhandlung – abgesehen von der Beratung durch mein Betreuer Prof. Dr. Michael Sarnthein – nach Inhalt und Form meine eigene Arbeit ist.

Ich habe diese Arbeit, ganz oder zum Teil, an keiner anderen Stelle im Rahmen eines Prüfungsverfahrens vorgelegt, veröffentlicht oder zur Veröffentlichung eingereicht.

Kiel, den 20 April 2010 Nabil Khélifi

Contents

Abstract

Pliocene changes in Mediterranean Outflow Water (MOW) and its potential influence on northern North Atlantic thermohaline circulation prior and during the onset of Northern Hemisphere Glaciation (NHG; 3.7 – 2.6 Ma) were investigated at westernmost Mediterranean Site ODP 978 (1930 m w.d.) and along the northeast Atlantic continental margin, at Sites DSDP 548 (1250 m w.d.) and ODP 982 (1135 m w.d.). Foraminiferal $\delta^{18}O$ records (and geomagnetic events) formed the base for stable isotope stratigraphy which led to a major revision of age control at Site 982. The Nd isotopic composition (ε_{Nd}) of bottom seawater served to trace back the origin of water masses. Sea surface temperatures (SST) were reconstructed from the alkenone unsaturation index ($U^{k'}_{37}$) and Mg/Ca estimates on planktic shells. Bottom water temperatures (BWT) were estimated from Mg/Ca measured on epibenthic foraminifera. Epibenthic $\delta^{13}C$ records were used as tracer of bottom water ventilation. This investigation consists of four interrelated studies.

Study 1 provides new insights from proxy intercomparison. $U^{k'}_{37}$-based vs Mg/Ca-based SST estimates at Site 982 show that SST values derived from alkenones are ~1°C higher than those based on Mg/Ca in planktic foraminifera. However, both proxies report similar climate trends. Over the period of fairly global stable climate between 3.7 and 3.3 Ma both proxies record a large orbital-scale variability that may be linked to changes in the strength and position of the North Atlantic atmospheric pressure systems and the position of the North Atlantic Current (NAC). From ~3.3 to 3.0 Ma northeast Atlantic SST underwent a major drop, a result that may contradict the PRISM concept assuming a time slice of largely constant climate conditions.

Study 2 documents a major and long-term Upper Pliocene intensification of the Mediterranean outflow, 3.5 – 3.3 Ma. ε_{Nd} values higher than -11 to -9 show that MOW spread continuously over the northeast Atlantic throughout the Upper Pliocene and reached up to the Rockall Plateau from 3.4 until 2.7 Ma and after 2.55 Ma. From 3.5 – 3.3 Ma, northeast Atlantic Sites 548 and 982 showed a singular and persistent increase in bottom water salinities (BWS) by ~2 psu and in densities (BWD) by 1 kg m^{-3}, which was matched by a ~1 to 3°C increase in BWT at Sites 548 and 982. This event of increased MOW flow was coeval with a unique and long-term rise in BWS by ~1 psu and in BWD by ~1 kg m^{-3} of WMDW at West Mediterranean Site 978 which partly forms the source of MOW by turbulent entrainment. These changes were most likely

linked to a major aridification in the Mediterranean region following a key change in the African monsoon system. Precisely at the same interval, surface waters of the Alboran Sea showed an increase of nutrient contents (decreasing planktic $\delta^{13}C$). The increase was most likely linked to an enhanced Atlantic inflow of nutrient-enriched surface waters that had to compensate for the enhanced outflow of MOW.

Study 3 concerned the onset of major NHG from ~3.0 to 2.7 Ma, when the long-term average BWT and BWS at S. 548 decreased by 3°–4°C and 2 psu, respectively, until 2.82 Ma (MIS G10). However, BWT and BWS at the shallower (and most distal) S. 982 continued to oscillate at a level that was 3°C and 1.5-psu higher than today. Generally, BWD then was slightly higher at S. 982 than at S. 548. Accordingly, it appears that the coeval enhanced production of upper North Atlantic Deep Water (NADW) may have diluted and/or rather displaced the core of the MOW tongue upward in the region off Brittany up to a level shallower than 1250 m w.d. (S. 548), although BWD still was about 0.5-kg m^{-3} higher than today.

Study 4 concerned potential links between the strength of MOW salt discharge and upper NADW formation. The increased advection of salt with MOW from 3.5 – 3.3 Ma did not translate into any trends of better ventilation ($\delta^{13}C$) of Lower NADW and Upper NADW, except for a single potential response of (distal) Upper NADW at Caribbean Sea S. 999. Likewise, the distinct change in MOW advection and salt injection after 2.9 Ma was not linked to any coeval change in the ventilation of NADW. In total, the influence of MOW salt injections into the North Atlantic Meridional Overturning Circulation (MOC) may be too small to produce any significant effects.

Kurzfassung

Die vorliegende Arbeit befasst sich mit dem Wandel des Mittelmeerwasserausstroms (MOW: Mediterranean Outflow Water) im Oberen Pliozän und seinem potentiellen Einfluss auf die nördliche thermohaline Zirkulation des Nordatlantiks vor und während des Einsetzens der Vereisung der nördlichen Hemisphäre (NHG; 3.7 – 2.6 Ma). Untersucht wurden im westlichsten Mittelmeer, Bohrprofil ODP 978 (1930 m w.d.), sowie Bohrung DSDP 548 (1250 m w.d.) und ODP 982 (1135 m w.d.) entlang des nordöstlichen atlantischen Kontinentalhangs. Das $\delta^{18}O$ Signal von Foraminiferen bildet die Basis für die stabile Isotopenstratigraphie, wobei die Alterseinstufung von Bohrprofil 982 erheblich revidiert wird. Die Nd-Isotopenzusammensetzung (ε_{Nd}) des Tiefenswassers dient dazu, die Herkunft der Tiefenwassermassen zu verfolgen. Die Wasseroberflächentemperatur (SST) wird anhand untersättigter Alkenone ($U^{k'}_{37}$) und am Mg/Ca Verhältnis planktischer Foraminiferenschalen rekonstruiert. Tiefenwassertemperaturen werden aus dem Mg/Ca-Verhältnis epibenthischer Foraminiferen abgeschätzt. Mit Hilfe epibenthischer $\delta^{13}C$ Werte, werden die Tiefenwasserventilation und damit Änderungen der Tiefenströmung abgeleitet. Die Arbeit umfasst vier unterschiedliche, aber eng miteinander korrelierte Sachgebiete.

Studie 1 vergleicht die Ergebnisse zweier unterschiedlicher Näherungswerte (Proxies) für Wasseroberflächentemperatur, $U^{k'}_{37}$ und Mg/Ca-Verhältnisse am Bohrprofil 982. Diese Temperaturen sind bei Alkenon-Werten etwa 1°C höher als bei Mg/Ca Verhältnissen planktischer Foraminiferen. Letztlich zeigen beide Proxies jedoch die gleichen Klimatrends, so während einer langen globalen klimastabilen Periode zwischen 3,7 und 3,3 Ma eine große orbitale Variabilität. Sie kann vielleicht mit der wechselnden Stärke und Position der atmosphärischen Drucksysteme im Nordatlantik sowie mit der Position der Nordatlantischen Strömung in Verbindung gebracht werden. Vor 3,3 – 3,0 Ma kühlten die Wasseroberflächentemperaturen auf Site 982 dramatisch ab, ein Ergebnis, das möglicherweise im Widerspruch zum PRISM-Konzept von damals mittelfristig konstanten Temperaturen steht.

Studie 2 dokumentiert eine wesentliche und langanhaltende Verstärkung des Mittelmeerausflusses im Pliozän vor 3,5 – 3,3 Ma. Hohe (ε_{Nd}) Werte von -11 bis -9 zeigen, dass während des Oberen Pliozäns das MOW beständig in den Nordostatlantik eindrang, und von 3,4 bis 2,7 Ma sowie nach 2,55 Ma, bis hin zum Rockall Plateau vorstieß. Vor 3,5 – 3,3 Ma,

zeigt sich an Bohrprofil 548 und 982 ein singulärer und dauerhafter Anstieg der Tiefenwasser-Salinität (BWS) um ~2 psu sowie der -Dichte (BWD) um 1 kg m^{-3}, zeitgleich mit einem Anstieg der Tiefenwassertemperatur an Site 548 und 982 um ~1° bis 3°C. Dieses Ereignis war gleichzeitig mit einem einmaligen und langanhaltenden Anstieg der BWS um ~1 psu und BWD um ~1 kg m^{-3} im Tiefenwasser nahe der MOW Quelle, bei Site 978. Diese Änderungen waren vermutlich an eine größere Aridifikation der Mittelmeerregion gekoppelt, als Folge eines Wechsels im Afrikanischen Monsun-System. Genau zu dieser Zeit nahm der Nährstoffgehalt im Oberflächenwasser der Alborán-See zu (signifikant abnehmende $\delta^{13}C$-Verhältnisse). Der Anstieg war wahrscheinlich mit einem erhöhten Zufluss von nährstoffreichem atlantischen Oberflächenwasser verbunden, welches den erhöhten Ausfluss des Mittelmeerwassers zu kompensieren hatte.

Studie 3 Mit dem Einsetzen der großen NHG vor ~3,0 bis 2,7 Ma, genauer: bis vor 2.82 Ma (MIS G10), sank die durchschnittliche BWT an Lokalität 548 um 3° – 4°C und die Salinität um 2 psu. Die gut 100 m flacher gelegene Bohrlokation 982 zeigte weiter Werte, die 3 °C und 1,5 psu höher oszillierten als heute. Generell lagen die Tiefwasserdichten (BWD) bei Site 982 leicht höher als bei Site 548. Entsprechend zeigt sich, dass die damals ansteigende Produktion von oberem Nordatlantischen Tiefenwasser (NADW: North Atlantic Deep Water) die salzreiche Wasserzunge aus dem Mittelmeer verdünnte und/oder sie in die Region vor der Bretagne auf Wassertiefen von weniger als 1250 m (Site 548) angehoben hat. Allerdings war damals die erniedrigte Tiefenwasserdichte (BWD) an Site 548 noch immer ~0,5 kg m^{-3} höher als heute.

Studie 4 erfasst eine potentielle Verknüpfung zwischen dem Salzeintrag durch den Mittelmeerausstrom (MOW) und der Bildung von Oberem Nordatlantischen Tiefenwasser (NADW). Der erhöhte Salzeintrag im MOW zwischen 3,5 – 3,3 Ma zeitigte keine bessere Durchlüftung (erhöhtes $\delta^{13}C$) des Unteren und Oberen Nordatlantischen Tiefenwassers (NADW). Ausgenommen ist vielleicht als Resonanz ein damaliger Anstieg der Ventilation im Oberen NADW in der (weit entfernten) Karibik bei Site 999. Gleichermaßen erscheinen die Veränderungen von MOW Advektion und Salzeintrag in der Zeit nach 2,9 Ma nicht mit Veränderungen in der Durchlüftung des Nordatlantischen Tiefenwasser (NADW). Der Einfluss der Salz Injektionen durch Mittelmeerausstromwasser (MOW) ist wahrscheinlich zu gering, um signifikante Änderungen zu bewirken.

مَرج البحرين يلتقيان بينهما برزخٌ لا يبغيان فبأي آلاء ربكما تكذبان (الرحمن 19 – 21)

He has let free the two sees meeting together. Between them is a barrier that they do not transgress.
(The Holy Qur'an 55: 19–21)

إلى الوالدين و كل أفراد الأسرة الكريمة ...

This thesis is dedicated to my parents and all my family ...

Acknowledgments

First of all I'd like to express all the gratitude and respect to the person who supported me generously until the end, with great patience, sincere advice, and friendship since we first met in the general paleoceanographer's family during the ICP 8 in Biarritz in 2004. To my "Doktorvater" Professor Michael Sarnthein, I owe a lot my success in passing the doctor degree. I learned from him everything from how to write-up proposals, generate data, and make stories out of them, write-up manuscripts and the thesis, ending with how to be "rational" in scientific thoughts. During 3 and a half years, I profited as much as possible from this leading scientist.

I would like to acknowledge generous financial support from the SysTem for Analysis, Research and Training (START) and the German Academic Exchange Service (DAAD). To the DAAD employee Cornelia Hanzlik-Rudolph I have special gratitude for her kind help.

I enjoyed my stay as a member of the large international working group of marine paleoclimatology at the "Institut für Geowissenschaften" of Kiel University. In particular, I'd like to thank the leader of the group Prof. Ralph Schneider for his kind help and generous support.

I must also thank many scientists who helped me, guided me, and with whom I had fruitful discussions during my PhD work and/or during several international meetings. From Kiel: Martin Frank, Nils Andersen, Dieter Garbe-Schönberg, Uwe Pflaumann, Mara Weinelt, Ann Holbourn, Wolfgang Kuhnt, Birgit Schneider, Guillaume Leduc, Syee Weldeab, Andres Rüggeberg, Thomas Blanz, Dirk Nürnberg, Brian A. Haley, and others. From other universities: Gerald Haug, Maureen Raymo, Christina Ravelo, Harry Dowsett, Alan Haywood, Michael Kucera, Isable Cacho, Antje Voelker, Luc Lourens, Uwe Mikolajewicz, Ralf Tiedemann, Jeroen Groeneveld, Michael Rogerson, Kira Lawrence, David Naafs, and many others.

"Vielen Dank" to the scientists and colleagues at the "Institut für Geowissenschaften" and IFM–GEOMAR with whom I shared a great "Kieler" life (!) in front of the Baltic Sea: Mohamed Aquit, Johan Etourneau, Elfi Mollier-Vogel, Tim Bolliet, Anke Dürkop, Veronica Krossa, Camille Butruille, Jenny Lezius, Yiming Wang, Ulrike Westernströer, Marcus Regenberg, Sebastien Meier, Gretta Bartoli, Jian Xu, Claudia Sieler, Uta Kreps-Kansow, Cyrus Kars, Opeyemi Salau, Christian Schwab, Rina Zuraida, Nathalie Tepe, Laura Bordelon, Liya Jin, Sven Nielsen, Jacek Raddatz, Roland Stumpf, Peter Appel, Nouri-Said Rahmoun, Nelson Boniface, Janne Repschläger, and others. I also appreciate the kind help of Rüdiguer Thomas, Hanno Kinkel, Stefanie Maack, and Bettina Kaste.

I would like to thank the technicians who helped with geochemical analyses and mass spectrometry: Karin Kißling, Silvia Koch, and Jutta Heinze, also my assistant students who helped a lot with sample preparation and lab work: Hartmut Kühn, Daniel Weimer, Maaiken Fonck, Frauke Menzel, Marius Isken, Jan-Henning Haas, and Miriam Ibenthal.

This thesis was supported generously by the "Deutsche Forschungsgemeinschaft" (DFG) and the Integrated Ocean Drilling Program (IODP). Many thanks to Walter Hale and the local staff of the IODP in the Bremen Core Repository (BCR) for their kind help with sampling.

Finally I'd like to thank my university professors at the University of Sfax, Tunisia. From them I learned the Geosciences. Many friends in Germany, Tunisia, France, and elsewhere have shown a lot of kind support and interest. To all of them, "chokran" (thank you) I won't forget that!

Chapter 1
Introduction and Objectives

1. Questions related to global Pliocene climate evolution

1.1. Preamble: Updated definition of Pliocene and Quaternary stages

Following the International Subcommission on Stratigraphic Classification (ISSC, 2009), the Pliocene series is reduced to stages named Early Pliocene (Zanclean) from ~5.33 to 3.6 Ma (Ma = Mega annum) and Upper Pliocene (Piacenzian) from ~3.6 to 2.59 Ma. With this new definition the Gelasian (2.59 – 1.81 Ma) is shifted from the Pliocene Epoch to the Peistocene (Fig. 1).

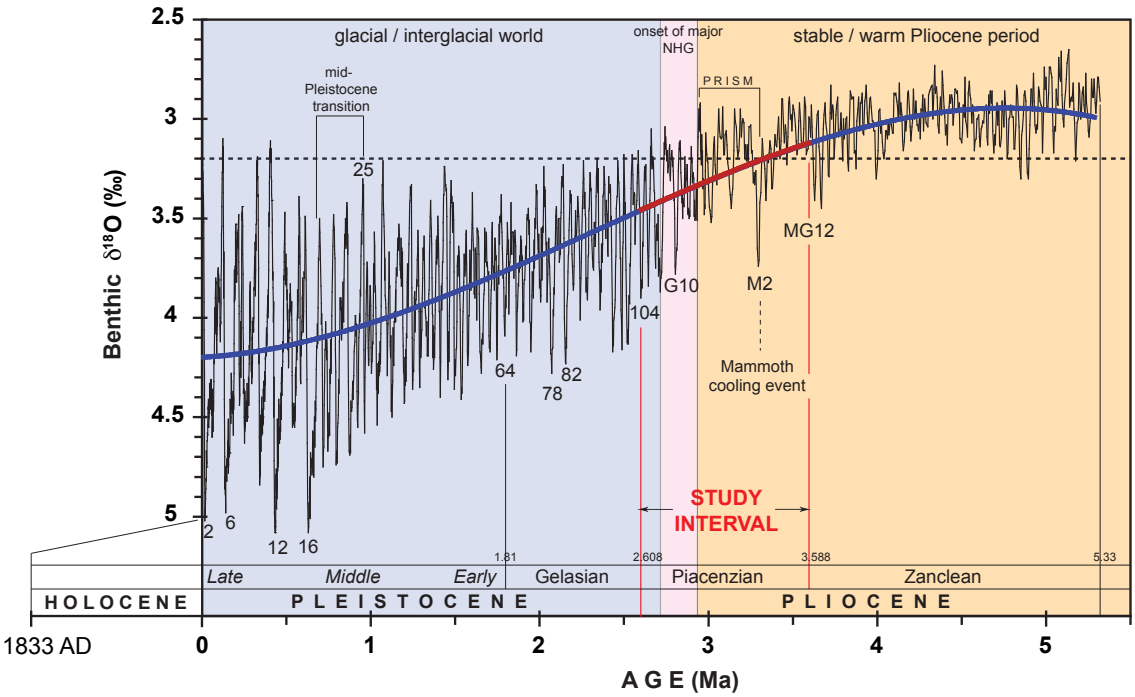

Figure 1.1. Plio-Pleistocene global cooling trend over the last ~5.33 Ma as shown by increasing (stacked) benthic oxygen isotope ratios (LR04; Lisiecki and Raymo, 2005). Most recent definition of Pliocene and Quaternary of ISSC (2009) as indicated. NHG = Northern Hemisphere Glaciation.

1.2. Pliocene climate units

Beyond orbital oscillations, benthic $\delta^{18}O$ records (stacked in LRO4, Lisiecki and Raymo, 2005; Fig. 1) suggest two long-term phases that may be important for evaluating paleoceanographic records of the Mediterranean Sea. An Early Pliocene warm period "Golden Age" from ~5.33 to 2.95 Ma, which was warmer than today (Crowley, 1991; Jansen et al., 2007), and a period of climatic deterioration that started near 2.95 Ma and led to high-magnitude Quaternary-style climates with glacial/interglacial cycles (summarized in Sarnthein et al., 2009).

During the warmer-than-present Early Pliocene period (5.33 – 2.95 Ma), the greatest warming was most likely located in high latitudes (cf. Dowsett et al., 2009b). Warming of high-latitudes may have resulted in much reduced sea ice, ice sheets, and higher sea level of about +25 m (Dowsett and Cronin, 1990; Dwyer and Chandler, 2009; Naish and Wilson, 2009). In mid-latitudes, winter and summer temperatures were also higher than today, as shown by the distribution patterns of planktic foraminifera and terrestrial fauna and flora (Dowsett et al., 1996; Salzmann et al., 2009).

Different modes of High- vs. mid-latitude interactions should have affected necessarily the state of Mediterranean climate through atmospheric and oceanic connections (e.g., Eshel, 2002; Lionello et al., 2006; Rohling et al., 2008a). To study these linkages, one needs to trace orbital-scale records of long-term Mediterranean evolution to be compared with coeval North Atlantic records.

Moreover, long-distance teleconnections such as between the Mediterranean climate and the African monsoon, especially after the progressive restriction of the Indonesian throughflow, ca. 4–3 Ma (ITF; Cane and Molnar, 2001; Karas et al., 2009), should have influenced the Mediterranean freshwater budget and climate through the discharge of the Nile, and other North African ancient rivers (as during the Late Quaternary; Rossignol-Strick, 1985). These links need to be tested by aridity records with precise timing, such as Mediterranean pollen and sea surface salinity curves.

During the restoration of open marine conditions from ~5.3 to 4.5 Ma (see Spezzaferri and Tamburini, 2007), the Mediterranean (-Paratethyan) region was humid enough to produce a negative freshwater budget (Evaporation/Precipitation), which in turn has maintained a short-lasting period of estuarine circulation mode (~5.33 – 5.2 Ma; van Gorsel et al., 1980; van Harten, 1984). Both modeling experiments (A. Haywood; A. Federov; pers. comm. 2009) and

pollen records (Suc, 1984; Fauquette et al., 1998b) show a warm (1°–5°C), humid (400–1000 mm/yr), and less seasonal Mediterranean climate with dense vegetation, perhaps continuing until much later (~3.5 Ma). Still poorly understood is whether the transition from estuarine to modern anti-estuarine circulation was a single event or followed after an oscillating circulation regime.

Subsequent to ~3.5 Ma, Mediterranean climatic rhythm (summer droughts; Suc, 1984) with higher evaporation and less precipitation (Keigwin and Thunell, 1979) was established. The origin of the forcing behind this change is as yet unknown (e.g., changes in the freshwater budget or closing of the advection of Paratethyan freshwater). Also, there is a lack of studies on whether this key change in Mediterranean climate may have had any impact on North Atlantic Meridional Overturning Circulation (MOC) through the advection of Mediterranean Outflow Water (MOW) (Reid, 1979; Bigg et al., 2003).

Prior to the termination of the Early Pliocene warm period, a short-lasting cold oscillation near 3.3 Ma marked the global climate at marine isotope stage (MIS) M2 (Fig. 1). This stage was the coldest period among a suite of other orbital-scale oscillations such as MIS Gi4 (ca. 3.67 Ma), KM2 (ca. 3.12 Ma), and G20 (ca. 3.01 Ma). It is still unknown, whether these cold stages had any repercussion on Mediterranean climate.

A global progressive cooling started only after MIS G17 (ca. 2.95 Ma) and was marked by a major climatic deterioration starting after at MIS G10 (ca. 2.8 Ma) leading to Quaternary-style high climatic variability with glacial/interglacial cycles (Bartoli et al., 2005; Sarnthein et al., 2009; Fig. 1). One may expect that this onset of major Northern Hemisphere Glaciation (NHG) has altered the response of the Mediterranean climate to the coeval climatic variability (Vergnaud-Grazzini, 1985; Thunell et al., 1987; 1991). One may consider a cooling of surface waters near the locations of deep-water convection, which may trigger enhanced deep-water formation and MOW advection. On the basis of pollen spectra, summer droughts similar to today became more persistent already after 3.6 – 3.2 Ma (Suc, 1984), which is much earlier than the onset of major NHG, a further unsolved question.

In addition, we may expect with the onset of NHG an onset of marked millennial-scale changes in temperature and precipitation on top of obliquity and precessional cycles (Draut et al. 2003; Bartoli et al., 2006). However, to trace this variability we would need centennial-scale resolution records that were not established by this study.

2. Questions related to the geodynamic history of the Mediterranean Sea

After the isolation of the Mediterranean Sea during the Messinian Salinity Crisis from ~5.96 to 5.33 Ma (Krijgsman et al., 1999a; Duggen et al., 2003; Betzler et al., 2006), the tectonic-driven opening of a marine gateway at the Strait of Gibraltar ~5.33 Ma restored open marine conditions (McKenzie, 1999; Garcia-Castellanos et al., 2009). However, it was important to know whether there were any further geodynamic changes of the Gibraltar seaway, which may have changed the sill aperture, and thus influenced the volume of MOW advection into the North Atlantic over the Pliocene.

3. Summary of objectives to be tested

Based on the outlined questions and in view of an almost general lack of studies on Pliocene changes in MOW, except for pioneering studies of Loubere (1987a; 1987b; 1988), the major goals of this thesis comprise the following targets:

1. To reconstruct Pliocene changes in the Mediterranean hydrological cycle as record of local climate variations, based on multiproxy records with orbital-scale resolution. In particular, we establish records of changes in Mediterranean Sea surface hydrology and properties of deep-water (temperature, salinity, density). These records enable us to monitor changes in the local E/P freshwater budget near to the Gulf of Lion, a major Mediterranean source of deep-water formation.

2. To reconstruct changes in MOW properties and advection in the North Atlantic. For this purpose, we establish records of changes in bottom-water salinity and density of MOW. This target required a proper selection of key study sites along the northeast Atlantic continental margin, which is along the northward-directed tongue of MOW.

3. To separate changes in MOW flow intensity from changes in the depth level of the MOW tongue, a target we have not fully accomplished because of a lack of monitoring sites in the northeast Atlantic.

4. To assess linkages between Mediterranean climate and the African monsoon system, moreover with changes in the Indonesian Throughflow (ITF; as forced by gradual northward drift of Australian plate). To reach this goal, we compare our records with

published continental and marine records focusing on Upper Pliocene changes in African and Indian monsoon intensity.

5. To find clues for the interactions of high- vs. mid-latitude climate system during the Upper Pliocene. The Mediterranean region today forms a transition between temperate and subtropical latitudes, near to the southern limit of the westerlies (and so even during peak glacial times; e.g., Pflaumann et al., 2003). Therefore, the Mediterranean Sea may monitor an impact of the Upper Pliocene warming observed in high- to mid-latitudes. In particular, this concerns testing the results of General Circulation Models (GCM) of Mediterranean climate change, which claim that atmospheric and oceanic heat transport from the Equator to the North Atlantic may caused warming of the Mediterranean and Europe during that time (A. Haywood et al., 2000b; A. Haywood, pers. comm. 2009).

6. To get an idea on a potential northward expansion of subtropical climate (Hadley cell) during the Upper Pliocene (to test the model of Federov et al., 2010). This major aim includes the question how to translate this climate forcing into a record of MOW variability.

7. To study the potential feedbacks of MOW incursion into the MOC of northern North Atlantic, i.e., to test models of Reid (1979) and Bigg et al. (2003), and to trace clues for a potential but questionable origin of Upper Pliocene global climate change from a Mediterranean and subtropical perspectives.

Chapter 2
Modern Ocean Setting, Climatology, and Site Selections

1. The modern Mediterranean Sea – Advection of the MOW

The Mediterranean is a landlocked, semi-enclosed marginal sea of the Atlantic Ocean, which is divided by the Strait of Sicily in two main sub-basins: Western and eastern Mediterranean (Fig. 2.1). This study focuses on the western basin, where Eastern Mediterranean Deep Water (EMDW) and Western Mediterranean Deep Water (WMDW) mix together with the Mediterranean Intermediate Water (MIW) to form the MOW after through the Strait of Gibraltar, the only connection of the Mediterranean Sea to the open (Atlantic) ocean. With 284 m sill depth and a minimum width of 14 km, the Plio-Quaternary Strait of Gibraltar maintains today an inflow of 1.68 Sv (1 Sv = 10^6 m^3 s^{-1}) with 36.2 psu salinity and outflow of 1.60 Sv with an average flow velocity of 2.1 m^3 s^{-1} and 38.4 psu salinity (Béthoux et al., 1979; Bryden and Kinder, 1991), which leads to an average of 3.5 Gt/day salt export to North Atlantic intermediate waters (Fig. 2.1). The geodynamics of the Strait of Gibraltar were stable since at least 5 Ma ago. Accordingly, water circulation and exchange patterns were largely similar until today (Blanc, 2002). Geodynamic stability of the Strait of Gibraltar offers the possibility to discuss Pliocene changes in MOW purely in terms of climate, independent of any geodynamic influence.

The Mediterranean climate regime is governed by the interaction/competition between the high-to-mid-latitude (over central and northern Europe) and subtropical (over North Africa) atmospheric systems (Lionello et al., 2006) (Fig. 2.2). The latitudinal shift of these climatic systems results in a pronounced contrast between seasons in the Mediterranean regions. While warm and dry conditions prevail during summers, winters are mild-to-cold and wet (Eshel, 2002; *see* Rohling et al., 2008a).

In summer, the northward displacement of the subtropical high-pressure belt results in droughts around most of the Mediterranean basins (Saaroni et al., 2003; Ziv et al., 2004). The western Mediterranean may still stay under the influence of polar front depressions. During winter, the subtropical conditions are displaced southward and the northern sector of the Mediterranean is under the influence of the temperate westerlies that dominate over central and northern Europe (Lolis et al., 2002). Climate variability in the Mediterranean is also under the effect of the North Atlantic Oscillation (NAO). Low NAO index phase is associated with wet conditions over the

western Mediterranean (Maheras et al., 1999; Dünkeloh and Jacobeit, 2003). However, the effect of NAO on the eastern basin has remained unclear, except via the dependence of the so-called Mediterranean Oscillation (MO) on NAO (Dünkeloh and Jacobeit, 2003; *see* Rohling et al., 2008a).

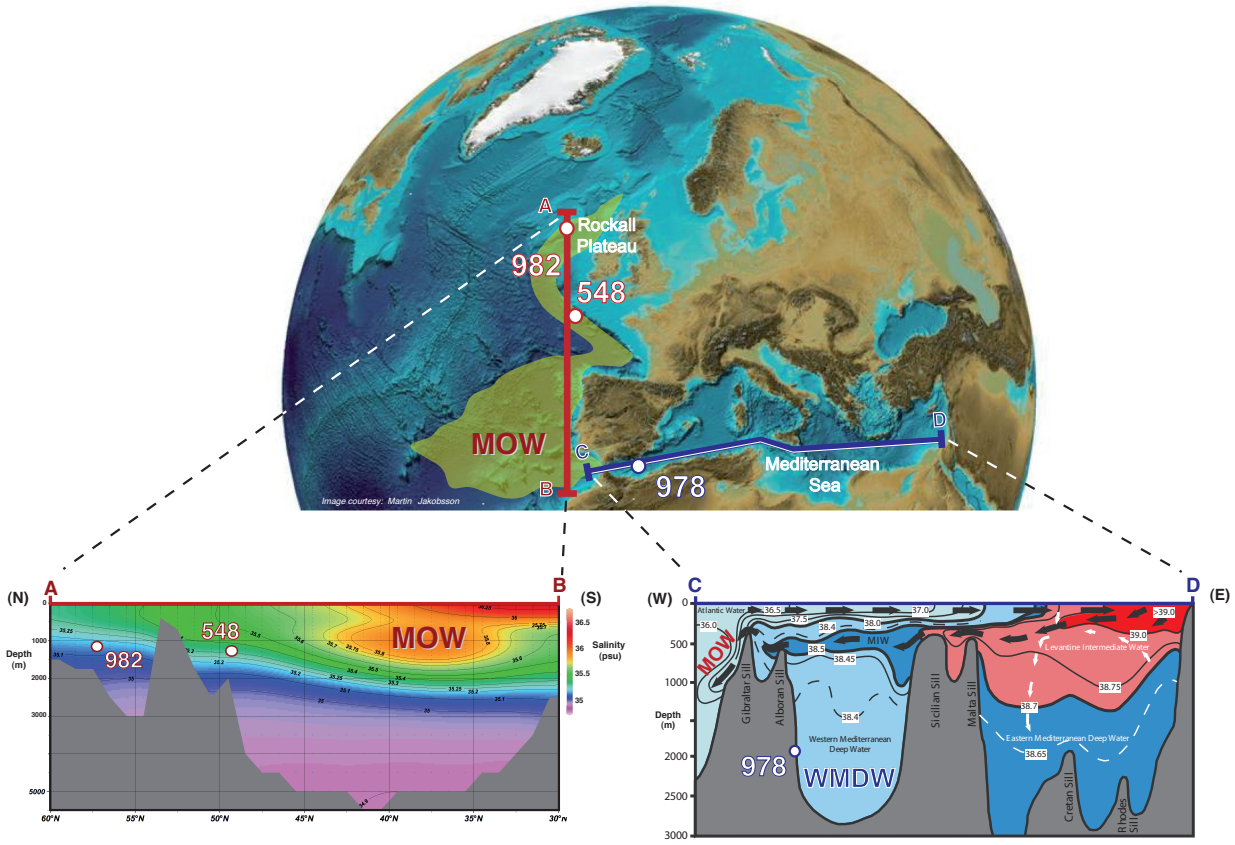

Figure 2.1. Modern hydrographic transects.

(A – B): North – South cross-section showing water masses in the northern North Atlantic with location of Sites 548 (48°N, 12°W; 1250 m w.d.) and 982 (57°3´N, 15°5´W; 1135 m w.d.). MOW = Mediterranean Outflow Water.

(C – D): West – East cross-section showing water mass circulation in the Mediterranean Sea during winter (after Wüst, 1961) with location of Site 978 (36°N, 2°W; 1930 m w.d.). Salinity isolines and arrows show directions of water circulation (Rohling et al., 2008a).

To a large degree it has been unknown, at which time the modern seasonal regime was first established in the Mediterranean, after the modern circulation pattern had been basically installed during the Lower Pliocene (*see* Spezzaferri and Tamburini, 2007; Rohling et al., 2008a). This can be recorded in marine sediments which may reflect, whether the basin hydrography was either under the influence of the African monsoon system through the freshwater discharge of the Nile River and other North African paleo-drainage systems or not (Rohling and Bryden, 1992; Scrivner et al., 2004). Thus it is unknown to which extent the freshwater budget during the Pliocene was altered by the African monsoon system.

Today, the influence of African monsoon is almost neglected. Accordingly, the Mediterranean Sea is a concentration basin, where evaporation losses (E) exceed the freshwater inputs resulting from precipitation (P) and river runoff (R) (Béthoux, 1979; Gilman and Garett, 1994; Bryden and Kinder, 1991). This feature results in an important surface water salinity increase over all the Mediterranean (36.2–39.5 psu; MEDATLAS, 1997) (Figs. 2.1; 2.3). During the Pliocene, Mediterranean freshwater budget may have been different due to an increased or reduced monsoonal effect as shown, for example, by some proxy records of vegetation change (Suc, 1984).

In the Mediterranean Sea, the vertical distribution of water masses consists of surface (0–200 m), intermediate (200–600 m) and deep waters (>600 m) (Pinardi and Masetti, 2000). The anti-estuarine circulation in the Mediterranean Sea is mainly driven by thermohaline forcing (in addition to wind stress), which depends on the basin's freshwater and heat budget (POEM Group, 1992; Robinson et al., 2001). In the Strait of Gibraltar an eastward surface flow of warm (15 °C) Atlantic water (AW) with normal salinity of 36.2 psu overlies the westward flow of little colder (13 °C) but more saline (38.4) and thus denser (1029.7 kg m^{-3}) subsurface waters (Candela, 2001), the result of both net evaporation loss and net cooling (Garrett, 1994). This subsurface MOW falls down to 1000 – 1500 m water depth in the northeast Atlantic Ocean (e.g., Wüst 1961; Stommel et al., 1973; Reid, 1979; Price et al., 1993) (Fig. 2.1). It is the objective of this study to investigate whether or not the anti-estuarine circulation, which maintains the "subsurface" advection of MOW, has continued or been reversed over the Pliocene.

After passing the Strait of Gibraltar, the AW mixes with upwelled MIW creating Modified Atlantic Water (MAW), which migrates eastwards forming anticyclonic gyres (Heburn and La Violette, 1990) (Fig. 2.3). In the northern sector of the Mediterranean Sea MAW forms mesoscale cyclonic gyres in the Gulf of Lions, where a strong cooling caused by the Mistral winds results in the formation of WMDW (MEDOC group, 1970; Leaman and Schott, 1991; Rohling et al.,

1998b). Along its migration to the East through the Strait of Sicily, the salinity values of MAW increase significantly due to continued evaporation (Wüst, 1961). For example in the Levantine Basin, salinities reach 39.5 psu. The joint influence of high salinity, enhanced mixing, and evaporation (as a consequence of cold winter continental winds) is leading to favorable conditions for active vertical convection and the consequent formation of the Levantine Intermediate Water (LIW) (Figs. 2.1; 2.3). From its source, the LIW spreads over the entire Mediterranean basins as MIW (150–600 m w. d.) and finally enters the Atlantic Ocean through the Strait of Gibraltar (see Rohling et al., 2008a and references therein) (Fig. 2.1). The interaction of LIW with cold surface waters in various northern sectors of the Mediterranean Sea results in a series of sites with deep-water formation, which are responsible for strong deep-sea ventilation of the entire Mediterranean (Pinardi and Masetti, 2000). In particular there is (1) the Aegean (Aegean Deep Waters, AeDW), (2) the Adriatic (Adriatic Deep Waters, ADW), and (3) the Gulf of Lions for the western basin (WMDW formation) (Fig. 2.3). While today the relative contributions of these sites to MOW are large (e.g., 0.3 Sv from WMDW), different climatic conditions during the Pliocene may have resulted in different main contribution to MOW.

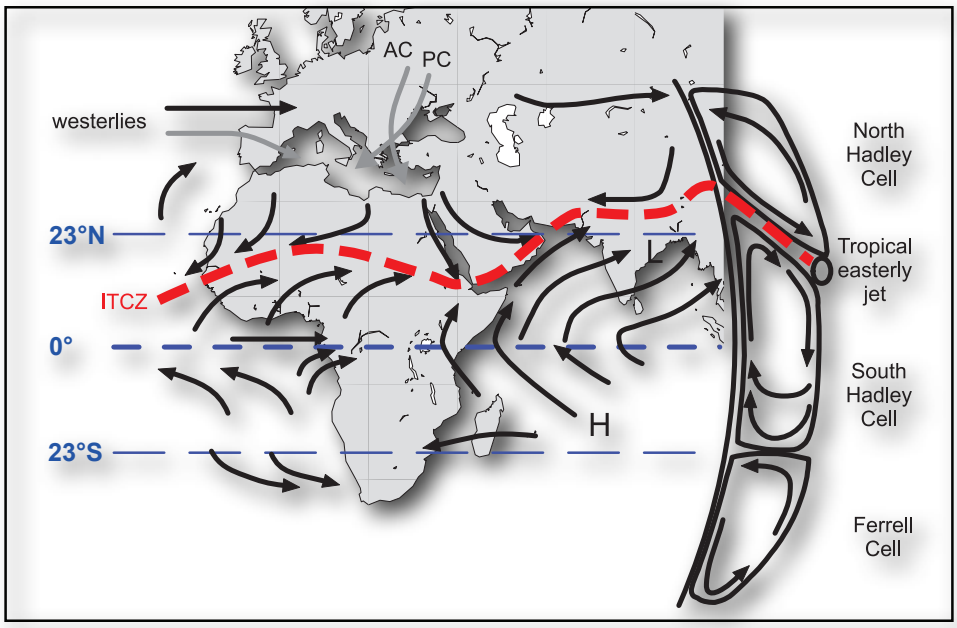

Figure 2.2. Scheme of Northern Hemisphere atmospheric circulation during summer (with vertical N-S transect at right margin). Black arrows represent main wind directions. ITCZ = Intertropical convergence zone; H and L = areas of high and low sea level pressure, respectively. Main air masses reaching the Mediterranean Sea in winter are labeled as grey arrows. AC = Arctic continental air masses; PC = Polar air masses (slightly modified after Marino, 2008; Rohling et al., 2008a).

2. The modern Northeast Atlantic – Mixing and dilution of MOW

Once entered into the Gulf of Cadiz, salinity and density of the MOW decrease rapidly because of mixing with the overlying less saline North Atlantic Central Water (NACW) and Labrador Sea Water from below (Zenk, 1975; Talley and McCartney, 1982). The resulting diluted outflow spreads between 700 and 1500 m far into the North Atlantic (Fig. 2.1), forming the only tongue of warmer and saltier waters beneath the thermocline in the Atlantic (Reid; 1979). Here MOW is split into an upper and a lower branch. The upper branch is centered at 750 m, flowing northward along the Portuguese continental slope up to the Greenland-Scotland Ridge, while the lower main core layer is centered at 1250 m. Both masses meander both along the West European continental margin to the North (due to Coriolis forcing; Baringer and Price, 1997b) and to the west and southwest (Zenk and Armi, 1990). The MOW tongues are characterized by relatively high oxygen values and low nutrient concentrations, *i.e.*, high $d^{13}C$ values of "dissolved inorganic carbon" (DIC) due to their origin in the oligotrophic Mediterranean Sea (Zenk and Armi, 1990) (Fig. 2.1). Also, the MOW tongues are populated by many submesoscale coherent vortices or so called "Meddies" (for Mediterranean eddies) (McDowell and Rossby, 1978; Armi and Zenk, 1984; Käse and Zenk, 1987).

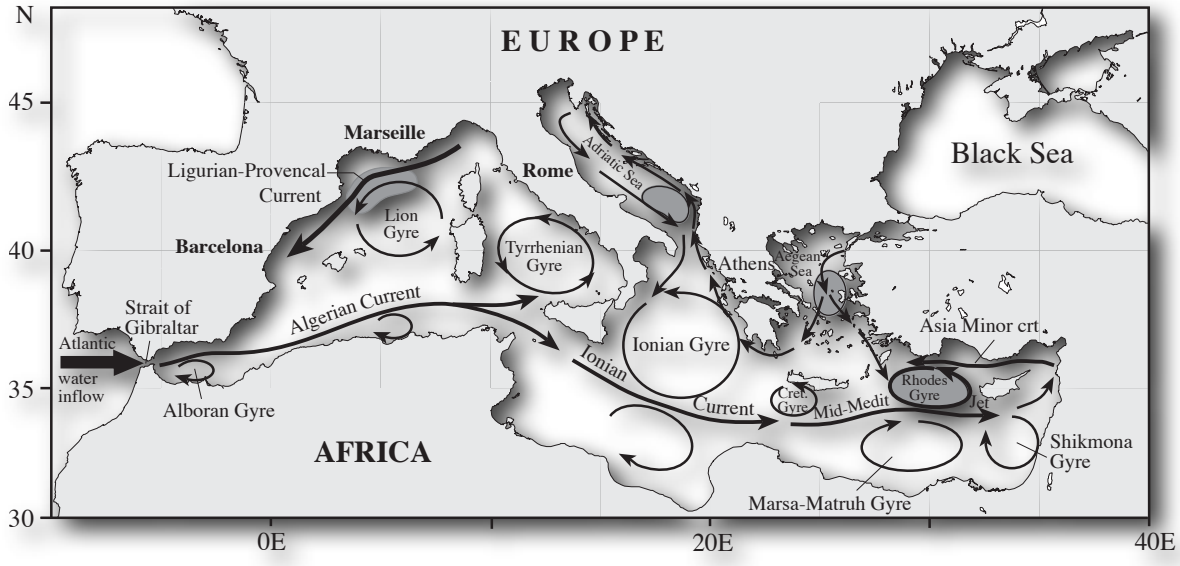

Figure 2.3. Surface water circulation in the Mediterranean Sea (after Vergnaud-Grazzini et al., 1988). Shaded areas indicate zones of intermediate and deep water formation (from Rohling et al., 2008a).

After turning northwards from the Gulf of Cadiz, MOW flows along the eastern boundary of the northeast Atlantic. This flow reaches the Rockall Trough near 1200 m w. d. (McCartney and Mauritzen, 2001) (Fig. 2.1). Finally, a diluted version of MOW may rise up to depths of less than 600 m over the Wyville-Thomson Ridge and up to the Norwegian Sea, thereby possibly contributing significantly to the high salinity of the Norwegian Current and its transport (model of Reid; 1979) (Fig. 2.1). While McCartney and Mauritzen (2001) agree that the MOW may be admixed to the "Nordic Seas Inflow" from below, they argue against any direct advection of MOW to the north of Rockall Plateau. Rather, they argue that the eastern boundary undercurrent starts to be diluted and may expulse its mass transport of MOW into the subtropical gyre. Today, the North Atlantic Drift Current (NADC) maintains the relatively warm climate over western Europe and Scandinavia (Bigg, 1996), also by the release of heat during North Atlantic Deep Water (NADW) formation (*see* Siedler et al., 2001). Whether a mixing from below or a direct advection of the MOW to the Nordic Seas is prevailing today and/or during the Pliocene is as yet unclear. For this reason our study tries to constrain the Pliocene density properties of the MOW eastern boundary undercurrent, in particular where it mixes with NADC over Rockall Plateau.

3. Strategy to select site locations

To study changes in the physical and chemical properties (temperature, salinity, density, and ventilation) of MOW over the Upper Pliocene, we need a proper strategy for selecting key study sites. In the North Atlantic, no sites occur at proper water depths (i.e., 700 – 1500 m) to study the westward flow of MOW. However, two sites monitor today the northward flow along the Northeast Atlantic continental margin: DSDP Site 548 (Goban Spur; 1250 m w. d.) and ODP Site 928 (Rockall Plateau; 1135 m w. d.) (Fig. 2.1) (Table 2.1). A horizontal and slight vertical gradient between Site 548 and Site 982 may help to constrain the water mass distribution along the northeast Atlantic continental margin. To properly monitor the actual properties of MOW prior to mixing with Atlantic water masses, we employed a site near to its source region, ODP Site 978 (Alboran Sea; 1930 m w. d.). Today this site in the westernmost Mediterranean is bathed by WMDW that only forms ~25% of the total MOW volume (see Rohling et al., 2008a) (Fig. 2.1). Accordingly, Site 978 cannot be expected to provide a perfect record of the variations in MOW composition. Nevertheless, any Pliocene variations in the other constituents of MOW, that is the composition of EMDW and MIW, may be linked closely to each other. This postulate is based on the assumption that all main sites of Mediterranean deep-water convection were under the influence of similar Mediterranean climate variability.

Site	Location	Region	Water Depth	Target
978	36°13´N, 2°3´W	Alboran Sea	1929 m	- Changes in the hydrological cycle of West Mediterranean Sea - Changes in the properties of WMDW
548	48°54´N, 12°09´W	Goban Spur	1251 m	- Changes in the properties of MOW (fairly proximal)
982	57°3´N, 15°5´W	Rockall Plateau	1134 m	- Distal properties of MOW - Possible influence of MOW on North Atlantic MOC

Table 2.1. Rationales for study site selection

Chapter 3
Methods and Strategy

1. Sediment sample preparation

Ocean sediment cores were sampled at the East Coast (LDEO, Columbia University) and Bremen (MARUM, University of Bremen) IODP core repositories. To reach orbital to millennial scale resolution, samples were spaced 10–20 cm at Site 978, and 10 cm at Sites 548 and 982. Sediment samples are 2 cm-wide and amount to 20 cm^3. Sample processing is summarized in Fig. 3.1.

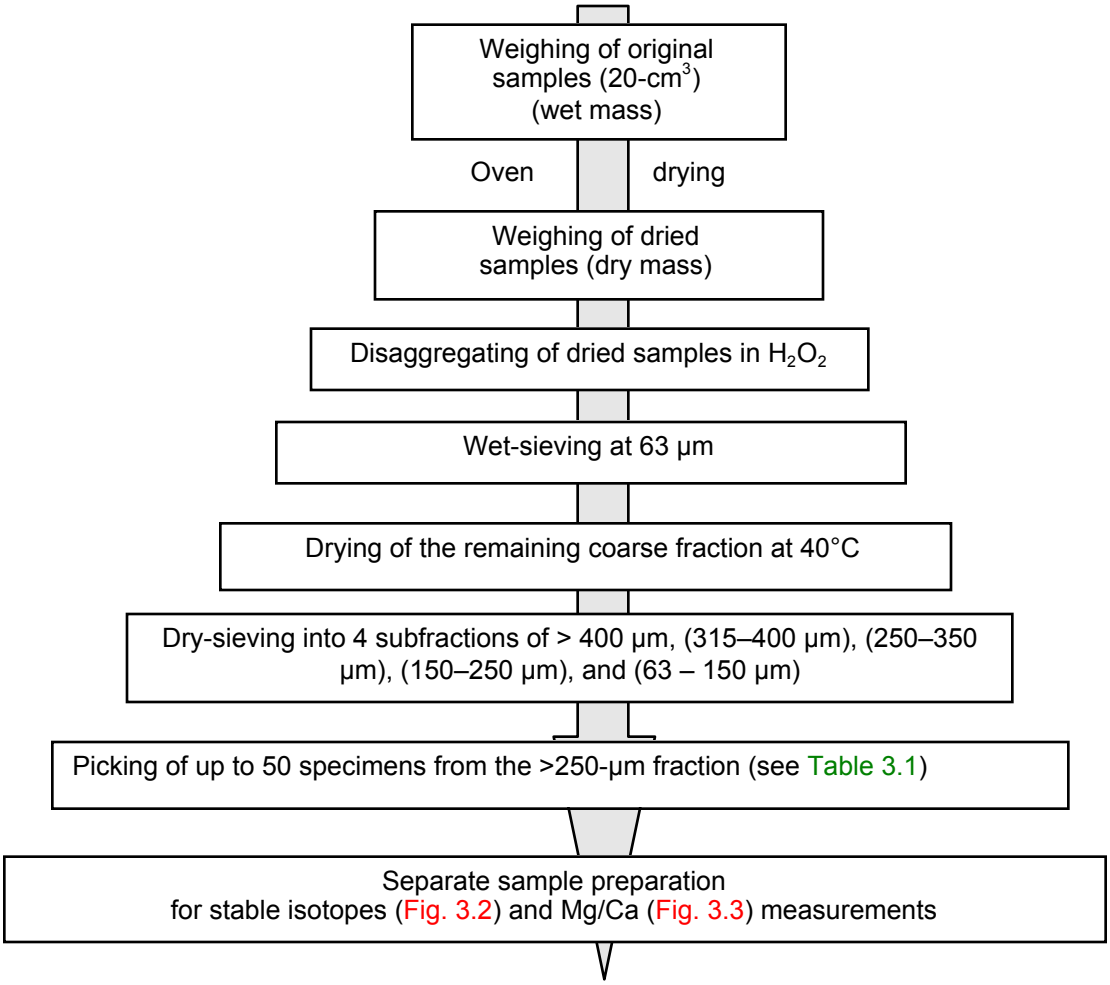

Fig. 3.1. Flow-chart of sample processing

2. Nd analyses

2.1. Extraction of the Fe-Mn Oxyhydroxide coatings

The Nd isotopic composition of bottom seawater was extracted from the authigenic Fe–Mn oxyhydroxide coatings in bulk sediment samples to reconstruct past water mass origin. Different from other stable isotopic or element ratio proxies, it is the benefit of using radioactive Nd isotopes that they remain unbiased by biological processes. Due to a residence time in seawater of 600 to 2000 years, Nd isotopes are increasingly used as a quasi-conservative water mass tracer for the present and past ocean (*cf.* Frank, 2002). Our analytical procedures for the extraction of the seawater-derived Nd in the Fe–Mn oxyhydroxide coatings followed Gutjahr et al. (2007) and are summarized in Fig. 3.2.

2.2. Analysis with an ICP-MS

Once the seawater fraction of Nd in the metal-oxide coatings of the sediment has been extracted by leaching (Fig. 3.2), the Nd in the leached solutions were chemically treated and purified following Cohen et al. (1988). The Nd isotope composition was measured at the mass spectrometry facility of IFM-GEOMAR using a *Nu* instruments multi collector–inductively coupled plasma mass spectrometer (MC–ICPMS) and a *Thermo* TRITON thermal ionization mass spectrometer (TIMS).

Nd isotope ratios are expressed as ε_{Nd} values, which correspond to the deviation of the measured $^{143}Nd/^{144}Nd$ ratio of a sample from that of the chondritic uniform reservoir CHUR (0.512638) multiplied by 10,000:

$$\varepsilon_{Nd} = (\{^{143}Nd/^{144}Nd_{\ sample} / {}^{143}Nd/^{144}Nd_{\ CHUR}\} - 1) \times 10^4$$

Measured $^{143}Nd/^{144}Nd$ was normalized to $^{146}Nd/^{144}Nd$ (= 0.7219) to correct for instrumental mass bias (Jacobsen and Wasserburg, 1980). Repeated measurements of the JNdi-1 standard (a Nd isotopic reference introduced by Tanaka et al., 2000) showed an error of external 2σ precision ±0.3 ε_{Nd} units. All Nd isotope ratios presented in this study were normalized to the widely accepted value for the standard JNdi-1 of 0.512115 (Tanaka et al., 2000).

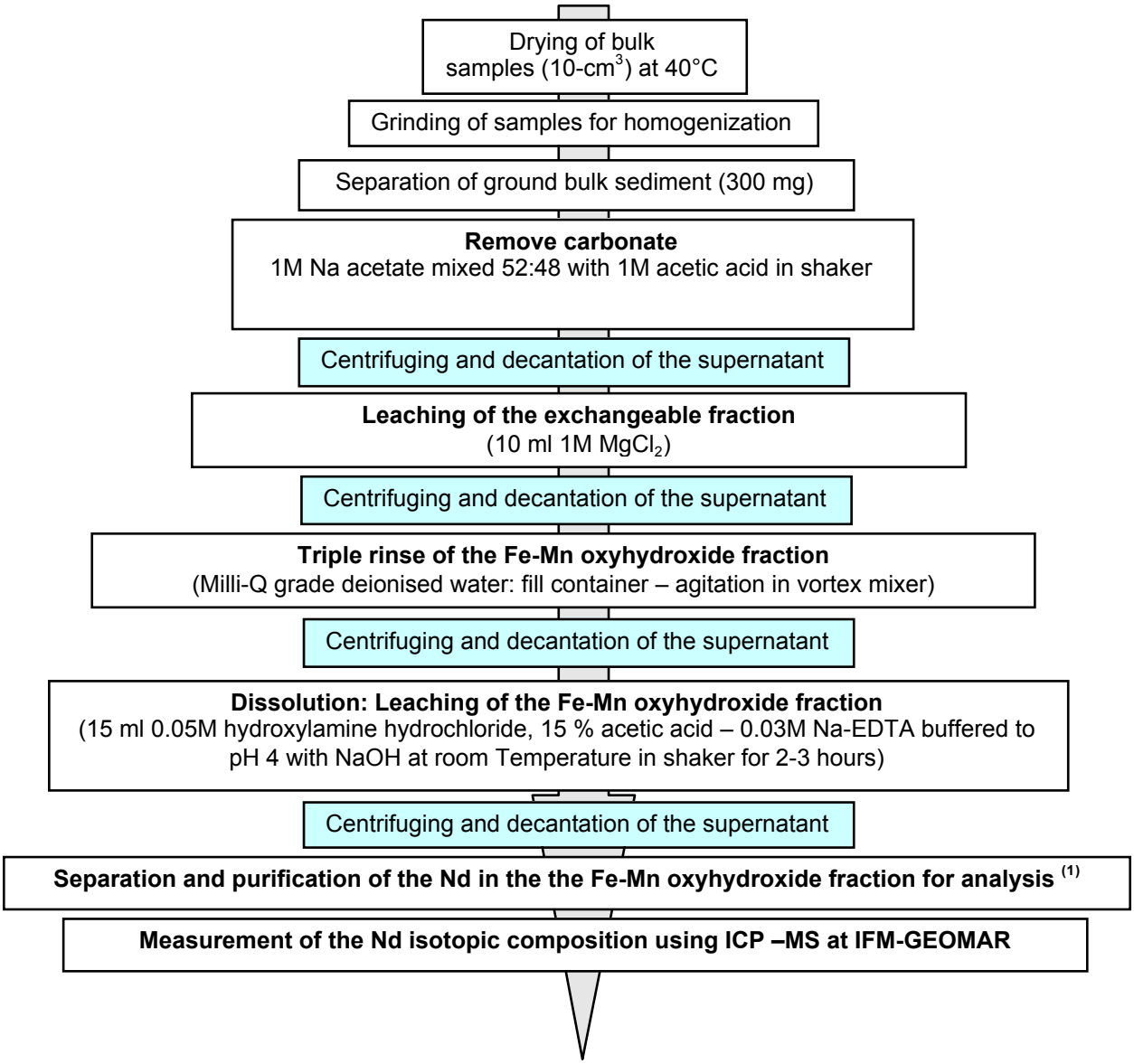

Fig. 3.2. Flow-chart of the extraction of Fe–Mn oxyhydroxide coatings (leaching according to Gutjahr et al., 2007).

---

(1) To further ensure that no Nd was leached from the clays, several Nd and Sr isotopic analyses of complete bulk sediment dissolutions were made after the leaching of the sediment, for comparison with the leached Sr and Nd isotope compositions (Gutjahr et al., 2007). Results show that the potential clay-derived Nd contribution was less than measurement error (±0.3 ε_{Nd} units), which may indicate the extraction of a Nd pure sea-water signal.

3. Selection of planktic and benthic species for geochemical and isotopic analyses (Mg/Ca and $\delta^{18}O$, $\delta^{13}C$)

Benthic and planktic species that we used for various geochemical and isotopic analyses are summarized in Table 3.1.

To reconstruct local hydrological changes in the westernmost Mediterranean Site 978, stable isotope signals of surface to subsurface waters are based on the warm and mixed-layer-dwelling species *Globigerinoides ruber* (white) that today develops preferentially in the autumn (Pujol and Vergnaud-Grazzini, 1989). In case *G. ruber* specimens were scarce or missing, *Globigerina bulloides,* which is known to calcify in late spring/early summer in the Alboran Sea (Rohling et al., 1995), was picked. In intervals where both *G. ruber* and *G. bulloides* were scarce, the today-extinct subtropical and temperate species *Globigerinoides obliquus* was picked (Last Occurrence (LO) near the Plio/Pleistocene boundary; Bizon and Müller, 1978). Planktic species were not used to produce a Mg/Ca-based sea surface temperature (SST) record to avoid a potential effect of highly saline Mediterranean waters on the Mg/Ca signal (Ferguson et al., 2008).

Mg/Ca-based BWT were based on both benthic foraminifers *Cibicidoides wuellerstorfi* and *C. mundulus.* We follow van Morkhoven et al. (1986) in considering *C. kullenbergi* to be a junior synonym of *C. mundulus* (*see* Holbourn and Henderson, 2002). In the Mediterranean (S. 978) we noticed that *C. mundulus* shows 2 different morphotypes: An Atlantic-like “opaque” morphotype (similar to that found at Sites 548 and 982) and a well preserved, more abundant, transparent, and “glassy” morphotype that we picked for our analyses. These morphotypes show different Mg/Ca ratios; the “glassy” morphotype exhibits a consistent interspecific offset in Mg/Ca of almost +2.25-mmol mol^{-1} (+5°C) from the Mg/Ca values of the “opaque” morphotype and also of *C. wuellerstorfi*, as determined from the difference between averaged values downcore. The offset is most likely due to a differential vital effect of both morphotypes of *C. mundulus* and of *C. wellerstorfi* (Yu and Elderfield, 2008; Healey et al., 2008). Likewise the effect of high bottom-water salinity may be ruled out because it would likewise affect the Mg/Ca ratios of both morphotypes and of *C. wellerstorfi* in the same manner. Therefore we corrected the Mg/Ca-based BWT values of both *C. wuellerstorfi* and the “opaque” morphotype of *C. mundulus* for the offset of 2.25 mmol mol^{-1}. In case we had not normalized the data to the Mg/Ca values of the “glassy” morphotype of *C. mundulus*, the resulting BWT estimates would drop

to levels significantly lower than those found for northeast Atlantic Sites 548 and 982, a level that is clearly unrealistic (*see* Chapter 5: Proxy intercomparison).

At Site 548, the aim was to produce a reliable stratigraphy based on the planktic $\delta^{18}O$ record, as the benthic $\delta^{18}O$ record may contain a possibly dominant MOW signal, and thus does not reflect properly global ice volume changes. To generate a planktic $\delta^{18}O$ record we picked the today-extinct *Neogloboquadrina atlantica* (s) specimens that were the most abundant overall the sediment sections. The benthic $\delta^{18}O$ record was established mainly based on *C. mundulus* (most continuous occurrence), *C. wuellerstorfi*, and partly on *Uvigerina* spp. (plus few other species, incorporating existing records of Loubere, 1987; 1988; see summary of species used in Table 3.1). Mg/Ca-based BWT were based mainly on *C. mundulus*. Due to the scarcity of *C. wuellerstorfi*, it was not possible to produce a complete Mg/Ca-based record of BWT but only a coarse, discontinuous record to be compared with the BWT record of *C. mundulus* (*see* Chapter 5: Proxy intercomparison).

At Site 982, planktic $\delta^{18}O$ and Mg/Ca-based SST records were based on *Neogloboquadrina atlantica* (s) specimens. Benthic $\delta^{18}O$ records were established mainly using the more abundant *C. mundulus* species. *C. wuellerstorfi* specimens were missing over some intervals and were picked only in case *C. mundulus* specimens were scarce or absent. However, separate Mg/Ca-based BWT records were generated from both species, each for proxy intercomparison (*see* Chapter 5: Proxy intercomparison).

TABLE 3.1. SPECIES USED IN THIS STUDY

Record	***Core depth (mcd)***	***Species***	***# Tests***	***Size Fraction (µm)***
Site 978				
Planktic $\delta^{18}O$, $\delta^{13}C$	371.00 – 398.10	*Globigerinoides ruber*	5 – 25	(250-400)
	420.30 – 438.38	*Globigerinoides ruber*		
	391.89 – 420.60	*Globigerina bulloides*	3 – 30	
	437.40 – 438.10	*Globigerinoides obliquus*	3 – 15	
Benthic $\delta^{18}O$, $\delta^{13}C$ (†)	371.00 – 438.38	*Cibicidoides wuellerstorfi*	3 – 10	> 250
Benthic Mg/Ca	371.98 – 438.38	*Cibicidoides wuellerstorfi*	5 – 15	> 250
	371.79 – 435.30	*Cibicidoides mundulus*	4 – 12	

Site 548					
Planktic $\delta^{18}O$, $\delta^{13}C$		127.60 – 167.03	*Neogloboquadrina atlantica (s)*	3 – 30	(250-400)
Benthic $\delta^{18}O$, $\delta^{13}C$ (†)		128.70 – 166.51	*Cibicidoides wuellerstorfi*	1 – 10	> 250
		127.60 – 167.03	*Cibicidoides mundulus*		
		143.89 – 165.25	*Cibicidoides robertsonianus*		
		124.99 – 143.90	*Uvigerina* spp.	4 – 12	
Benthic Mg/Ca		132.91 – 142.10	*Cibicidoides wuellerstorfi*	3 – 12	> 250
		128.22 – 167.03	*Cibicidoides mundulus*		
		129.20 – 144.40	*Cibicidoides robertsonianus*		
Site 982					
Planktic $\delta^{18}O$, $\delta^{13}C$		57.51 – 89.88	*Neogloboquadrina atlantica (s)*	15	(250-400)
Planktic Mg/Ca		57.51 – 89.88	*Neogloboquadrina atlantica (s)*	3 – 30	(250-400)
Benthic $\delta^{18}O$, $\delta^{13}C$ (†)	**Hole A**	68.58 – 72.74	*Cibicidoides mundulus*	2 – 6	> 250
		79.67 – 84.18	*C. mundulus, C. wuellerstorfi*		
	Hole B	57.51 – 59.67	*C. mundulus, C. wuellerstorfi*		
		66.27 – 68.63	*C. mundulus, C. wuellerstorfi*		
		74.47 – 89.88	*C. mundulus, C. wuellerstorfi*		
Mg/Ca Benthic		58.11 – 84.04	*Cibicidoides wuellerstorfi*	3 – 12	> 250
		57.51 – 86.54	*Cibicidoides mundulus*		

At Deep Sea Drilling Project (DSDP) Site 548, 41 out of 48 data of endobenthic *Uvigerina* spp., and 43 out of 416 data of epibenthic *Cibicidoides* spp. are from Loubere (1987) for the benthic $\delta^{18}O$ record. To adjust these $\delta^{18}O$ values to our dataset we corrected them by an empiric value of +0.31. This offset may be due, for example, to contamination of sample gas by reference gas during ionization for analyses generated before the 1990s (Ostermann and Curry, 2000).

For increasing the temporal resolution at Ocean Drilling Program (ODP) Site 982, we supplemented the existing benthic $\delta^{18}O$ record of Venz and Hodell (2002) and Lisiecki and Raymo (2005) by 290 data (see Fig. 4.2 and Table 4.1 in Appendices).

(†) A correction factor of +0.64 was applied to $\delta^{18}O$ values of *Cibicidoides* spp. to normalize them to $\delta^{18}O$ values of *Uvigerina*, which are known to be in equilibrium with ambient seawater (Shackleton, 1974). Parallel measurements did not reveal any systematic offset between $\delta^{18}O$ of *C. wuellerstorfi* and *C. mundulus*. Various studies have shown that both species have nearly equal isotopic values (e.g., Woodruff et al., 1980; Duplessy et al., 1984). $\delta^{13}C$ values of *C. wuellerstorfi* and *C. mundulus* reflect the $\delta^{13}C$ of $\sum CO_2$ (e.g., Shackleton et al., 1973; Shackleton and Hall, 1984; Hodell and Venz, 1992).

4. Stable isotope analyses

Stable isotope measurements served for establishing an oxygen isotope stratigraphy and for the reconstruction of changes in sea surface salinities (SSS) in the western Mediterranean Sea (planktic $\delta^{18}O$), and in bottom water salinities (BWS) and densities (BWD), and the ventilation of MOW in both its Mediterranean source region and the northeast Atlantic (benthic $\delta^{18}O$). The preparation of foraminifera samples is summarized in Fig. 3.3. Measurements of $\delta^{18}O$ and $\delta^{13}C$ were performed on the Kiel device I / Finnigan MAT251 mass-spectrometer at the Leibniz Laboratory in Kiel. Isotopic data were presented by comparison to the Vienna PeeDee Belemnite (VPDB) standard. The analytical precision amounts to ±0.07‰ for $\delta^{18}O$ and ±0.05‰ for $\delta^{13}C$. Benthic $\delta^{18}O$ values were corrected for species-specific offsets relative to *Uvigerina peregrina* (+0.64), the oxygen isotopes of which are considered to represent equilibrium with the ambient water masses (see Table 3.1).

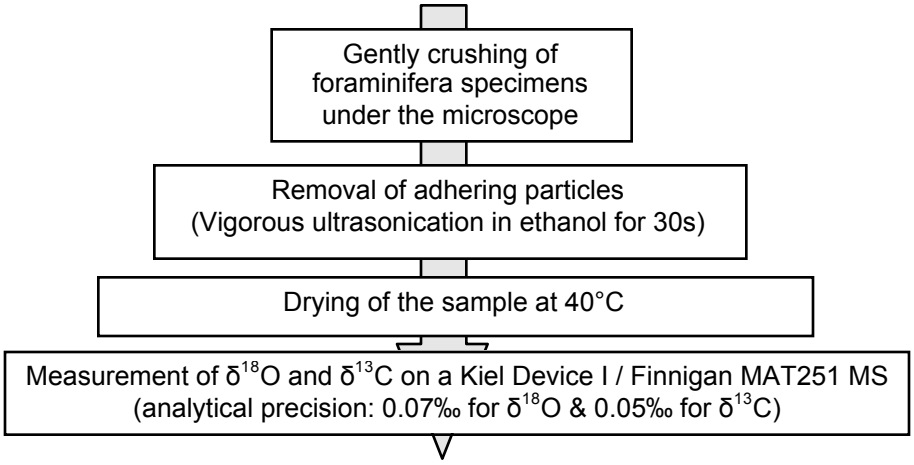

Fig. 3.3. Flow-chart of sample preparation for stable isotope analyses

5. Mg/Ca, Sr/Ca, and other trace elements

5.1. Mg/Ca paleothermometry technique

Over the past decades, Mg/Ca paleothermometry has developed to a widely used tool in paleoceanography. Mg/Ca ratios of carbonate shells show a species-specific exponential dependence on temperature at which the carbonate is secreted. The temperature controls both the inorganic distribution coefficient and the physiologic processes that affect the uptake of Mg into the calcite test (Nürnberg et al., 1995; Rosenthal et al., 1997). The incorporation of Mg into carbonate shells of various (planktic and benthic) foraminifera, ostracod, corals, and bivalve taxa has been calibrated against modern temperatures, though there is still a lack of calibrations for several species (e.g., Dwyer et al., 1995; Nürnberg et al., 1996; Elderfield et al., 2006; Regenberg et al., 2009).

The Mg/Ca paleothermometry method provides the advantage of direct quantitative estimate of BWT. Also, it is important that Mg/Ca ratios are measured on the same foraminiferal species as paired oxygen isotope analyses, which is a necessary condition to make reliable reconstructions of $\delta^{18}O_{seawater}$, salinity, and density (e.g., Cacho et al., 2006 for Late Quaternary Mediterranean deep water estimates). The Mg/Ca ratio in seawater is spatially constant and hardly changes on timescales of less than 1 Million years due to very long residence times of Mg and Ca (Broeker and Peng, 1982). Accordingly, in our study (~ 3,6–2.58 Ma) we decided not to correct for hypothetical changes in the Mg/Ca ratio in seawater. The uncertainty of the method is modest (*e.g.*, ± 1°C; Lear et al., 2000). The evidence of dissolution effects on Mg/Ca content of (epi-) benthic shells is less certain compared to planktic foraminifera (*cf.* Lea, 2003). In the northeast Atlantic, Sites 548 and 982 are located above the foraminiferal lysocline (cf. Berger and Winterer, 1974) and the dissolution appears without an effect on Mg/Ca ratios. Likewise, in the western Mediterranean this bias is minimized by selecting the Site 978 that has a well-preserved calcite. Results from Cacho et al. (2006) from a core near Site 978 in the Alboran Sea (1841 m w.d.) showed no effect of dissolution on Mg/Ca in epibenthic foraminifera. Also, in ocean basins marked by low biological productivity, such as the Mediterranean Sea, the Calcium Carbonate Compensation Depth (CCD) (and the overlying lysocline layer) is located at deep water depths (Berger and Winterer, 1974).

Several caveats and secondary factors may affect Mg incorporation into foraminiferal tests and the resulting temperature estimates. First, multi-species calibrations of Mg/Ca vs. temperature

may result in a reduced accuracy of temperature estimates based on a single species. Moreover, high salinity values (Nürnberg et al., 1996; Groeneveld et al., 2008; Ferguson et al., 2008), pH (Lea et al., 1999; Russel et al., 2004), carbonate ion concentration (Russel et al., 2004), and carbonate ion saturation state (Rosenthal et al., 2006; Elderfield et al., 2006; Yu and Elderfield 2008) may exert an important role in controlling the incorporation of Mg during shell growth in addition to the temperature factor. Elderfield et al. (2006) argued that the greater response of Mg/Ca in benthic foraminifers to temperatures below 3°C (Martin et al., 2002) may be explained by to the effect of low carbonate ion saturation ($\Delta[CO_3^{2-}]$) in cold bottom waters on the uptake of Mg (see discussion in section 6.1). Results raised the validity of benthic Mg/Ca for use on the coldest bottom waters ("cold-end problem").

5.2. Cleaning protocol

Our preparation of foraminifera samples for Mg/Ca, Sr/Ca, and trace metal element analyses followed the methods described by Martin and Lea (2002; modified from Boyle, 1981; Fig. 3.4). Cleaning methods can include or not a reductive cleaning step. In this study, we decided to clean samples with a reduction step to get rid of possible Mn-carbonate that might be enriched in magnesium, moreover to be sure to eliminate any contaminants. Mg values derived by cleaning steps of oxidation plus reduction of benthic foraminifera amount to values that are almost 0.2 mmol mol^{-1} lower than values deduced from an oxidation step only (Elderfield et al., 2006). This comes close to a 10–15% difference found for planktic foraminifera (Barker et al., 2003; Rosenthal et al., 2004).

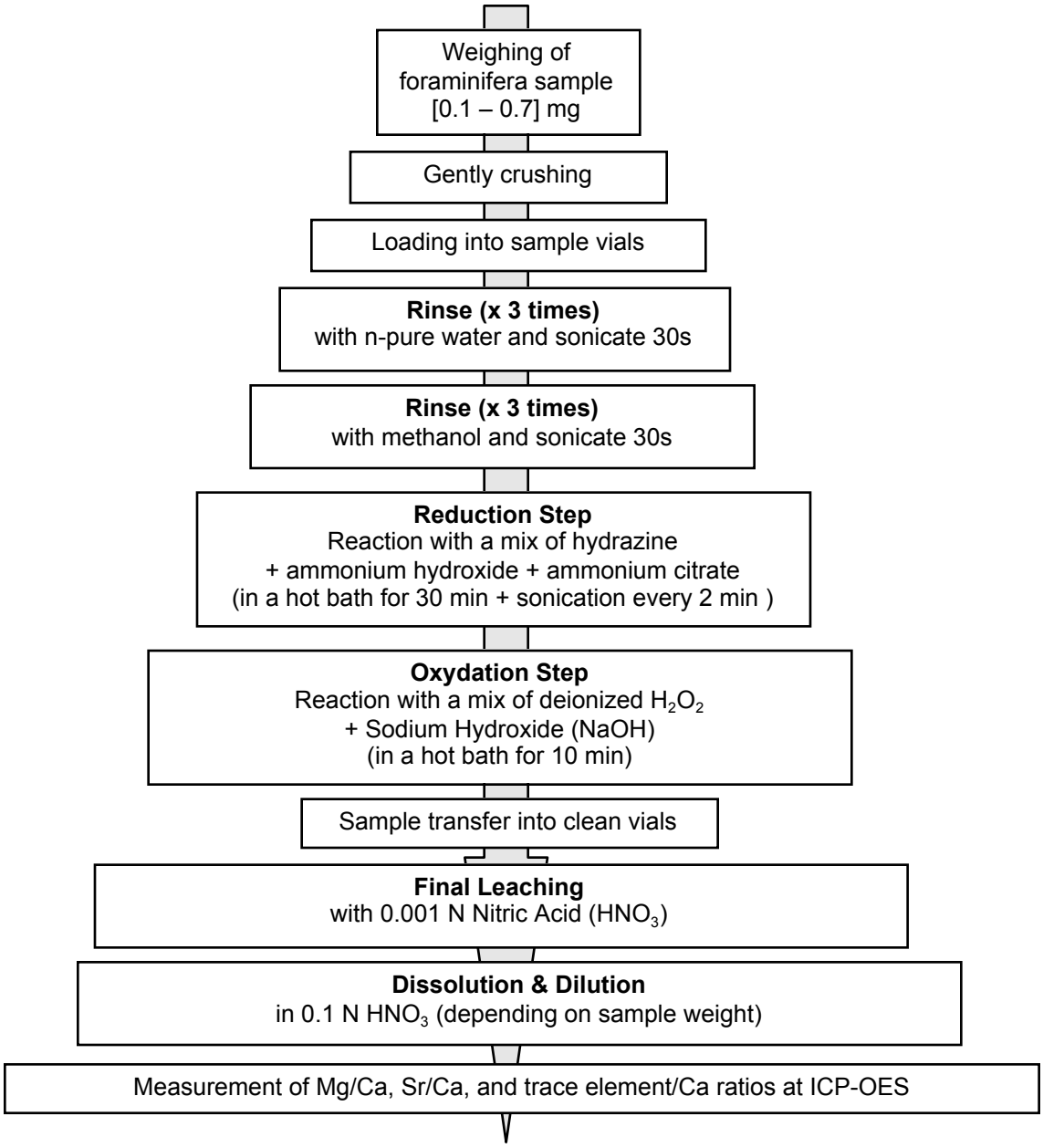

Fig. 3.4. Procedure of the cleaning protocol prior to Mg/Ca, Sr/Ca, and trace element/Ca analysis according to Martin and Lea (2002).

5.3. Analysis with ICP-OES

Mg/Ca values were measured simultaneously on an inductively coupled plasma–optical emission spectrometer (ICP–OES) at the Institute of Geosciences, University of Kiel. The use of simultaneous ICP–OES improved significantly the analytical quality by allowing simultaneous measurements of a series of elements. For example, the Ar concentrations indicate the stability of the machine. Also, elements such as Sr, Fe, Al, and Mn were used to monitor the degree of contamination in each measured sample, following Schmidt et al. (2004), as contaminants may persist even after careful cleaning.

The intensity ratio calibration followed the method of de Villiers et al. (2002). The analytical precision of Mg/Ca ratios was better than 0.1–0.2% relative to a standard deviation (RSD), equivalent to ±0.02°C. The standard deviation of repeated analyses of the same sample over different days amounts to 0.12 mmol mol^{-1}, equivalent to a temperature uncertainty of ±0.6°C.

To ensure the compatibility of Mg/Ca paleothermometry amongst different laboratories, a first intercomparison study of Rosenthal et al. (2004) showed that the reproducibility, an indicator of interlaboratory method precision, between 13 laboratories worldwide measuring the same sample material was significantly worse than ~8% RSD, which translates into a Mg/Ca-based temperature reproducibility of ± 2–3°C. This variability range is larger than the difference between the Last Glacial Maximum and the Holocene. Thus the authors at that time suggested the need of introducing a generally agreed solid standard to be employed by all laboratories such as the PDP-standard for stable isotope analyses.

A certified limestone reference material (ECRM 752-1) was first presented by Greaves et al. (2005) as consistent standard solution to be used within and between laboratories. However, liquid standard solutions may not retain their initial composition over the time of measurement. Based on new solid consistent standard material, it became recently possible to perform an interlaboratory comparison amongst 25 laboratories including Kiel laboratory (Greaves et al., 2008). Results show that solid standards are suitable as reference materials for determinations of foraminiferal Mg/Ca. However, the repeatability an indicator of interlaboratory precision, increased with a decrease in Mg/Ca ratio from 0.78% at Mg/Ca of 5.56 mmol mol^{-1} to 1.15% at Mg/Ca of 0.79 mmol mol^{-1}. Also, the interlaboratory reproducibility for Mg/Ca determinations was significantly worse than the repeatability (4.5%–8.7%). In summary, the interlaboratory variability appears dominated by inconsistencies among instrument calibrations and a need for

improved interlaboratory compatibility. This caveats applies particularly to temperatures deduced from low Mg/Ca ratios of benthic and cold-water foraminifers (“cold-end problem”).

5.4. Temperature calibration of Mg/Ca ratios

SST estimates from Mg/Ca obtained from *N. atlantica (s)* at Site 982 were based on the multispecies calibration equation developed by Anand et al. (2003), which presumably also applies to extinct species. For comparison, the most recent multispecies calibration equation developed by Regenberg et al. (2009) produced nearly equal temperature estimates (Equations 1 and 2).

$$\mathbf{Mg/Ca = 0.38 \exp^{[0.09 \times SST]}} \text{ (Anand et al., 2003) (Eq. 1)}$$

$$\mathbf{Mg/Ca = 0.29 \exp^{[0.101 \times SST]}} \text{ (Regenberg et al., 2009) (Eq. 2)}$$

Calibrations established for the epibenthic genus *Cibicidoides* revealed linear, yet mainly empirical exponential relationships between Mg/Ca and temperature (e.g., Lear et al., 2002; Elderfield et al., 2006). Many of the calibrations used are based on data of several species, which may increase the uncertainties of temperature estimates.

Since there is no regional single-species calibration neither for *C. wuellerstorfi* nor for *C. mundulus* in the westernmost Mediterranean Sea and the Northeast Atlantic at water depths of MOW, BWT estimates were deduced using the global Mg/Ca-temperature calibration defined for common *Cibicidoides* species in a temperature range below 5°C (Equation 3; Elderfield et al., 2006).

$$\mathbf{Mg/Ca = 0.9 \exp^{[0.11 \times BWT]}} \text{ (Eq. 3)}$$

The temperature sensitivity of this calibration is similar to that previously derived by Lear et al. (2002), which was also defined for *Cibicidoides* species *sensu lato* in a temperature range extending up to 18°C. We preferred not to use the calibration of Lear et al. (2002) because it relies mainly on *Cibicidoides* Mg/Ca data from the Little Bahama banks that may be elevated because of secondary high-Mg calcite overgrowths (*see* Elderfield et al., 2006; Sosdian and Rosenthal, 2009).

5.5. Derivation of bottom-water salinity and density estimates

Using the Mg/Ca-based BWT and benthic $\delta^{18}O$, we calculate the $\delta^{18}O_{water}$ signal by solving equation 4:

$$\mathbf{T = 16.9 - 4.0\ (\delta^{18}O - \delta^{18}O_{water})}\ \text{(Shackleton et al., 1974)}\ \text{(Eq. 4)}$$

$\delta^{18}O_{water}$ values (vs. PDB) are converted to SMOW (Standard Mean Ocean Water) values by adding 0.27‰. To extract the signal of BW salinity, we deduce from $\delta^{18}O_{water}$ record the global ice volume effect by employing the variability of the LR04 benthic $\delta^{18}O$, assuming that the latter record is mainly representing Pliocene changes in ice volume and hardly variations in BWT. Assuming that the present overall slope between BWS and $\delta^{18}O_{water}$ (~0.6‰ ≈ 1 psu; Craig and Gordon, 1965) is valid for the Pliocene, we may determine a BWS signal. The latter is converted into bottom-water density record following Fofonoff and Millard (1983). Due to large uncertainty ranges, our discussion was only based on the major and long-term trends in the bottom-water density record. A flow chart of density proxy techniques is presented in Fig. 3.5.

Fig. 3.5. Flow chart of density proxy techniques

(1) Global ice-volume variations for the Plio-Pleistocene are deduced from the LR04 benthic $\delta^{18}O$ stack of Lisiecki and Raymo (2005), assuming that this record is mainly controlled by sea levels changes. Modern $\delta^{18}O$ of 3.25‰ corresponds to 0 m in sea level. Past sea level estimates were determined from the difference from the modern level.

(2) After correction for the global ice effect, local $\delta^{18}O_{water}$ is assumed to be directly linked to local bottom water salinity. However, this relationship [BWS:$\delta^{18}O_{water}$] is highly regional and most likely dependent on seasonal changes in Mediterranean latitudes. In the northeast Atlantic we decided to use the equation (5) of Craig and Gordon (1965) for Atlantic bottom water:

$$\mathbf{Salinity = (\delta^{18}O_{water} + 20.68) / 0.59}\ \text{(Eq. 5)}$$

When applying the outlined approach for the West Mediterranean, our salinity estimates come very close to those calculated from the equation (6) of Cacho et al. (2006) established for the West Mediterranean Deep Water (WMDW):

$$\mathbf{Salinity = (\delta^{18}O_{water} + 17.37) / 0.48}\ \text{(Eq. 6)}$$

(3) Modern BWS in the WMDW are near 38.5 psu at Site 978. In the northeast Atlantic modern BWS are near 35.6 psu at S. 548 and near 35 psu at S. 982.

→

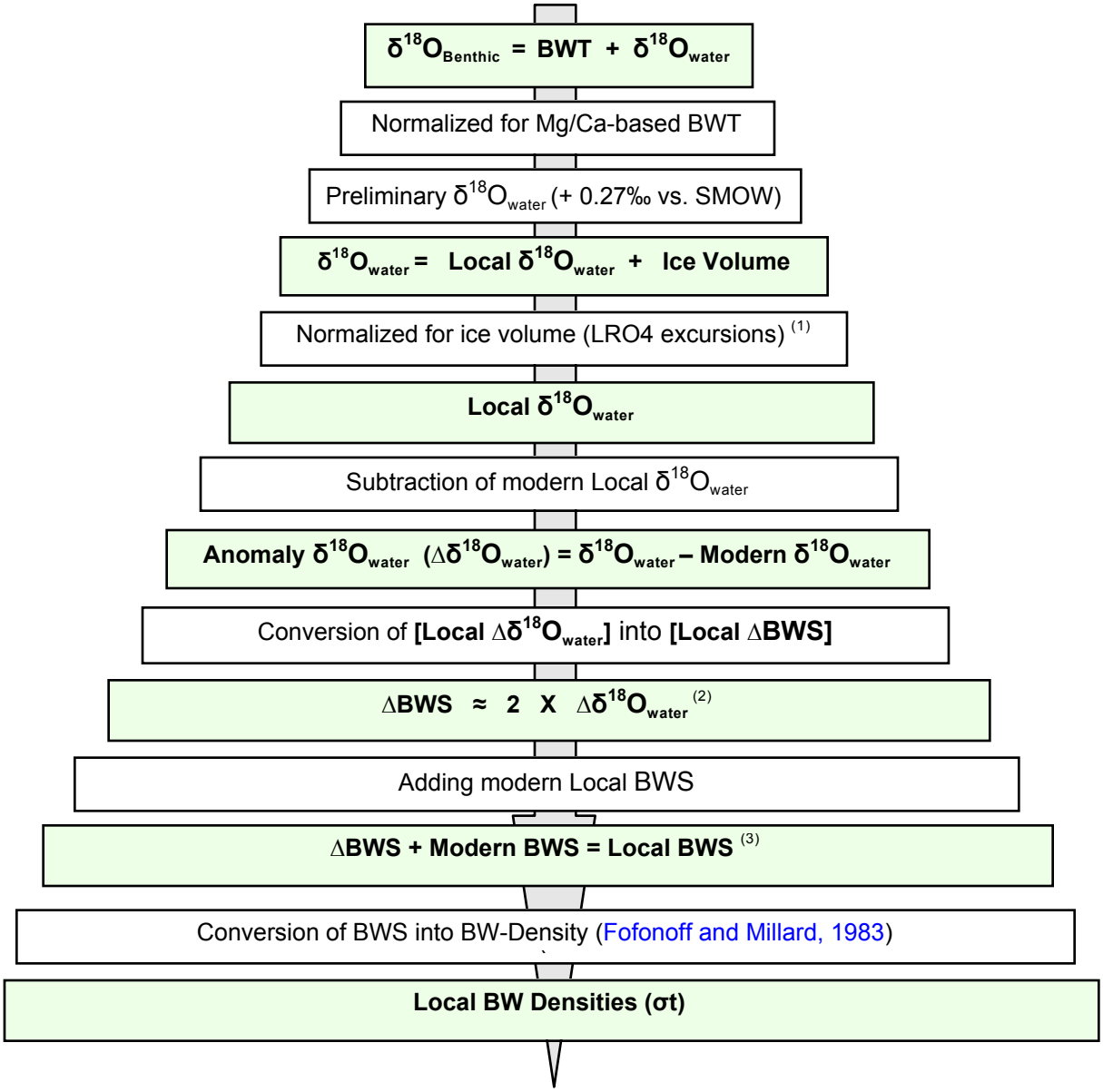
$\delta^{18}O_{Benthic}$ = BWT + $\delta^{18}O_{water}$
Normalized for Mg/Ca-based BWT
Preliminary $\delta^{18}O_{water}$ (+ 0.27‰ vs. SMOW)
$\delta^{18}O_{water}$ = Local $\delta^{18}O_{water}$ + Ice Volume
Normalized for ice volume (LRO4 excursions) (1)
Local $\delta^{18}O_{water}$
Subtraction of modern Local $\delta^{18}O_{water}$
Anomaly $\delta^{18}O_{water}$ ($\Delta\delta^{18}O_{water}$) = $\delta^{18}O_{water}$ – Modern $\delta^{18}O_{water}$
Conversion of [Local $\Delta\delta^{18}O_{water}$] into [Local ΔBWS]
ΔBWS ≈ 2 X $\Delta\delta^{18}O_{water}$ (2)
Adding modern Local BWS
ΔBWS + Modern BWS = Local BWS (3)
Conversion of BWS into BW-Density (Fofonoff and Millard, 1983)
Local BW Densities (σt)

6. Analyses of Alkenones

6.1. Alkenones-paleothermometry technique – an overview

To study Upper Pliocene changes in the hydrological cycle in the western Mediterranean Sea, we need sea surface temperature and salinity records. Alkenones were measured on 182 ocean sediment samples retrieved from Site 978-A every 30–40 cm over the interval studied to reconstruct SST. Estimates of $\delta^{18}O$ sea-surface water were based on the equation of Bemis et al. (1998) after deducing the effect of SST from Planktic $\delta^{18}O$ record. $\delta^{18}O_{surface\text{-}water}$ signal was not converted to surface salinity changes because of the absence of a reliable equation for the Alboran Sea. $\delta^{18}O_{surface\text{-}water}$ reflects mainly changes in the freshwater budget of the westernmost Mediterranean and to a limited extent Atlantic inflow $\delta^{18}O_{surface\text{-}water}$ signal. Changes in $\delta^{18}O_{sw}$ signal were interpreted directly as mainly linked to local variability in surface salinities.

The alkenone unsaturation index ($U^{k'}_{37}$) is strongly correlated to annual average SST in the modern Ocean (Brassell and Eglinton 1984; Brassell et al., 1986; Prahl et al., 1988) and has been increasingly calibrated from modern ocean surface sediments (Prahl and Wakeham, 1987; Sikes et al., 1991; Müller et al., 1998; Conte et al., 2006).

$$U^{k'}_{37} = C_{37:2} / (C_{37:2} + C_{37:3}) \quad \text{(Eq. 7)}$$

The $U^{k'}_{37}$ index utilizes long-chain ketones identified in several species of Prymnesiophyceae, in particular the ubiquitous marine coccolithophorid *Emiliania huxleyi* (Volkman et al., 1980) are useful for paleotemperature reconstruction (Marlow et al., 1990; Brassell, 1993; Conte et al., 2006). However, the application of calibration obtained from *E. huxleyi* for example could be problematic for the Pliocene since these unicellular haptophytes first occurred about 0.27 Ma ago. While some precaution remains when discussing the absolute values of alkenone-based SST, the applicability of alkenones to estimate Pliocene SST is to some extent valid. Indeed, the co-occurrence of alkenone synthesis similar to today and *E. huxleyi* ancestors in ocean sediments since the Eocene (Marlowe et al., 1990) may indicate that the production was performed by these predecessors in a same manner as today. Moreover, it has been argued that the relationship between $U^{k'}_{37}$ and C_{38} methyl ketone indexes for the Pliocene is the same to that of Late Pleistocene (Herbert et al., 1998). However, the alkenones may experience some

biochemical evolution and diagenesis (Prahl et al., 1989; Freeman and Wakeham, 1992; Rosell-Melé et al., 1995a).

Today, alkenone peaks in the western Mediterranean are associated with low SST (~14°C) during the spring and with warmer SST (~18–21°C) during the fall. Major production depths are 50 and 30 m w. d., respectively. Coccolithophorid production is seasonal and the water depth variable, however, systematically similar in both seasons (Sicre et al., 1999).

6.2. Analytical technique

Alkenones were extracted in Kiel lab with the help of a technician. Alkenones were analyzed at a multidimensional double column gas chromatograph system (MDGC). Sample and standard replicates show a temperature uncertainty of ±0.3°C. The procedure of alkenone extraction is summarized in Fig. 3.6.

6.3. Alkenone-SST calibration

Generally, estimating of SST derives from the original publication of Prahl and Wakeham (1987) and revised by Prahl et al. (1988). In this study, the global field-based calibration of Conte et al. (2006), which includes the Mediterranean data set from Ternois et al. (1997) was used.

$$\mathbf{SST = -0.957 + 54.293\,(U^{k'}_{37}) - 52.894\,(U^{k'}_{37})^2 + 28.321\,(U^{k'}_{37})^3} \quad \text{(Eq. 8)}$$

Mean standard error of estimation using this equation is ±1.2°C. The equation covers a large SST range (-1 to 30 °C) and seems therefore suitable for high Pliocene SST in the Mediterranean Sea.

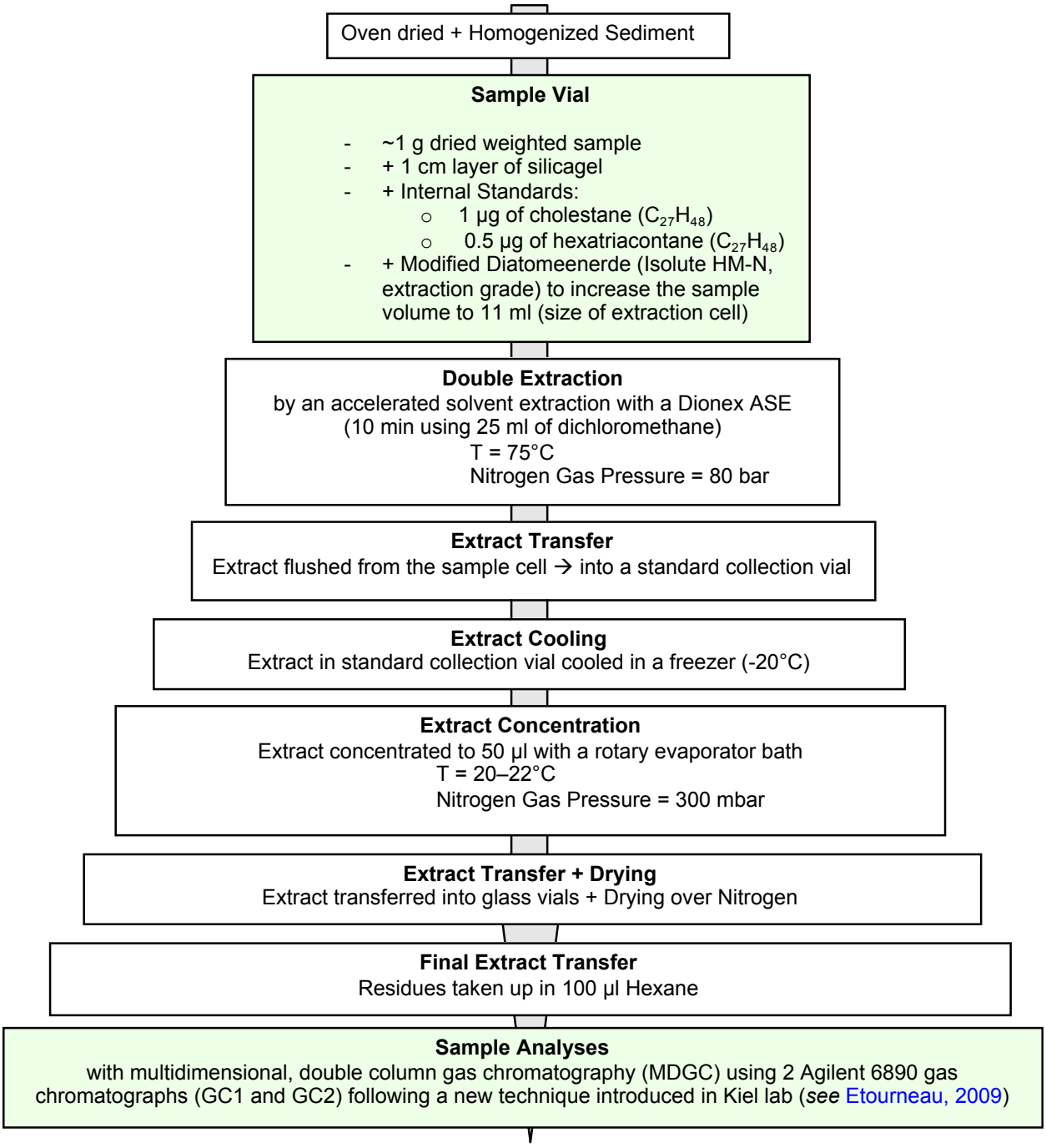

Fig. 3.6. Procedure of Alkenone extraction prior to measurement at multidimensional, double column gas chromatography (MDGC)

7. Summary of methods

Methods used in this study are summarized in Table 3.2.

MOW proxies	Parameters used
Origin of bottom water	ε_{Nd}
Sea surface temperature	$U^{k'}_{37}$ + Mg/Ca
Bottom water temperature	Mg/Ca (*C. wuellerstorfi* + *C. mundulus*)
Bottom water salinity ($\delta^{18}O_w$)	Mg/Ca + $\delta^{18}O$ (epibenthic)
Bottom water density	Mg/Ca + $\delta^{18}O_w$ (epibenthic)
Bottom water ventilation	$\delta^{13}C$ (epibenthic)
Age scale	Geomagnetic reversals + $\delta^{18}O$ records tuned to LRO4

Table 3.2. MOW Proxies versus Parameters used

Chapter 4
Age Models

1. Age control at western Mediterranean Site 978

The Site 978 age model for the Upper Pliocene (3.62 – 2.72 Ma ago) integrates evidence from biostratigraphy, magnetostratigraphy (ODP Leg 161, Shipboard Scientific Party, 1996a), and from tuning orbital precession-scale oscillations of the planktic $\delta^{18}O$ record to the LR04 record (Lisiecki and Raymo, 2005; Fig. 4.1b). The epibenthic $\delta^{18}O$ record was not used for defining an age model for Site 978 (Hole A) because it does not reflect the signal of global ice volume oscillations but derives its signature from regional, yet unexplained changes in local bottom water salinity and temperature in the Mediterranean Sea.

Three biostratigraphic datums (ODP Leg 161, Shipboard Scientific Party, 1996a) were identified for the interval 3.62 – 2.72 Ma ago: (1) The Last common Occurrence Datum (LOD) of *D. tamalis* was identified at 372.70 mbsf and provides an age of 2.78 Ma, coeval with marine oxygen isotope stage (MIS) G9, which represents the top of the sequence investigated. (2) The LOD of *Sphaeroidinellopsis* spp. led to an identification of MIS KM6 (3.22 Ma) at 398.69 mbsf. (3) LOD of *G. puncticulata* was found at 436.76 Ma and provides an age of 3.57 Ma (MIS MG11).

Based on magnetostratigraphy, we identified both the top (3.22 Ma ago) and base (3.33 Ma ago) of the Mammoth subschron at 400.7 mbsf and 408.4 mbsf, respectively. The Gauss/Gilbert boundary (~3.58 Ma ago) and the associated MIS MG11 / MG12 boundary were identified at 436 mbsf (Fig. 4.1b).

On the basis of these age control points we tuned the planktic $\delta^{18}O$ record of Hole 978A to the LRO4 (Lisiecki and Raymo, 2005) reference record by graphical correlation of peaks and stage boundaries, using the *AnalySeries 2.0.3* software (Paillard et al., 1996; Fig. 4.1b). The planktic $\delta^{18}O$ record shows an overall $\delta^{18}O$ increase from MIS Gi1 (~3.6 Ma ago) to MIS G5 (~3.4 Ma ago). Subsequently, isotope stages oscillated around a constant average of -0.25‰ vs. PDB. In contrast, the LRO4 global record shows overall an $\delta^{18}O$ increase only much later, starting from MIS G17 (~2.95 Ma ago) / MIS G10 (2.82 Ma ago).

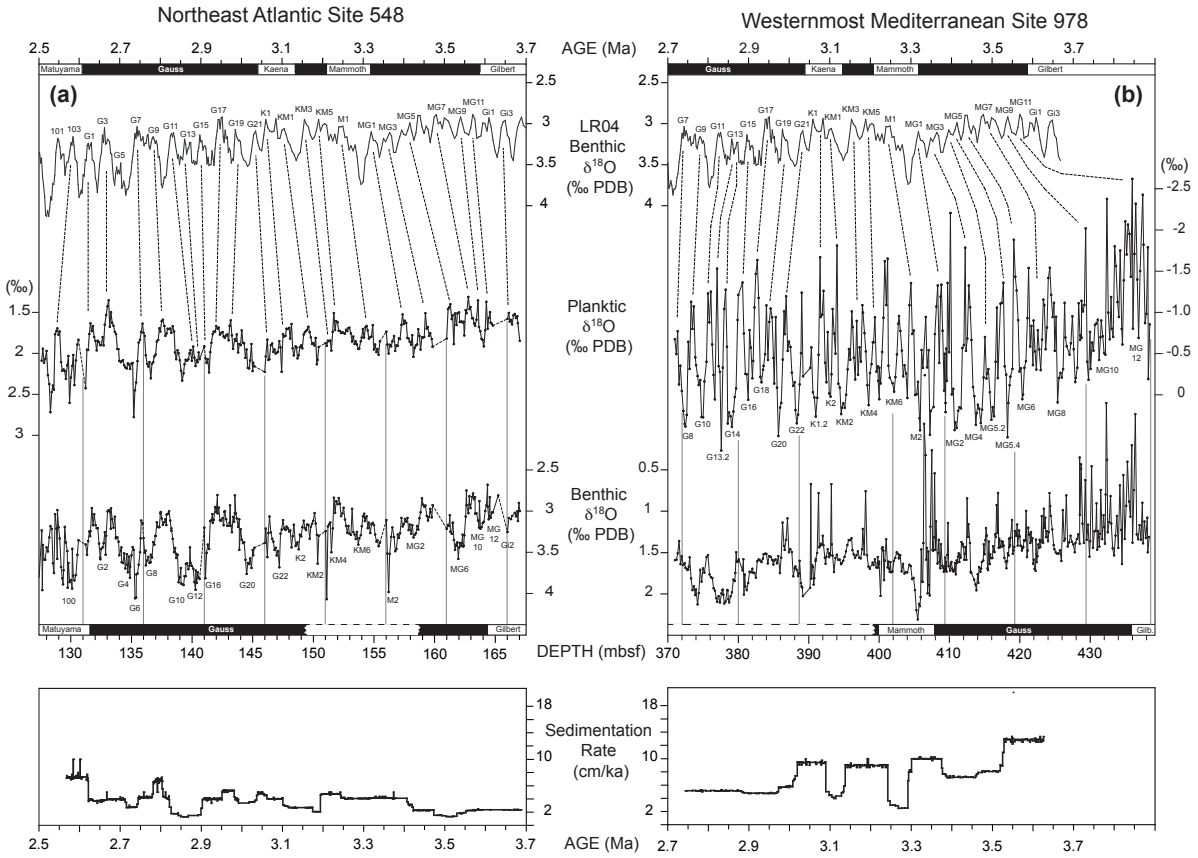

Figure 4.1. Age control and sedimentation rates for Deep Sea Drilling Project (DSDP) Site 548 (A) and Ocean Drilling Program (ODP) Site 978 (B). Isotopic stages are labeled and tuned (with hatched lines) to benthic $\delta^{18}O$ stack LR04 (Lisiecki and Raymo, 2005). Age ranges of magnetic stratigraphy are plotted for comparison. For Site 548, no magnetic polarity reversals were defined between 158.58 and 149.32 mbsf (Graciansky et al., 1985), likewise for Site 978 between 400 and 370 mbsf (Shipboard Scientific Party, 1996a). Vertical solid lines mark potential losses of sediment sections at core breaks.

Planktic $\delta^{18}O$ oscillations between cold and warm marine isotope stages had amplitudes of 1.5 – 2.0‰. Of course these stages can hardly be compared as structures with the common features of the benthic LRO4 stack because the planktic oscillations integrate the effect of SST and SSS changes in addition to the global ice volume effect. As in the LRO4 signal, a bipartite feature marks MIS G13; likewise MIS K1 is split into two substages; MIS KM5 shows a more distinct bipartite feature than in LRO4. A twofold excursion in both the planktic and benthic δ18O

records also marks the prominent cold MIS M2, a record that is difficult to correlate. Probably the second excursion already belongs to MIS M2 (Fig. 4.1b).

The suite of marine isotope stages MG12 – MG9 (~3.58 – 3.54 Ma ago) shows pronounced negative excursions both in the planktic and benthic $\delta^{18}O$ records during interglacial stages, a result of low SSS as discussion further below (see Chapter 6). Near to the Gauss/Gilbert boundary (~3.58 Ma ago) the isotope signal varied highly in amplitude; thus the identification of MIS Gi1 is not clear.

In total, the age model for Hole 978A covers an interval from 3.627 to 2.729 Ma, resulting in sedimentation rates of 5.1–12.7 cm/1000 years and sampling intervals of 1000–1500 to 2500 years, occasionally of 4000–8000 years (Fig. 4.1). At some core breaks, the time resolution deteriorates up to 10,000–12,500 years (e.g., between 389.18–390.2 mcd and 380–380.6 mcd).

2. Age control at northeast Atlantic Site 548

The Site 548 age model for the Upper Pliocene (3.65 – 2.57 Ma ago) likewise integrates evidence from (1) shipboard biostratigraphy (DSDP Leg 80, Müller, 1985), (2) magnetostratigraphy of DSDP Leg 80 (Graciansky et al., 1985), and (3) the planktic and benthic $\delta^{18}O$ records obtained from Hole 548 (Fig. 4.1a).

The biostratigraphy is based on the last appearance datums (LAD) of the calcareous nannofossils *Discoaster pentaradiatus* and *D. surculus*, which occur at 136.1–133 mbsf. This extinction event is related to the onset of the first culmination of major Northern Hemisphere Glaciation (Berggren, 1972) at the end of MIS G7 (~2.74 Ma). In addition, the LOD of the planktic foraminifera *Globorotalia margaritae* at 164.95 mbsf marks the end of the lower Pliocene (Mazzei et al., 1979) and the base of Gauss Chron (MIS MG12, ~3.58 Ma).

The biostratigraphic age control at Hole 548 was supplemented by the geomagnetic reversal stratigraphy (Townsend, 1985). It shows the top (2.608 Ma ago) and base of the Gauss Chron (3.588 Ma ago) at 132.8–131.6 and 165.7–164.2 mbsf, respectively, by a sequence of 7 cores with positive magnetic inclination. This normal-polarity interval does not show any reversal that might indicate the negative Kaena subchron. Possibly, the coring break and distinct gap near 156 mbsf that may hide the short-lasting polarity reversal of the Mammoth subchron.

Such as at Site 978, orbital-scale stratigraphy was obtained from tuning the largely parallel oscillations of planktic, and in particular benthic $\delta^{18}O$ records of Site 548 to the LR04 benthic $\delta^{18}O$ stack and timescale of Lisiecki and Raymo (2005). However, the benthic $\delta^{18}O$ signal is still partly uncommon because of the admixture of MOW, which does not contain the signal of the global $\delta^{18}O_{ice\text{-}effect}$ (Fig. 4.1a). MIS 104 was placed at the Gauss/Matuyama boundary near 131.6 mbsf. However, different from LR04 MIS 104 is bipartite in the Site 548 planktic $\delta^{18}O$ record, a feature that is also found in the Site 982 benthic $\delta^{18}O$ record (see section 3). On the other hand, the duplicity may simply result from a duplication of sediment sections in core sections immediately above and below a core break at 131 mbsf. Subsequent to MIS 104, stages 103 to 101 were only identified in the planktic $\delta^{18}O$ record, whereas the benthic record is dominated by noise (Fig. 4.1a).

Prior to MIS 104, structures and amplitudes in both planktic and benthic $\delta^{18}O$ records largely resemble MIS stages G1 to G10 as shown by the standard LR04 record, except for an uncommonly positive $\delta^{18}O$ excursion for glacial MIS G8. Interglacial MIS G11 and G13 appear

far “colder” than suggested by LRO4, likewise glacial MIS G12, which is almost as $\delta^{18}O$ positive as MIS 10 in the benthic record. Parts of MIS G13 to G15 were lost in a 27-cm hiatus at a core break near 141 mbsf. The suite of benthic and planktic MIS G16 to G20 differs slightly from LRO4, in particular with cold MIS G18 being hardly preserved. MIS G20 is the best-defined structure in the benthic $\delta^{18}O$ record. Here almost 85 cm were skipped from sampling near a core break at 146 mbsf, because of a soupy sediment structure due to drilling disturbance. It appears likely that significant parts of lower MIS G20 and G21 were not preserved in our $\delta^{18}O$ records. MIS G22 appears “colder” than to be expected from the LRO4 signal. With the absence of magnetostratigraphy, it was difficult to define the marine stages of the Kaena subchron. MIS K2 is clearly displayed, likewise the bipartite MIS K1 in the benthic record. MIS KM1 is well defined in both $\delta^{18}O$ records. However, KM2 and part of KM3 were lost in a coring-gap hiatus near 151 mbsf. MIS KM3 and KM4 are poorly represented by amplitude. The planktic $\delta^{18}O$ record clearly shows the suite of stages KM5, KM6, and M1, in particular the typical “stair” step structure subsequent to MIS M2.

A core break below MIS M1 at 156 mbsf resulted in a sediment loss of ~50 cm and a disturbance in the sample section added a further 25-cm of sediment loss (Shipboard Scientific Party, 1985). Accordingly, it was difficult to find a clear record of the pronounced cold MIS M2. Prior to MIS M2, the planktic $\delta^{18}O$ record of stages MG1, MG2, and MG3 resembles closely the coeval section in LRO4. Between 161 and 159.84 mbsf, the sediment record of Hole 548 suffered from a further drilling hiatus, where parts of MIS MG4 and MG5 were lost. Right below the gap we find the distinct positive excursion characteristic for MIS MG6, where the benthic $\delta^{18}O$ amplitude comes close to that of “cold” MIS G20 and clearly exceeds that in LRO4, a feature not seen in the planktic $\delta^{18}O$ record. Accordingly, the extreme excursion of benthic $\delta^{18}O$ may result from a decrease in bottom water temperature of MOW or more likely, an increase in bottom-water salinity during MIS MG6. Further downcore, MIS MG7 to MG11 clearly identified per analogy to LRO4, except for an intensive MIS MG10 reflected in both planktic and benthic $\delta^{18}O$ records. A sharp negative excursion of the magnetic inclination indicates the location of the Gauss/Gilbert boundary at ~167 mbsf, between MIS MG12 (~3.59 Ma ago) and Gi1 (~3.60 Ma ago). A major part of MIS Gi2 (~3.62 Ma ago) was lost in a coring gap near 166 mbsf.

On the basis of these stratigraphic correlations, the resulting age model covers an interval from 3.65 to 2.57 Ma ago and results in sedimentation rates of 1.4–7.2 cm/1000 years (Fig. 4.1a) and sampling intervals of 700–3500 years. Single sampling intervals may increase up to 7,900 to 32,000 years at core breaks near MIS G20, M2, and Gi2, where minor sediment sections were probably lost.

3. Age control at northeast Atlantic Site 982

This Chapter section was written up in cooperation with M. Sarnthein

By now (several refs.), the age control at Site 982 for the Upper Pliocene (3.65 – 2.50 Ma ago) was based on both magnetic reversals in Hole A (Channell and Lehmann, 1999) and the epibenthic $\delta^{18}O$ record mostly obtained from Hole B (Venz et al., 1999; Venz and Hodell, 2002; tuned to LR04 by Lisiecki and Raymo, 2005; Fig. 4.2).

The positive magnetic polarity of the upper Gauss Chron (2An) is resolved at Site 982 by a well-defined section with positive inclination, ending with a sharp decrease in magnetic polarity at 57.03 mcd in Hole A (Fig. 4.2). However, the position of this Gauss/Matuyama boundary (~2.608 Ma ago in LR04) is not located at the same composite depths in the three holes A, B, and C drilled in parallel at Site 982. In Hole A the top of Gauss is located close to 57.23 mcd (50.70 mbsf), a depth previously employed by all authors for calibrating MIS stratigraphy since Venz and Hodell (2002). In contrast, Hole B shows the boundary (midpoint of reversal) almost 1 meter deeper, at 58.06 mcd (52.55 mbsf), a discrepancy that we took care of in this study, in part by measuring additional $\delta^{18}O$ record over a short crucial core section in Hole B between 57.51 and 59.67 mcd (Fig. 4.2). However, there are a number of subsequent short-term positive oscillations in magnetic polarity up to 54.81 mcd, as yet unexplained, excursions that we lump with the Matuyama chron in harmony with Channell and Lehmann (1999) (Fig. 4.2).

Figure 4.2. Age control for Ocean Drilling Program (ODP) Site 982. (A) Magnetic polarity reversals are from Shipboard inclination data for Holes A (green) and B (red) (Channell and Lehman, 1999). M/G = Matuyama/Gauss. (B) Isotopic stages are labeled and tuned (hatched lines) to benthic $\delta^{18}O$ stack LR04 (C) (Lisiecki and Raymo, 2005). (D) Age model of Shipboard Scientific Party (as cited by Lawrence et al., 2009) is displayed for comparison. Vertical brownish bars mark potential losses of sediment sections at core breaks in Hole B. Note particular discrepancies between $\delta^{18}O$ records of Holes A, B, and C between 68 and 72 m c. d. (composite depth).

→

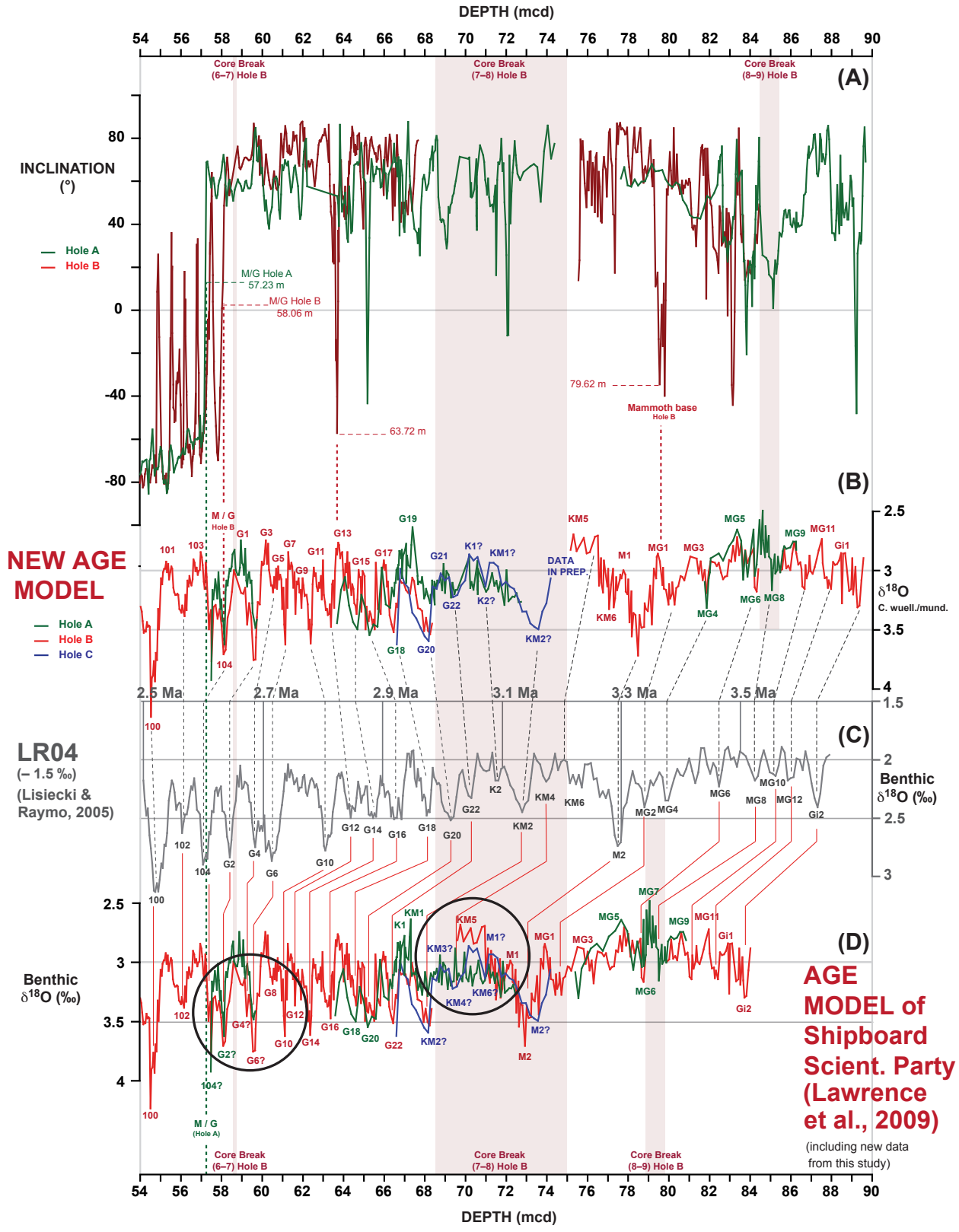
DEPTH (mcd)
54 56 58 60 62 64 66 68 70 72 74 76 78 80 82 84 86 88 90
Core Break (6–7) Hole B
Core Break (7–8) Hole B
Core Break (8–9) Hole B
(A)
INCLINATION (°)
80
40
0
-40
-80
Hole A
Hole B
M/G Hole A 57.23 m
M/G Hole B 58.06 m
63.72 m
79.62 m
Mammoth base Hole B
(B)
NEW AGE MODEL
Hole A
Hole B
Hole C
M / G Hole B
DATA IN PREP
2.5 Ma
2.7 Ma
2.9 Ma
3.1 Ma
3.3 Ma
3.5 Ma
δ18O C. wuell./mund.
2.5
3
3.5
4
(C)
LR04
(– 1.5 ‰)
(Lisiecki & Raymo, 2005)
Benthic δ18O (‰)
1.5
2
2.5
3
(D)
Benthic δ18O (‰)
2.5
3
3.5
4
M / G (Hole A)
AGE MODEL of Shipboard Scient. Party (Lawrence et al., 2009)
(including new data from this study)

The core fit between Holes A, B, and C is poorly established below 55 mcd, as it cannot rely on any oscillations in the magnetic susceptibility record, which dropped down to background levels (Shipboard Scientific Party, 1996b; Chapter 4–Fig. 2). Color reflectance below 50 mcd was only measured in holes A and B. The core fit was also based on gamma ray density (GRAPE). However, the GRAPE record is showing only minor oscillations, insufficient for any clear signal correlation. Moreover, the correlations between holes A and B don't appear unique (stringent).

In addition, our new benthic $\delta^{18}O$ data sets measured on holes A, B, and C from 63.67 to 74.19 mcd (see Table 4.1 in Appendices) don't confirm the present core fits proposed by the Shipboard Scientific Party (1996b) – shown in Fig. 4.2d using the old stratigraphy of Venz and Hodell (2002; tuned to LR04 by Lisiecki and Raymo, 2005). We need to suggest therefore several corrections of the spliced record that forms the composite depth section for Site 982. Based on a correction of numerous glacial/interglacial $\delta^{18}O$ oscillations, we now produced a series of new tie points between the cores in holes A, B, and C to construct a new splice. Also, there is a strange problem with different absolute $\delta^{18}O$ levels of the records in holes A, B, and C (66.37 – 69.47 m c.d.). Below 68.36 mcd a further correction of the composite depth was established by shifting core B-8 farther downcore by ~6.8 m (Fig. 4.2b). This shift resulted from a ~6.8-m coring gap in Hole B from 68.36 to ~75.2 mcd.

Because most of the published marine-isotope stratigraphy at Site 982 relies on the largely continuous benthic $\delta^{18}O$ record measured on sediments from Hole B (just with adding few short stratigraphic sections from holes A and C to bridge core breaks in Hole B), one needs to be consistent and to switch from the Hole-A to the Hole-B position of the magnetic reversal, that is to 58.06 mcd for defining the Gauss/Matuyama boundary and the associated MIS 104 (~2.608 Ma ago) in the same hole. Accordingly, Fig. 4.2 is showing the $\delta^{18}O$ records running in parallel for the sediment sections of holes A, B, and C. The new short sections of the $\delta^{18}O$ record now constrain the Hole-B core gaps as close as possible at 68.58–74.19 and 84.57–86.18 mcd.

As result, the Gauss/Matuyama boundary now clearly corresponds to MIS 104 (~2.608 Ma ago) as defined by Lisiecki and Raymo (2005). However, different from the LR04 record, MIS 104 appears to be bipartite, with a second cold stage in the upper part, a narrow structure likewise shown in the $\delta^{18}O$ records from holes A and B (and similar to the record of Site 548).

Subsequent to MIS 104, the suite of MIS 103–100 well reflects all details of amplitudes and structures as defined in LR04. The influence of MOW was obviously that weak that it did not change anymore significantly the benthic $\delta^{18}O$ signal.

Prior to MIS 104 (now defined according to Hole-B evidence; 58.06 mcd), stages G1 to G3 closely resemble the structures and amplitudes displayed in the LRO4 reference record, likewise the suite of MIS G4, G5, G6, G7, G8 and G9, except for the $\delta^{18}O$ excursion at glacial MIS G4, which is somewhat less positive than the LR04 signal (Fig. 4.3). The new tuning also results in an amplitude of G10, which clearly exceeds those of all preceding "cold" MIS, as suggested by LR04 (Fig. 4.2). The stage features in both records continue to be quite similar from MIS G11 (~2.83 Ma ago) back to G20 (~3.01 Ma ago). MIS G11 and in particular MIS G13 depict bipartite peaks as suggested by LR04, although G13 appears somewhat "warmer" than expected. Also, MIS G13 coincides with a well defined but short-lasting negative excursion in inclination within the Gauss Chron near 63.72 mcd (Fig. 4.2). However, this feature was not identified in holes A and C and not described in the standard polarity time scales of Lowrie and Alvarez (1981). Moreover, the amplitude of MIS G13 is higher ("warmer") than that of the bipartite MIS G17 (however a similar feature is seen at ODP Site 846; Tiedemann et al., 1994). The amplitude of MIS G19 in holes B and C is as high as to be expected from LR04, which is much lower than the amplitude of MIS G17, in contrast to Hole A, where the amplitude clearly exceeds that of LR04. Likewise, the broad and marked positive $\delta^{18}O$ excursion of MIS 20 in holes B and C is by far more distinct and thus comes much closer to that suggested in LR04 than the G20 excursion found in Hole A (Fig. 4.2). However, we do not understand yet the generally more negative $\delta^{18}O$ level in Hole A records, although the relative amplitudes of $\delta^{18}O$ excursions are largely the same in all three holes.

Prior to MIS G20, the coring gap at Hole B from 68.36 to 69.33 mcd (now expanded to ~75.2 mcd according to the ~6.8-m core-fit) was partly bridged by almost 40 epibenthic $\delta^{18}O$ data points from Hole A (Fig. 4.2). Its results do not show the proper amplitudes of MIS as postulated by LRO4. In particular, the amplitude of MIS G21 was not as high as to be expected from LRO4, where MIS G21 is as high as MIS G19. On the other hand, the bipartite feature characteristic of MIS K1 was clearly identified, whereas the succession of MIS K2, KM1, and KM2 was not well identified. However the new $\delta^{18}O$ record obtained finally from Hole C contains the "common" succession of MIS as reflected by LR04 from MIS G21 until KM2 and confirms the core fit between holes A and C (Fig. 4.2).

In summary, it appears that stages G21, G22, K1, K2, and from KM1 – KM4 were lost in the ~6.8-m gap of the core break between cores B7 and B8, and hence the composite depths need to be corrected accordingly. Further isotope analyses for data from Hole C are in progress in

order to identify stages KM3 and KM4 in the composite record and to establish the link to stages KM5 to MG1/MG2 in Hole B (Khélifi and Sarnthein, in prep.).

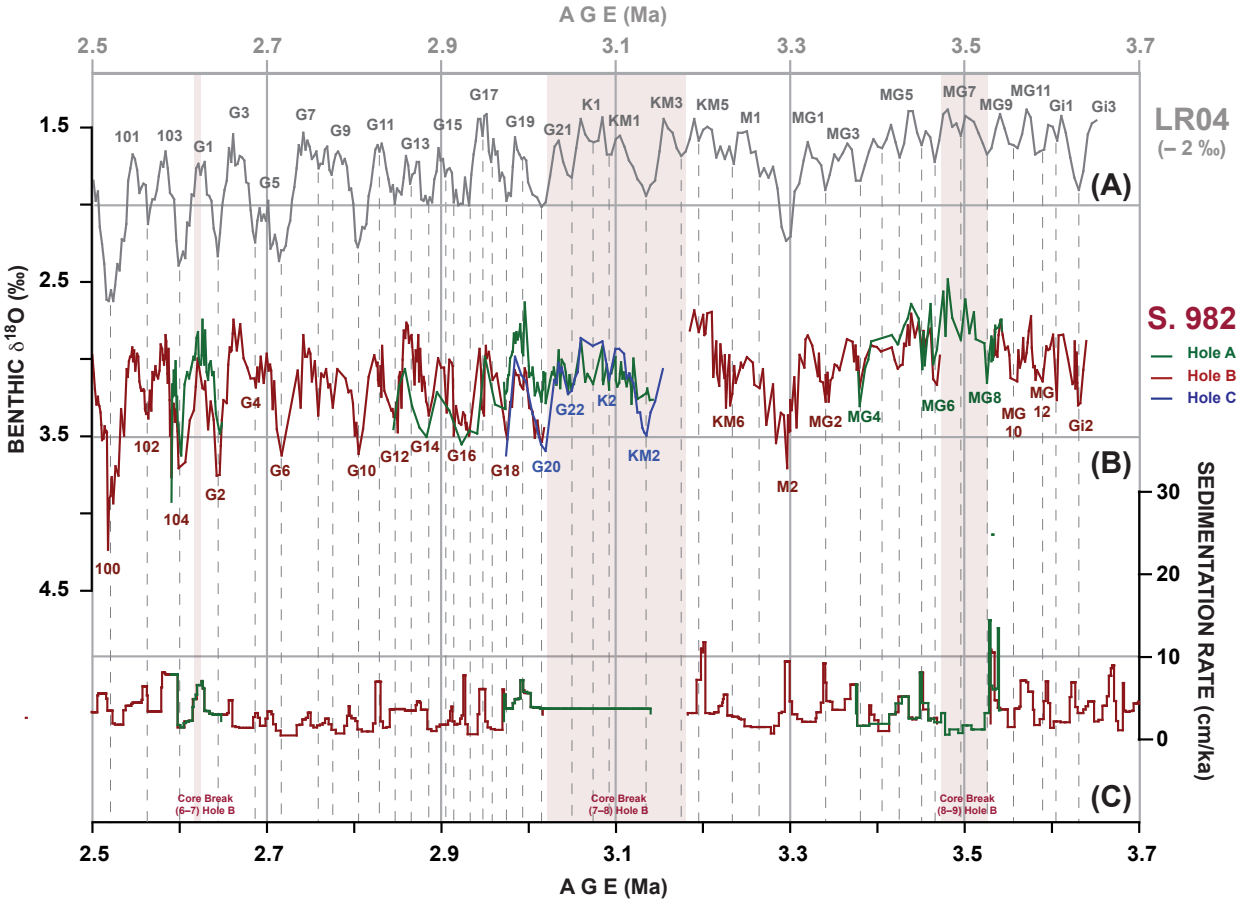

Figure 4.3. Newly established $\delta^{18}O$ records and marine isotope stages (B) for ODP Site 982 versus age and LR04 ice volume record (A) (Khélifi and Sarnthein, in prep.) and resulting sedimentation rates (C).

On the basis of these new stratigraphic correlations it turns out that the chronology of the $U^{k'}_{37}$ record over the onset of NHG (published by Lawrence et al., 2009; see Chapter 5) now needs to be shifted by 80 to more than 160 kyr (e.g., lower MIS M2 versus MIS KM2) toward lower ages. On the basis of this stratigraphy the sampling resolution of our study amounts to 1000–2000 years, in rare cases up to 5000 years.

Near 79.62 mcd a significant positive excursion in $\delta^{18}O$ can be aligned with a well-defined negative-inclination event within the Gauss Chron (Fig. 4.2). This event probably represents the base of the Mammoth subchron and indeed clearly matches the extremely “cold” MIS M2/MG1 boundary as expected (~3.3 Ma; Lisiecki and Raymo, 2005). The upper part of the Mammoth subchron was probably lost due to a kind of “burn-down” process, that is, major post-depositional downcore bioturbation has largely distorted the negative magnetic signals in the upper portion of the sediment layer during the subsequent time of positive inclination. Further downcore, the majority of stages are similar to those defined in the reference LRO4 record. The magnetization intensities were too low for defining any location of the Gauss/Gilbert boundary (Fig. 4.2).

Chapter 5

New insights from proxy intercomparison: Uk'37-based vs Mg/Ca-based sea surface temperature estimates in the northeast Atlantic

1. Quantitative records of Pliocene sea surface temperature in the North Atlantic

Quantitative records of Pliocene sea surface temperature (SST) in the North Atlantic are essential for understanding the last major change in Earth's climate from relatively stable and warm (more ice free) to more variable and colder climates that were marked by glacial-to-interglacial Quaternary cycles (Lisiecki and Raymo, 2005). Moreover, SST records are needed for a better understanding of the degree and extent of Upper Pliocene warming in North Atlantic high latitudes.

Combining two or more independent geochemical proxies for SST reconstruction (e.g., Mg/Ca and alkenone unsaturation / $U^{k'}_{37}$ index) may reduce the uncertainty of SST reconstructions for the North Atlantic, where the majority of records are only based on a single proxy. For example, SST reconstructions from planktic foraminiferal assemblages, that use quantitative micropaleontological census counts (e.g., Dowsett and Poore, 1990), may face problems of reduced foraminiferal populations or extinct species, when translating these Pliocene data into modern SST estimates. Mg/Ca-based SST reconstructions may also respond to factors other than temperature such as dissolution (Regenberg et al., 2006) and/or salinity (Kisakürek et al., 2008). Also, a combination of alkenone and Mg/Ca proxy records potentially permits to reconstruct different temperatures for different habitats of coccolithophorids and foraminifers (Elderfield and Ganssen, 2000) and for different seasons (Leduc et al., 2010).

To date, two studies have compared the alkenones and Mg/Ca proxies on pre-Pleistocene timescale in the east equatorial Pacific (EEP) warm pool (Dekens et al., 2008) and in the North Atlantic (Robinson et al., 2008). Results of the first study suggest that the long-term SST trends in both proxy records likewise reflect mean annual SST in the EEP. Possible influences of seasonality and subsurface plankton growth were found insignificant in these Plio-Peistocene records. The latter observation was (over?) interpreted as evidence for a stability of the $U^{k'}_{37}$ – Mg/Ca relationship through time (Dekens et al., 2008). In the North Atlantic, there is a large-

scale agreement between $U^{k'}_{37}$ - and Mg/Ca-based SST estimates for the Upper Pliocene at four DSDP Sites transecting the North Atlantic Current (NAC), when differences in the calibration, the habitat depth, and the seasonality are considered (Robinson et al., 2008).

2. Aspects of Methodology

In this study, we present a further approach for the North Atlantic, which compares a $U^{k'}_{37}$ SST record of Site 982 (Lawrence et al., 2009) to a new Mg/Ca-based record from *Neogloboquadrina atlantica* (s). The comparison of both records is focused on the times prior and right after the onset of major Northern Hemisphere Glaciation (NHG), i.e., from ~3.7 – 2.6 Ma and based on a revised stratigraphy at Site 982 (Khélifi and Sarnthein, in prep.) (see Chapter 4; Fig. 4.2).

The $U^{k'}_{37}$ -SST record of Lawrence et al. (2009) is based on the equation of Prahl et al. (1988), which has been refined by means of several global core top calibration studies (Müller et al., 1998; Conte et al., 2006). These $U^{k'}_{37}$ -based temperatures at Site 982 may virtually approximate mean annual conditions (Müller et al., 1998). However, the $U^{k'}_{37}$ transfer function was derived for *Emiliania huxleyi* and thus actually only valid for the last 0.270 Ma. For older records, the transfer function was simply extrapolated.

The Mg/Ca-based SST record at ODP Site 982 may largely reflect probably the temperatures at the preferred calcification depth and living season of *N. atlantica* (s) (Fig. 5.1). Because this species is extinct, it is difficult to define the actual habitat and season of preference. *N. atlantica* (s) is a dominant species at high latitudes, that is a cold end-member of the *Neogloboquadrina* genus during the Pliocene. Many authors grouped it with *N. pachyderma* (s) (e.g., Dowsett and Poore, 1990), the habitats of which were explicitly defined by Simstich et al. (2002).

Under modern conditions, the apparent calcification depth of *N. pachyderma* (s) ranges from 30–100 m but can also occur much deeper, such as along a deepening pycnocline of 70–250 m w. d. in the eastern Nordic seas (Simstich et al., 2002). The flux of *N. pachyderma* (s) presently peaks twice a year (in spring and late summer/autumn) at mid-high latitudes, a productivity pattern typical for the sub-arctic setting (Jonkers et al., *in press.*). Accordingly, Mg/Ca-based

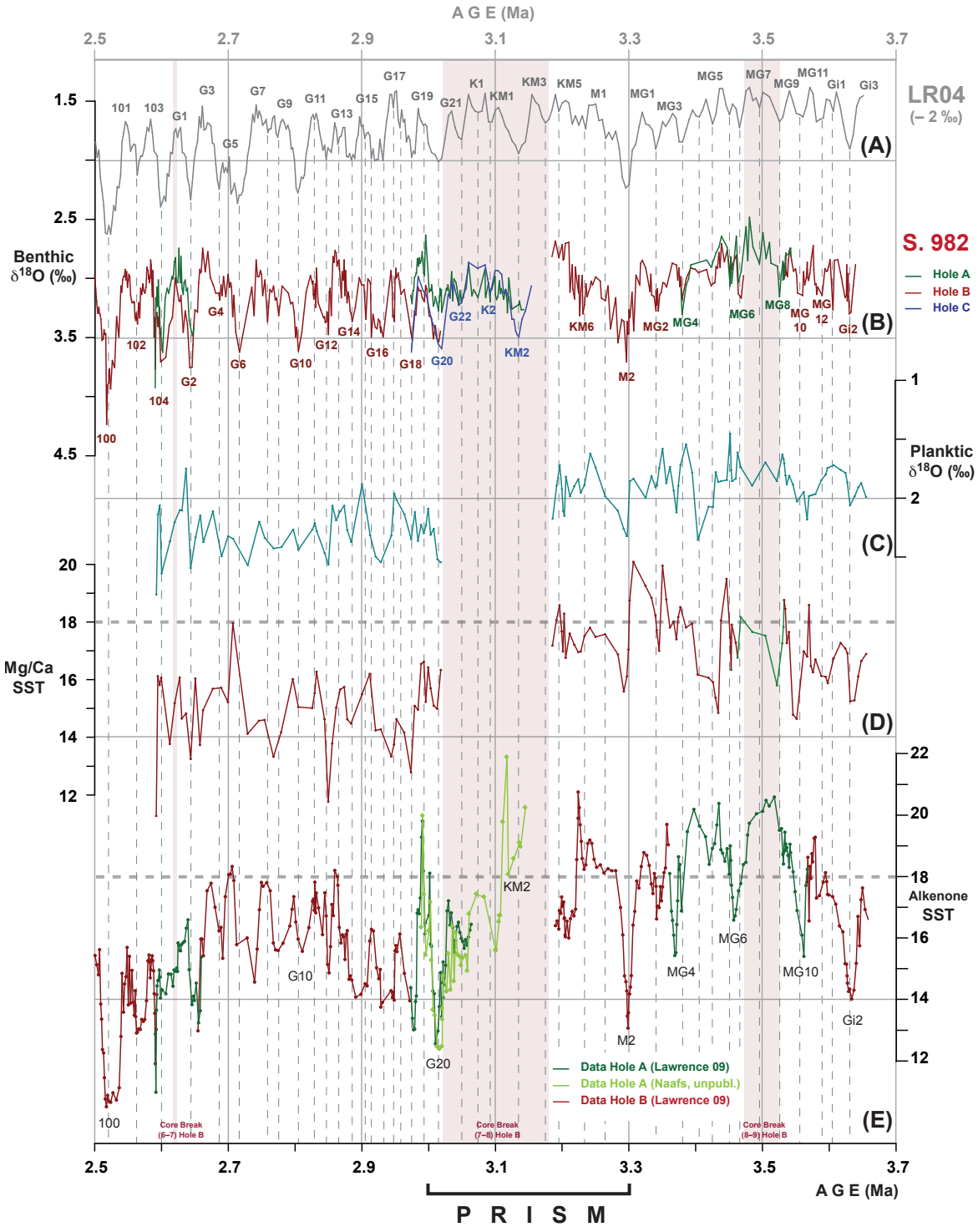

Figure 5.1. Mg/Ca-based sea surface temperature record of *Neogloboquadrina atlantica* (D) as compared to alkenone-based SST record at ODP Site 982 (E) (Lawrence et al., 2009; supplemented by unpublished data of D. Naafs). Planktic (C) and benthic (B) $\delta^{18}O$ records are plotted for comparison with global ice volume record LR04 (A) (Lisiecki and Raymo, 2005). The PRISM interval (Pliocene Research, Interpretation and Synoptic Mapping) from ~2.97 – 3.29 is labeled between MIS 19/18 – MIS M2/M1 (Dowsett et al., 1999).

temperature estimates from *N. atlantica* (s) may reflect mean annual temperatures near the thermocline, that are cooler than actual SST.

Mg/Ca-based SST from *N. atlantica* (s) record uses the Anand et al. (2003) equation that is widely used for extinct species. The main concern of applying this method is the dissolution, the impact of which varies regionally and spatially (Rosenthal and Boyle, 1993; Brown and Elderfield, 1996). Also, at a decreasing $\Delta[CO_3^{2-}]$ a loss in Mg^{2+} can occur (Schiebel et al., 2007). These factors may artificially lower SST estimates. However, this may not the case as intermediate water depths of ~1200 m are far above the lysocline and MOW is highly saline and saturated.

3. Intercomparison of $U^{k'}_{37}$ - and Mg/Ca-based SST records

In general, there is a good agreement between $U^{k'}_{37}$ and Mg/Ca SST records in terms of the timing and amplitude of many temperature changes (Fig. 5.1). However some trends such as the $U^{k'}_{37}$ -based cooling from 3.5 – 3.4 Ma and after 2.7 Ma do not match.

SSTs based on alkenones are in most samples warmer than Mg/Ca-based SSTs. In general, the long-term trends in both records show a pronounced 4°–5°C cooling from ~3.2 (after MIS KM5) to ~2.97 Ma ago (MIS G20/G18) (Fig. 5.1). A sampling gap (in Hole B) between 3.15 (MIS KM3) and 3.01 Ma (MIS G20) makes it difficult to constrain the time for the onset of this cooling more exactly, which marks the first step in the onset of major NHG, possibly starting only after 3.1 Ma (as recorded at nearby Site U1313; Naafs et al., in prep.).

From 3.7 – 3.3 Ma there is a slight long-term warming by 2-3°C in Mg/Ca-based SST, a trend already ending at 3.5 Ma in the $U^{k'}_{37}$ record. During that time, both proxies record a large short-term variability in amplitude. $U^{k'}_{37}$ -based SSTs oscillate between 14° and >20°C, that is ~3°-9°C warmer than the modern mean annual surface temperature in the northeast Atlantic (58°N, 20°W; ~11°C; Levitus and Boyer, 1994). Over the same time period, Mg/Ca-based SSTs were oscillating around 15°-20°C.

Both records show a further gradual warming from 2.97 – 2.70 Ma from ~14° to 17°C. Subsequently, from 2.70 – 2.58 Ma (MIS G5/G3 – 104) $U^{k'}_{37}$ -based SST reflect a second cooling trend down to less than 11°C, a value close to that of today.

On orbital scales both SST proxy records follow the variations of glacial-interglacial MIS as seen from the LR04 record (Fig. 5.1).

4. Discussion

As expected, SST values derived from alkenones are ~1°C higher than those based on Mg/Ca in planktic foraminifera. This can be explained by the generally shallower habitat of coccolithophorid algae as compared to *N. atlantica* (s), moreover by different seasons. Perturbations of the SST signal by environmental variables other than temperature (e.g., metabolic forcing) are also possible (e.g., Bard, 2001). Problems also include lateral contamination by reworked alkenones which are particularly abundant in glacial North Atlantic sediments and at sites located on or close to continental margins (e.g., Mollenhauer et al., 2005), when primary production is low (Weaver et al., 1999).

Lateral transport of the alkenone-bearing fine fraction (i.e., “allochthonous alkenones”) may bias in general the SST signal (e.g., Benthien and Müller, 2000; Ohkouchi et al., 2002). However this factor may be insignificant at S. 982 because both $U^{k'}_{37}$ - and Mg/Ca-based SST show nearly the same overall trends (Fig. 5.1). Most important, Site 982 lies on top of Rockall Plateau and hence suffers little from lateral near-bottom sediment input. Moreover, it lies below the NAC and hence one would expect the advection of too warm tracer particles from the subtropics, for which no evidence are found. Finally, the alkenone SST record generally corroborates the model that the SST calibration for $U^{k'}_{37}$ can be extended from the interval 0–270 ka back into the Pliocene.

Also, there is an uncertainty with the influence of $\Delta[CO_3^{2-}]$ that may explain in part the differences in short-term amplitudes between both proxies. Finally, other factors such as calcite overgrowth of Mg-rich coating may add some variance to Mg/Ca SST record. However, *N. atlantica* species look well preserved under the binocular.

When the global climate was fairly stable between 3.7 Ma (MIS Gi5) and ~3.3 Ma (MIS M2) as reflected in the LR04 $\delta^{18}O$ record, the amplitude (2–4°C) in both proxy records display a large orbital-scale variability (Fig. 5.1). This may be linked to the location (northeastern end of the NAC) of Site 982 that may be highly sensitive to changes in the strength and position of the North Atlantic atmospheric pressure systems and the position of the NAC, driven by orbital changes in the strength and the position of the westerlies (Lawrence et al., 2009). For example, during the glacial periods of the mid- to late Pleistocene the NAC had a west-east flow direction (Pflaumann et al., 2003) and the northward heat transport was reduced. Further studies to constrain past changes in the track of the NAC by comparison with other ODP/IODP sites are in progress (e.g., Naafs et al., in prep.).

A second forcing of the orbital scale variations may include a strong, high-latitude feedback mechanism to obliquity-induced insolation changes, decoupled from continental ice sheets, that have cooled or warmed a broad region of the northern high latitudes (Lawrence et al., 2009). The major cooling 3.2 – 2.95 Ma is also recorded in the planktic oxygen isotope record at Site 982 (Fig. 5.1c).

By contrast to PRISM concept the SST regime from ~3.3 to 3.0 Ma is not uniform but covers a time of dramatic change. Indeed, a new supplementary alkenone record from Hole A (Naafs et al., unpublished data) shows a pronounced ~5°C cooling right after ~3.1 Ma (MIS KM1) (Fig. 5.1). These results contradict other results (e.g., Cronin, 1991; Dowsett et al., 2009b), which all point toward an increased heat transport and intensified NAC during that time. However, the Hole A SST decrease may just represent a significant lateral shift in the position of the NAC. This idea may be corroborated by a new SST record from Site U1313, which shows a warming interpreted as an intensification of the NAC over the entire PRISM interval (Naafs et al., in prep.).

Chapter 6
Upper Pliocene Changes in Mediterranean Outflow Water

1. A major and long-term Pliocene intensification of the Mediterranean outflow, 3.5 – 3.3 Ma ago

This chapter section is based on:

Khélifi N., Sarnthein M., Andersen N., Blanz T., Frank M., Garbe-Schönberg D., Haley B.A., Stumpf R., Weinelt M., (2009). A major and long-term Pliocene intensification of the Mediterranean Outflow, 3.5–3.3 Ma ago: Geology, v. 37; no. 9; p. 811-814; DOI: 10.1130/G30058A.1.

1.1. Abstract

Largely continuous millennial-scale records of benthic $\delta^{18}O$, Mg/Ca-based temperature, and salinity variations in bottom waters were obtained from Deep Sea Drilling Project (DSDP) Site 548 (East Atlantic continental margin near Ireland, 1250 m water depth) for the period 3.7 to 3.0 Ma ago. High ε_{Nd} values of –10.7 to –9 show that this site monitored changes in Mediterranean Outflow Water (MOW) throughout the mid-Pliocene. Bottom water variability at Ocean Drilling Program (ODP) Site 978 (Alboran Sea, 1930 m water depth) provides a complementary record of MOW composition near its West Mediterranean source. Both sites show a singular and persistent rise in bottom water salinities by 0.7–1.4 psu, and in densities by ~1 kg m^{-3} from 3.5–3.3 Ma ago, which is matched by an ~3°C increase in bottom water temperature at Site 548. This event suggests the onset of strongly enhanced deep-water convection in the Mediterranean Sea and a related increase in MOW flow as a result of major aridification in the Mediterranean source region. In harmony with model suggestions, the enhanced MOW flow has possibly intensified Upper North Atlantic Deep Water formation.

1.2. Introduction

As a result of semi-arid continental climate, a freshwater deficit, and cold winters, the modern Mediterranean circulation is anti-estuarine; there is an inflow of Atlantic surface waters with 36.1 psu salinity at Gibraltar and an outflow of highly saline (38.4 psu), warm (13°C), and dense (1029.7 kg m^{-3}) waters below (Candela, 2001). This Mediterranean Outflow Water (MOW)

consists of a mixture of modified Levantine Intermediate Water (LIW) and Western Mediterranean Deep Water (WMDW). From the Strait of Gibraltar, ~2 Sv of MOW are advected both westward and northward along the eastern margin of (lower-salinity) Northeast Atlantic Intermediate Waters (NEAIW; McCartney and Mauritzen, 2001; Fig. 6.1.1). MOW prevails at water depths of 700–1500 m and is centered near 1000 m (Reid, 1979), where it admixes heat and salt to the northern North Atlantic. Today, this supply possibly contributes to preconditioning the Atlantic Meridional Overturning Circulation (MOC; Reid, 1979; Rahmstorf, 1998), generating 1–2 Sv of deep-water flow, and may have done so in the past (Bigg et al., 2003). Hence, MOW may have been a player in changing past ocean circulation and North Atlantic climate beyond the Mediterranean region, in particular at reduced Atlantic MOC. Nonetheless, this hypothesis is still little supported by observations (McCartney and Mauritzen, 2001) or modeling studies (Kahana et al., 2007).

MOW has undergone significant changes in response to different climatic episodes since it began to form after the end of the Messinian salinity crisis (ca. 5.0 Ma ago), when open marine conditions in the Mediterranean were reestablished. For example, Pliocene humid climates in the northern subtropics were linked to sapropel formation first in the eastern, and later in the western Mediterranean. During these episodes, surface waters became stratified, and a reduced density of LIW and WMDW strongly attenuated the flow of MOW (Béthoux and Pierre, 1999). For comparison, during recent glacial and semiglacial marine isotope stages (MIS) 2–4, when sea level fell by 50–120 m below the present level, MOW mostly continued to flow, albeit occasionally at reduced strength (Zahn et al., 1987; Schönfeld and Zahn, 2000). Sediment records from the Gulf of Cadiz suggest that millennial-scale climate variability of Dansgaard–Oeschger (D–O) cycles have controlled changes in MOW advection (Voelker et al., 2006), such as the density of WMDW (Cacho et al., 2006).

In contrast to late Quaternary changes in MOW, which have been studied in detail, little is known about the Pliocene history of MOW near the onset of major Northern Hemisphere Glaciation (NHG) 3.2–2.7 Ma ago (Bartoli et al., 2005). Pioneering studies of Loubere (1987; 1988) first identified MOW at Deep Sea Drilling Project (DSDP) Site 548 during the Pliocene, subsequent to ca. 3 Ma ago. On the basis of multiproxy records with orbital resolution, we now discuss a major mid-Pliocene intensification of MOW flow and its potential influence on North Atlantic Deep Water (NADW) formation. Our conclusions use estimates of Mg/Ca-derived bottom water temperature (BWT), $\delta^{18}O$-based salinity, bottom water density, and Neodymium (Nd) isotopes that help us to trace the origin of MOW at northeast Atlantic Site 548 (48°54´N, 12°09´W; 1250 m w.d.) back to west Mediterranean Ocean Drilling Program (ODP) Site 978

(36°13´N, 2°3´W; 1930 m w.d.) (Fig. 6.1.1). Here, Mg/Ca values are used as a direct record of temperature variability, disregarding a potential bias by changes in carbonate ion saturation (Yu and Elderfield, 2008). This study focuses on the interval 3.7–3.0 Ma ago, when global climate was still characterized by the warm Pliocene “Golden Age”, except for MIS M2 near 3.3 Ma ago, an early but short-lasting precursor signal of major climatic deterioration.

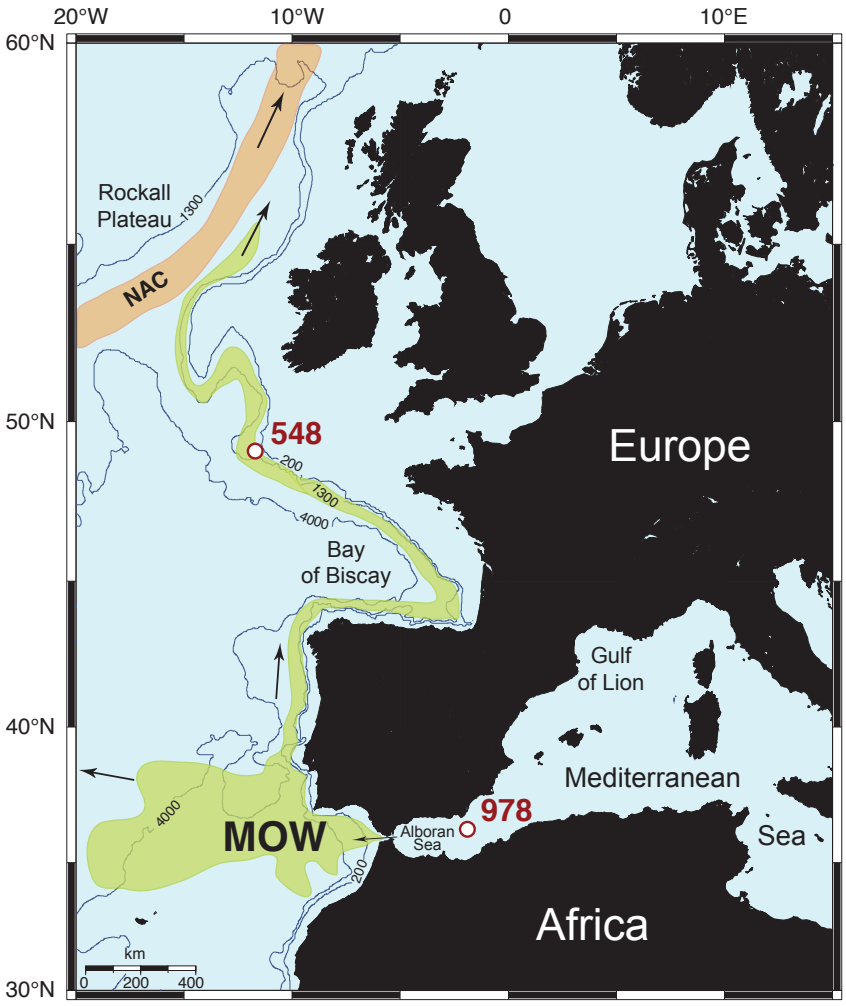

Figure 6.1.1. Locations of Deep Sea Drilling Project (DSDP) Site 548 (48°54´N, 12°09´W, 1250 m w.d.) and Ocean Drilling Program (ODP) Site 978 (36°13´N, 2°3´W; 1930 m w.d.), North Atlantic (surface) Current (= NAC), and highly saline tongue of Mediterranean Outflow Water (MOW; arrows) centered near 1000 m w.d. (Reid, 1979).

1.3. Evidence for the origin of MOW

Nd has an oceanic residence time of 600–2,000 years, which is on the order of the ocean global mixing time (cf. Frank, 2002). Thus, the isotope composition of Nd (ε_{Nd}), which is controlled by the signature of the weathering inputs in the source regions of water masses, can serve as quasi-conservative tracer of Atlantic water mass mixing and circulation. Today, MOW leaves the Mediterranean with a ε_{Nd} of –9.4 to –9.1 (Fig. 6.1.2; Tachikawa et al., 2004; this study), and subsequently becomes less radiogenic through mixing with Atlantic waters along its flow path west of Gibraltar (ε_{Nd} = –9.8; Muiños et al., 2008) up to the Bay of Biscay (ε_{Nd} = –11.1; Rickli et al., 2009) and west of Brittany (ε_{Nd} = –10.5; this study). In contrast, Labrador Sea Water (LSW) today shows ε_{Nd} values of –14 near its source (Lacan and Jeandel, 2005) and –12 in the Bay of Biscay as a result of admixed Atlantic waters (Rickli et al., 2009). Thus, the Nd isotopic difference between MOW and surrounding Atlantic waters, including NEAIW, should suffice to distinguish MOW influence in the sediment record at DSDP Site 548. Here our Pliocene ε_{Nd} seawater record shows fairly stable values of –10.7 (warm MIS) to –8.9 (cold MIS). These values come close to those found at Alboran Sea Site 978 (ε_{Nd} of –9.1 to –8.6) (Fig. 6.1.2), and thus strongly suggest a persistent advection of MOW little diluted by Atlantic waters. This interpretation is robust despite the fact that the ε_{Nd} signatures of mid-Pliocene deep waters in the western and eastern North Atlantic at 700–2700 m depth have shifted generally by +1.5 units (O'Nions et al., 1998; Muiños et al., 2008): No other water mass in the Pliocene North Atlantic had a Nd isotope signature radiogenic enough to produce the positive values found for MOW in our core.

Figure 6.1.2. Seawater Nd isotope composition (ε_{Nd}) at Alboran Sea Site 978 (red) and northeast Atlantic Sites 548 (blue) and 982 (green) as a function of age (Ma). ε_{Nd} values correspond to the deviation of the measured $^{143}Nd/^{144}Nd$ ratio of a sample from that of the chondritic uniform reservoir (CHUR; 0.512638) multiplied by 10,000. Horizontal dashed lines mark modern ε_{Nd} of North Atlantic Deep Water (NADW), Labrador Sea Water (LSW), Mediterranean Outflow Water (MOW), and Western Mediterranean Deep Water (WMDW) at different locations and water depths in the Mediterranean and the northeast Atlantic.

→

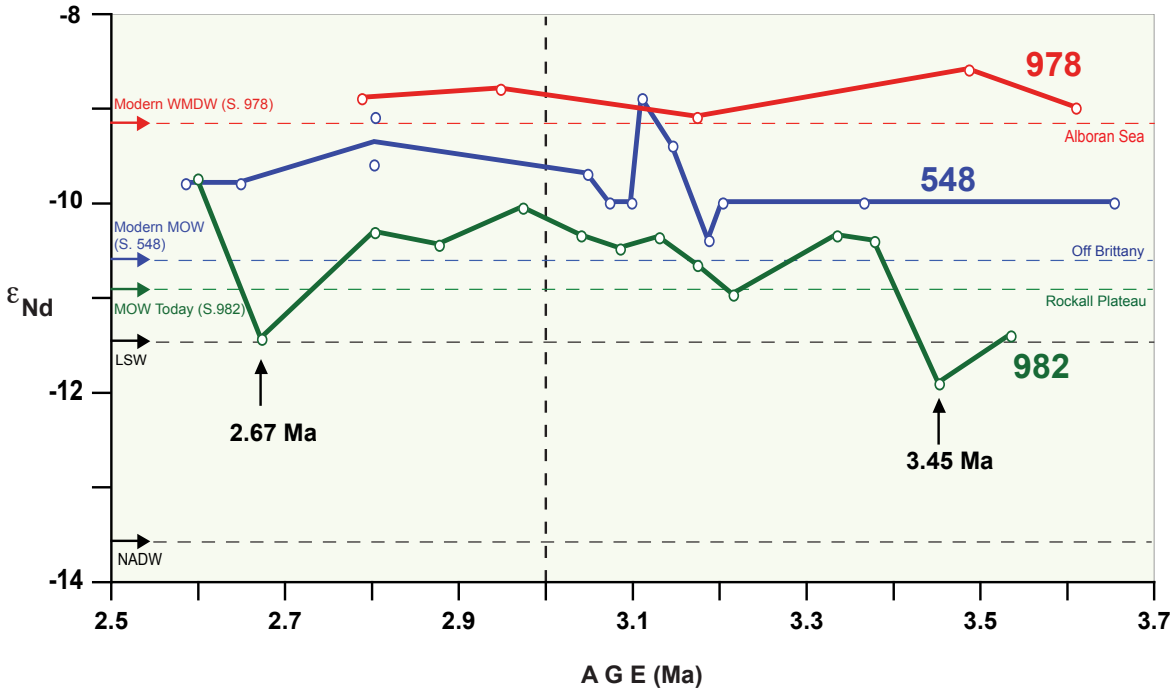

1.4. Correlative Temperature, Salinity, and Density Changes in Alboran Sea Bottom Water and MOW

The Mg/Ca-based BWT record from the Alboran Sea shows ongoing orbital-scale oscillations of 2 °C around an average level of 16 °C ± 3 °C over the interval 3.65–3.0 Ma ago, which is ~3 °C warmer than modern WMDW (Fig. 6.1.3b).

Unlike elsewhere in the ocean, benthic $\delta^{18}O$ variations of *Cibicidoides wuellerstorfi* do not reflect changes in global ice volume as depicted in the global $\delta^{18}O$ record LR04 (Lisiecki and Raymo, 2005), nor any other long-term trend, except for a single major positive excursion at cold MIS M2 and a series of exceptionally negative excursions from 1.5‰ down to 0‰ at 3.54–3.6 Ma ago (Fig. 6.1.3b).

Accordingly, the $\delta^{18}O_{water}$ values for Alboran Sea bottom water (1930 m) reached an extreme minimum around 1.3‰ at 3.65–3.5 Ma ago, with strong $\delta^{18}O$ oscillations that are real in view of highly regular precessional cycles in the corresponding benthic $\delta^{13}C$ record (Fig. 6.1.3b). Subsequent values increased gradually by ~0.35‰ to reach a level of 1.65‰ near 3.35 Ma ago. This high $\delta^{18}O_{water}$ level formed a plateau until 3.0 Ma ago that is only intersected by a number

of short-lasting negative and positive excursions, such as during MIS M2. Using the equation of Cacho et al. (2006), the major $\delta^{18}O_{water}$ shift at 3.5–3.35 Ma ago reflects an increase in bottom water salinity by ~0.7 psu (0.35‰-$\delta^{18}O_{water}$) and results in a gradual density rise by 1 kg m^{-3} from 3.5 to 3.3 Ma ago, when coeval Mediterranean BWT remained largely constant (Fig. 6.1.3b).

With a delay of ~70 ka, $\delta^{18}O_{water}$ (bottom water salinity) values at DSDP Site 548 display a similar long-term and basic rise by 0.7‰ (1.4 psu) from 3.45 to 3.3 Ma ago, up to a level that largely persisted until 3.0 Ma ago (Fig. 6.1.3a). However, different from ODP Site 978, the salinity increase at Site 548 paralleled an abrupt ~3 °C rise in BWT from 6 ° to 9 °C right after 3.4 Ma ago. This rise also led to a slight benthic $\delta^{18}O$ reduction from MIS MG5 to MG3, in contrast to a general $\delta^{18}O$ increase shown at LR04 (Lisiecki and Raymo, 2005; Fig. 6.1.3). In total, bottom water salinity and BWT changes at Site 548 induced a 1.5 kg m^{-3} rise in bottom water density from 3.5 to 3.3 Ma ago (Fig. 6.1.3a), precisely coeval with that at Site 978.

1.5. Discussion

New results by Yu and Elderfield (2008) suggest that the increase in Mg/Ca of *C. mundulus* near 3.4 Ma ago may reflect an increase in bottom water carbonate ion saturation ($\Delta[CO_3^{2-}]$) than a temperature rise at Site 548. However, increased $\Delta[CO_3^{2-}]$ would imply enhanced BW ventilation, and thus likewise an intensified MOW advection, such as increased BWT and heat transport would do. Moreover, Mg/Ca-based BWT measured in parallel on partially temperature-controlled *C. wuellerstorfi* largely match the oscillation trends measured on *C. mundulus*. Thus, it appears likely that our *C. mundulus* record also depicts a BWT signal. Most important, our BWT (5 °–13 °C at Site 548) ranges far above the notably controversial cold-end range of BWT (<5 °C) discussed by Yu and Elderfield (2008). Thus, changes in BWT may be far better recorded than previously suggested.

Major trends in BWT, salinity, and density at ODP Site 978 and DSDP Site 548 can be summarized as follows: Bottom waters in both the west Mediterranean and MOW along the northeast Atlantic continental margin (as traced by positive ε_{Nd} values) experienced a joint singular and long-lasting major increase in BW density by ~1–1.5 kg m^3 from 3.5 to 3.3 Ma ago. At Site 548, coeval BWT possibly increased by ~3 °C, whereas west Mediterranean BWT stayed largely constant. In addition, short-lasting prominent bottom water salinity drops occurred in the Alboran Sea ca. 3.6–3.5 Ma ago.

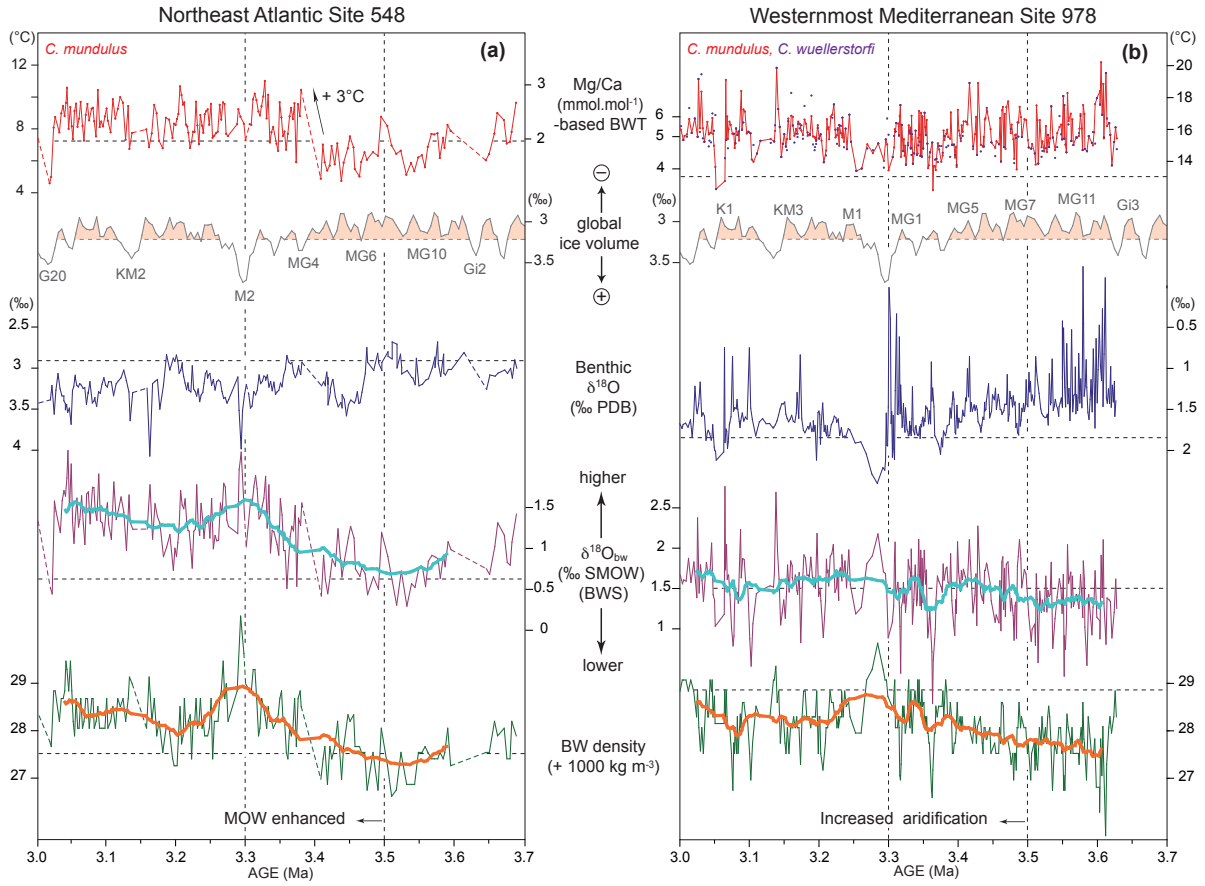

Figure 6.1.3. Pliocene changes in the properties of Mediterranean Outflow Water (MOW) at Deep Sea Drilling Project (DSDP) Site 548 (A) and (B) Western Mediterranean Deep Water (WMDW) at Ocean Drilling Program (ODP) Site 978. Epibenthic $\delta^{18}O$ is measured on *Cibicidoides* spp. at Site 548, on *C. wuellerstorfi* at Site 978, and compared with the stacked $\delta^{18}O$ LR04 (Lisiecki and Raymo, 2005). Mg/Ca-based bottom water temperature (BWT) was obtained from *C. mundulus* at Site 548 and from *C. mundulus* and *C. wuellerstorfi* at Site 978. Trend lines connect averages of paired measurements. Approximately 40 ka running means (thick lines) highlight long-term trends. Dashed horizontal lines show modern levels. Broken trend lines in records at Site 548 present potential sediment loss at core breaks. BW—bottom water; BWS—bottom water salinity; SMOW—standard mean ocean water; PDB—Peedee belemnite.

The concurrent event 3.5–3.3 Ma ago in bottom water composition at two far distant sites inside and outside the Mediterranean provides strong evidence that the 200-ka-long shift in bottom water salinity originated from a key change in Mediterranean overturning circulation and climate. For this period, major tectonic events around Gibraltar are unknown. The significant density increase is not mirrored in Mediterranean BWT at Site 978, the general level of which then was ~3 °C higher than today, nor is it seen in enhanced sea-surface salinity (SSS); instead, it is only reflected in a long-term ~1 °C cooling of sea-surface temperature (SST) in the Alboran Sea (Fig. 6.1.4), in contrast to the prominent 3 °C rise in MOW BWT at Site 548. For this reason, we conclude enhanced Mediterranean deep-water convection and MOW flow, which imply more vigorous heat and salt transport to the Atlantic at that time.

The intensification of MOW flow occurred >200 ka prior to the first pronounced glacial MIS M2. It did not entail any intensification, but a long-term reduction in Lower NADW ventilation (decreasing epibenthic $\delta^{13}C$ until 3.3 Ma ago; Kleiven et al., 2002).

As the $\delta^{18}O$ record LR04 (Fig. 6.1.3; Lisiecki and Raymo, 2005) shows that global ice volume has little increased during this time, the origin of increased Mediterranean convection was linked most likely to a major, possibly seasonal rise in subtropical aridity that started around the Mediterranean for reasons as yet unexplained. Other Mediterranean marine sediment sections in Sicily and Calabria (Lourens et al., 1996) do not record the 3.5–3.3 Ma event, except for two marine pollen records from the Gulf of Lion (Fauquette et al., 1998) near the main convection cell of west Mediterranean deep water, which document a basic shrinkage of (mega-) mesothermic forests and increased summer droughts around the northwest Mediterranean ca. 3.56–3.22 Ma ago (ages based on biostratigraphic datums calibrated to $\delta^{18}O$ stratigraphy). This shift to more steppic vegetation and drier summer climate around the Gulf of Lion strongly corroborates our conclusion on increased convection ca. 3.5–3.3 Ma ago.

Prior to this event, we see a pronounced drop in mid-Pliocene Mediterranean bottom water salinity at ODP Site 978 from 3.6 to 3.5 Ma ago (MIS Gi1–MG8). It was clearly aligned with a short-term extreme reduction in SSS by ~4 psu ($\Delta\delta^{18}O_{water}$ = 2‰) but not with any major change in SST (Figs. 6.1.3; 6.1.4). This SSS minimum suggests a major increase in continental humidity and freshwater discharge to the west Mediterranean Sea (in harmony with Fauquette et al., 1998). Possibly, the freshening also resulted in a short-term reduction of MOW flow, which may have been lost in Site 548 coring gaps. A further large negative bottom water salinity excursion at the beginning of MIS MG4, near 3.37 Ma ago, was not linked to any significant SSS or SST

oscillation, and thus cannot be related to any particular event in west Mediterranean climate change.

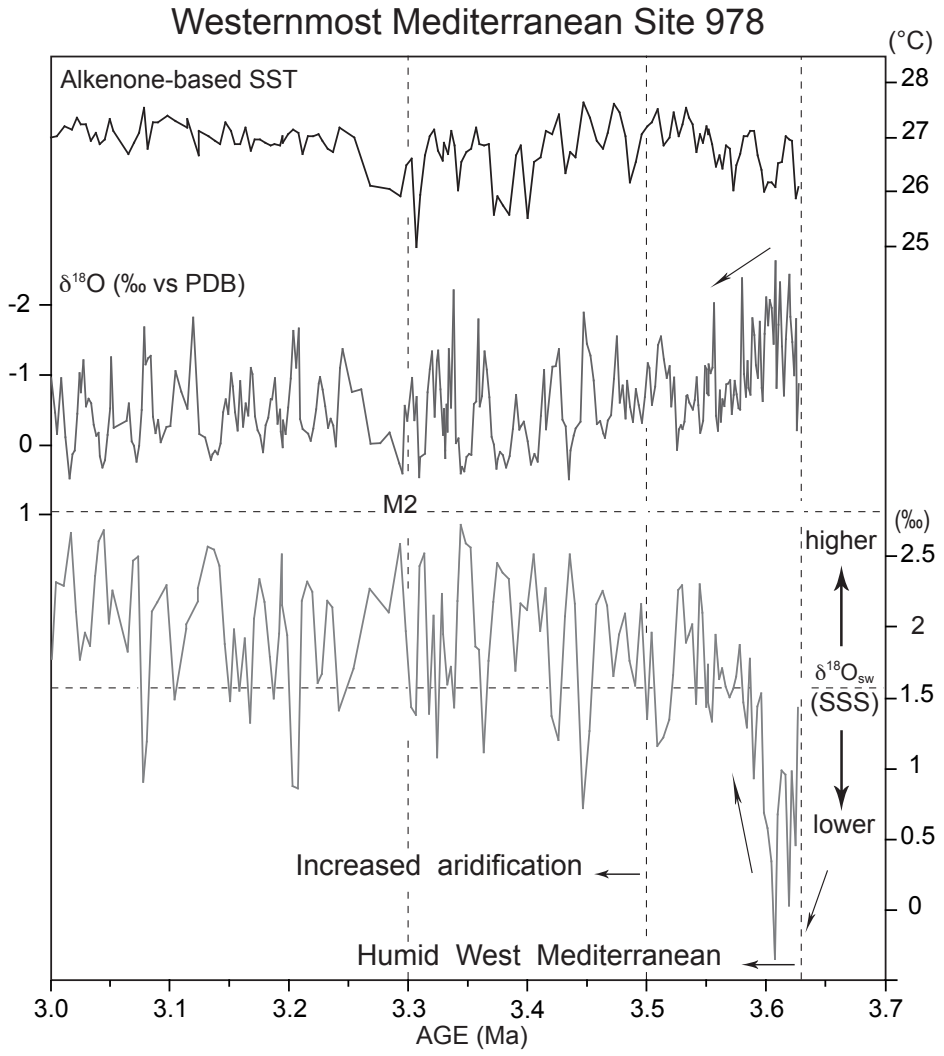

Figure 6.1.4. Record of changes in sea-surface properties at Ocean Drilling Program (ODP) Site 978. $\delta^{18}O$ is measured on *Globigerinoides ruber, Globigerina bulloides*, and *Globigerinoides obliquus*. Horizontal lines show modern levels. Labeled arrows outline major long-term trends. SSS—sea-surface salinity; SST—sea-surface temperature; SW—seawater; PDB—PeeDee belemnite.

1.6. Conclusion

High ε_{Nd} values trace the mid-Pliocene MOW flow from Gibraltar up to DSDP Site 548 at the northeastern Atlantic margin from 3.7 to 3.0 Ma ago. Both Mediterranean deep water at Alboran Sea (ODP) Site 978 and MOW at Site 548 show a distinct long-term rise in bottom water salinity by 0.7–1.4 psu between 3.5 and 3.3 Ma ago. This rise in bottom water salinity matches a possible 3 °C increase in BWT and, most importantly, a rise of MOW density by ~1 kg m^{-3}, thus suggesting a significant increase in MOW flow and Mediterranean deep-water formation over this time, which, in turn, has intensified Upper NADW formation. The enhanced MOW flow was linked to enhanced seasonal aridity in the Mediterranean zone, as documented by a distinct shift to more steppic vegetation and climate in pollen records from the Gulf of Lion (Fauquette et al., 1998). Near 3.6 Ma ago, a short-term extreme low in Mediterranean bottom water salinity matched a likewise extreme low in SSS, suggesting a major freshening of the Alboran Sea, and humid climates all over the western Mediterranean.

2. Potential links of changes in Mediterranean hydrological cycle to the African monsoon system and the Indian Ocean, 3.5 – 3.3 Ma

2.1. Mediterranean hydrological budget vs. East African climate change

The Mediterranean Sea's overall hydrological budget can be affected indirectly by the African monsoon system that feeds the Nile and other ancient rivers across the Sahara (Pachur and Altmann, 2006). Today, the African monsoon system exerts only a kind of "remote" influence on the Mediterranean, mainly through the Nile river discharge before the construction of the Aswan High Dam (Rohling et al., 2008a). However, in past periods the monsoon front (i.e., northward displacement of the ITCZ) was penetrating far beyond the central Saharan watershed (~21°N) all of the way to the Mediterranean, where significant runoff may reached along the wider North African margin. For example, during the insolation maximum of the Eemian interglacial maximum (MIS 5e; ~125 ka BP) both Libyan lakes and marine stable oxygen isotope data show evidence of a significant penetration northward of the monsoon front to flood the eastern Mediterranean via fossil river/wadi systems (Rossignol-Strick, 1983; Petit-Maire, 1985; Rohling et al., 2002b). Geochemical data also demonstrate that these waters indeed derived from the North African watershed (~21°N) and penetrated across the Libyan Sahara all of the way to the Gulf of Sirte in Libya (Osborne et al., 2008). The uninterrupted freshwater corridor across a currently hyperarid region of the Sahara marked orbital wet episodes in general and extremely humid periods such as the peak Early Holocene in particular (Pachur et al., 1987; Kröpelin, 1987), when precession was in its maximum.

Here we study a potential linkage between a key change in the western Mediterranean hydrological budget from wet to more dry conditions (3.5 – 3.3 Ma) (Khélifi et al., 2009) (Fig. 6.1.4 in section 6.1) and a coeval switch in the intensity of the African monsoon climate towards aridification of East African lakes (summarized in Maslin and Trauth, 2009).

A progressive vegetation shift from C_3 (~trees and shrubs) to C_4 (~tropical grasses) plants during the Plio-Pleistocene marked a step-function change from formerly wet to dry conditions in eastern African climate following the progressive rifting of East Africa (deMenocal, 1995; Levin et al., 2004; Sepulchre et al., 2006). The trend of drying in East Africa was punctuated by alternating short periods of extreme humidity and aridity (Fig. 13.2 in Maslin and Trauth, 2009). For example, a humid-lake phase occurred at ~3.6 Ma (Trauth et al., 2005; 2007; Maslin and Trauth, 2009) and corresponded to a maximum in "pollen humidity" in the Gulf of Lion (3.6 –

3.55 Ma) (Suc, 1984) and a minimum in SSS (~3 psu lower than today) and BWS (~0.5–1 psu lower than today) at Alboran Sea S. 978 (Khélifi et al., 2009) (Figs. 6.1.3; 6.1.4; Section 6.1).

This humid period did not entail any sapropel formation in the Mediterranean Sea (Lourens et al., 2004). The subsequent drop in humidity may reflect a key change in the hydrological budget and climate of North Africa and the Mediterranean Sea, probably caused by ceasing African river discharge following a weakening of the African monsoon system and/or southward displacement of the ITCZ to south of 21°N. The end of humid conditions (shift from C_3 to C_4) was reflected by a gradual ~4-psu increase in SSS at S. 978 reaching a modern level near ~3.53 Ma (Fig. 6.1.4; section 6.1).

As expected, the aridification of North Africa and the western Mediterranean after ~3.5 Ma was coeval with a gradual 1–2 psu increase in BWS of WMDW in the Alboran Sea from 3.5 – 3.35 Ma, and consequently with some delay, also in MOW as recorded in the northeast Atlantic (Fig. 6.4.2b; section 6.4).

Likewise, a large and deep-lake stage/period identified in most basins of the East Africa graben system from 2.65 to 2.5 Ma (Trauth et al., 2005; 2007) was indirectly recorded by an abrupt cease of MOW advection (3°C BWT drop and ~1-ε_{Nd} unit drop at Site 982; 1°–2°C BWT drop at Site 548, Figs. 6.1.2 and 6.4.1a in section 6.4; i.e., a period unfortunately not anymore analyzed at Site 978).

2.2. Discussion of potential forcings by changes in oceanography / geodynamics: The partial constriction of the Indonesian Gateway

According to the conceptual model of Cane and Molnar (2001), the northward movement of New Guinea since 5 Ma shifted the source of the Indonesian Throughflow (ITF) subsurface waters from the warm and saline equatorial West Pacific Warm Pool to the cooler and fresher subtropical North Pacific. This shift should have resulted in a distinct drop of SST (~2°C) at 100 m w. d. in the tropical eastern Indian Ocean and a reorganization of Pacific SSTs from a dominantly El Niño-like to a more frequent La Niña-like pattern. Both events may have contributed to droughts in eastern Africa and perhaps, to the initiation of major NHG (Cane and Molnar, 2001; Rodgers et al., 2000).

In contrast to Cane and Molnar (2001) recent General Circulation Model (GCM) simulations of Jochum et al. (2009) show that a widening of the Indonesian Seaway would result in reduced

Pliocene temperature values at 150 m w. d. as compared to today over the whole tropical Indian Ocean and thus, in lower precipitation in the equatorial Indian Ocean and off Somalia. This trend may indicate that a progressive closing of the Indonesian seaways may just result in subsurface temperatures larger than today and perhaps, in slightly enhanced evaporation/precipitation over East Africa after the Pliocene restriction of the ITF.

In contrast to these GCM results a recent study of Karas et al. (2009) shows an abrupt prominent cooling event (SST drop by ~3°C; SSS drop by >1‰ $\delta^{18}O_{seawater}$) of subsurface waters in the tropical eastern Indian Ocean at ~3.3 – 3.15 Ma, indicative of a throughflow of cooler and fresher North Pacific subsurface waters following the progressive constriction of the Indonesian gateway (Cane and Molnar, 2001). As result, we should also expect a subsurface cooling in the western tropical Indian Ocean, partly fed by the ITF. This would affect the equatorial surface and/or the coastal upwelling waters off Somalia (e.g., Schott et al., 2002). In turn, west Indian surface cooling would lead to a reduction of evaporation and a drop of precipitation over eastern Africa; whereas GCM simulations of Jochum et al. (2009) show reduced precipitation with warming subsurface waters. This would imply a decrease in river discharge into the Mediterranean basins, a significant increase in SSS and enhanced deep-water formation, and finally, an increased MOW incursion and salt discharge to the northeast Atlantic.

However, the outlined Indonesian forcings occurred only 200–300 ky after the onset of aridification in East Africa and the Mediterranean region (3.5 – 3.3 Ma ago). Moreover, East African lakes just showed a maximum extension after the 3.15 Ma SST event, near 3.1 Ma ago (Trauth et al., 2005; 2007). This humid event was also recorded in the western Mediterranean by a 0.5-psu drop in SSS and BWS of WMDW below the modern level (Figs. 6.1.4; 6.4.1b).

In view of these contradictions between the conceptual model of Cane and Molnar (2001) and the records of Karas et al. (2009) on the one hand and GCM simulations of Jochum et al. (2009) on the other hand, the progressive constriction of the Indonesian gateway and its impact on water mass properties in the tropical Indian Ocean apparently did not imply any significant influence on East African and Mediterranean climates.

2.3. Conclusion

A major Mediterranean hydrological change occurred around 3.5 to 3.3 Ma (Khélifi et al., 2009). This event most likely originated from key changes in the African monsoon system, as shown by increasingly dry conditions depicted in the terrestrial records from East Africa near that time (Trauth et al., 2005; 2007). This trend, in turn, might have been linked to the gradual Upper Pliocene constriction of the ITF (Cane and Molnar, 2001).

However it turns out, beyond the range of age uncertainty, that the major cooling of subsurface waters in the tropical Indian Ocean (Karas et al., 2009) as a result of reduced ITF (Cane and Molnar, 2001) occurred only at 3.3 – 3.15 Ma and thus has not exerted any effect on East African climate (Trauth et al., 2005; 2007) and hence on the Mediterranean Sea's overall hydrological budget.

3. Alboran Sea $\delta^{13}C$ records of nutrient contents and deep-water ventilation

3.1. $\delta^{13}C$ of planktic foraminifera: Tracer of nutrients (P, N) (Fig. 6.3a)

In the Alboran Sea, modern $\delta^{13}C$ values of DIC (dissolved inorganic carbon) are near 1.3–1.4‰ in the upper 25 m (Pierre et al., 1999). In general, the $\delta^{13}C$ of the near-surface dweller *Globigerinoides ruber* in the Mediterranean Sea with its low productivity amounts to 1.3–1.5‰ (Vergnaud-Grazzini et al., 1986), values that correspond closely to the $\delta^{13}C$ of DIC. For comparison, intermediate waters at 200–300 m show 0.75 – 0.85‰ $\delta^{13}C$ for DIC (Pierre et al., 1999).

Upper Pliocene $\delta^{13}C$ values at Site 978 vary from 0.8–1.2‰ to 0–0.5‰ over the interval ~3.55 – 2.7 Ma. This level is significantly lower than modern values, except for a marked positive excursion up to 1.2–1.5‰ near 3.165 Ma (MIS KM3) (Fig. 6.3a).

Prior to 3.5 Ma $\delta^{13}C$ average values were constant near 1.1‰, oscillating between 0.5 and 1.4‰. From 3.5 – 3.3 Ma they decreased extremely by 0.9‰ down to 0.3‰. Subsequently, a gradual 1-‰ increase marked the interval from 3.3 to 3.165 Ma. After this $\delta^{13}C$ maximum the values returned to oscillations at a low level of -0.5–0.5‰ from 3.15 – 3.05 Ma. Subsequently, the $\delta^{13}C$ record was marked by a constant average level of 0.6–1.0‰ until at least 2.7 Ma ago (the range of oscillations exceeds ~10 times the uncertainty of analyses) (Fig. 6.3a).

As outlined above, the ratio of ^{13}C to ^{12}C in *G. ruber* reflects the composition of the DIC of the water ambient to shell precipitation. There are two models to explain the trends of planktic $\delta^{13}C$ signals (Broecker and Peng, 1982). First, increased nutrient use and production of organic matter (OM) will result in an enhanced incorporation of ^{12}C into the OM. As the ^{12}C is extracted preferentially (over ^{13}C) by reoxidation during the photosynthesis, $^{13}C/^{12}C$ ratio in surface water DIC will be enriched, and thus $\delta^{13}C$ in planktic carbonate shells high.

The second model (Ganssen, 1983) argues as following: An increased nutrient supply will result in an enrichment of organic matter in the surface layer. This process results, in turn, in an increased production of ^{12}C from the remineralization of OM (90%) within the surface layer, thus yielding more negative $^{13}C/^{12}C$ ratios in DIC of the surface water ambient to foraminiferal shell precipitation. Thus the planktic $\delta^{13}C$ values will be low. Because of multiple evidences

(Ganssen, 1983; Weinelt et al., 2001; Wang et al., 1997; Gebhardt et al., 2008) we need to follow the latter concept: Planktic foraminifera living in the photic layer reflect mostly low $\delta^{13}C$ values, where the production of organic matter is high.

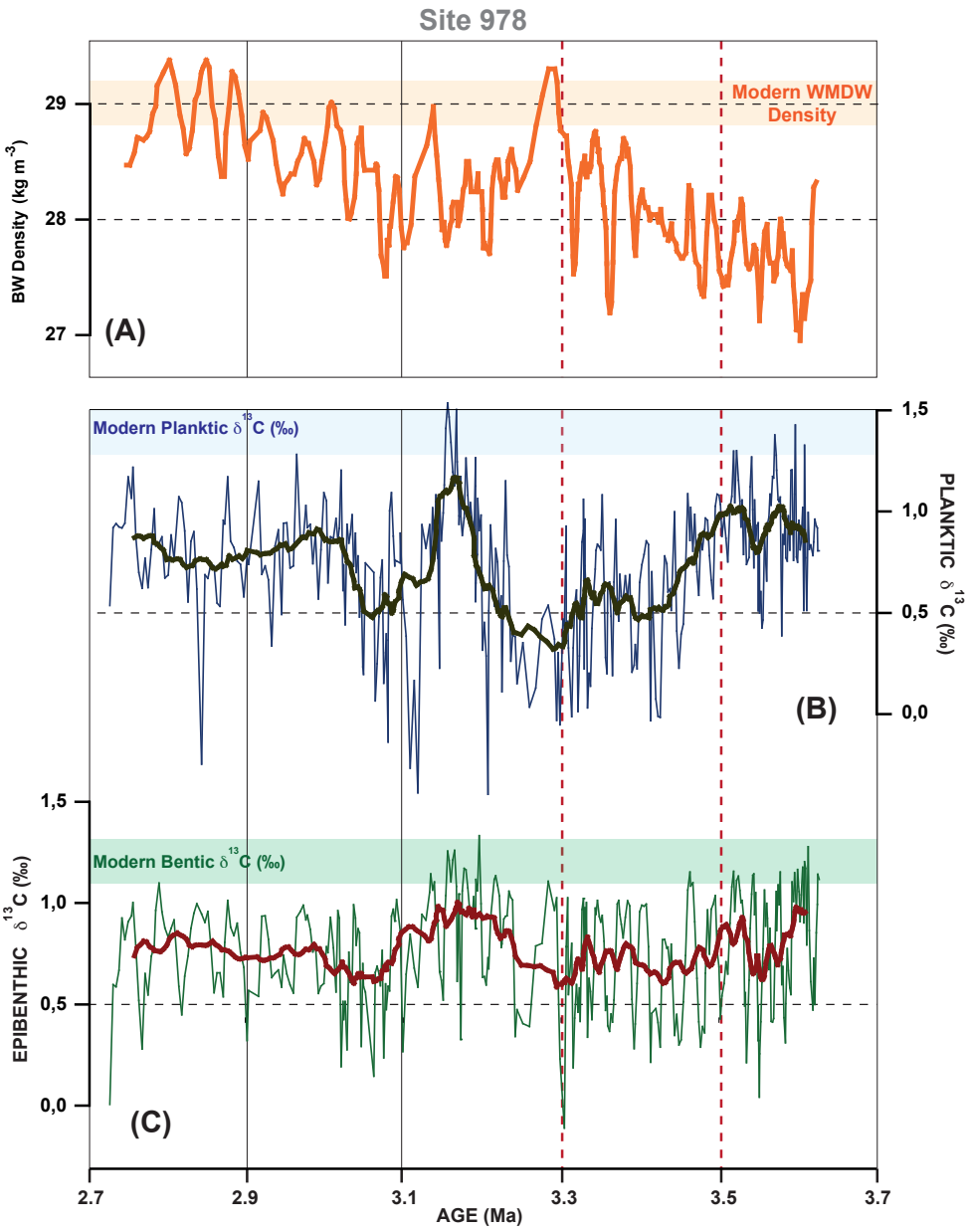

Figure 6.3. Nutrient contents (planktic $\delta^{13}C$) of Alboran sea surface waters (B) and deepwater ventilation (epibenthic $\delta^{13}C$) (C) versus changes in western Mediterranean deep water density Site 978 (A). Note inverse parallel trends between records (A) and (B) and clear orbital-scale variability (a 20 ky) in record (C).

The major planktic $\delta^{13}C$ decrease in the Alboran Sea from 3.5 Ma to 3.25 Ma (MIS MG7–M2) may therefore reflect an increase in nutrient and productivity supply in the surface layer (Fig. 6.3a). Here the question arises, whether the enhanced productivity was linked to circum Mediterranean discharge or to an increased advection/inflow of characteristically nutrient-enriched Atlantic surface waters (1.1–1.2‰ $\delta^{13}C$; Ganssen, 1983) to compensate for the increased outflow recorded during that time (section 6.1 and Khélifi et al., 2009).

A recent OGCM study of Alhammoud et al. (in press) indeed shows that the less water flows with MOW, the less Atlantic inflow is needed for compensation. Thus, the intensity of the complete inflow-outflow system will be reduced. Accordingly, any increase in MOW flow (as evidenced by an increase by 1.0–1.5 psu of BWS; see section 6.1) will necessarily result in a much enhanced, ^{13}C-depleted Atlantic inflow. This increased exchange also leads to a slight reduction in the overall Mediterranean salinities and a deepening of the thermocline, and accordingly to a drop by ~1‰ $\delta^{13}C$ of the DIC of surface waters at Site 978 in the westernmost Mediterranean Sea (Fig. 6.3a). This event was also paralleled by a long-term 1–1.5°C cooling of sea surface waters in the Alboran Sea (Fig. 6.1.4.). On the other hand, an increased deep water formation and export of MOW were necessarily linked to higher aridity, as confirmed by pollen (Fauquette et al., 1998), and thus to a reduced riverine input of ^{12}C enriched OM. Thus the low $\delta^{13}C$ level even stronger argues for an enhanced Atlantic inflow.

In turn, the salient positive excursion of planktic $\delta^{13}C$ values near 3.25 – 3.15 Ma (MIS KM2–M2) is most likely also the result of a short-term major decrease in the supply of nutrient-rich Atlantic surface waters and indeed is matching precisely a significant coeval minimum in the flow of MOW (Fig. 6.4.1).

3.2. $\delta^{13}C$ of benthic foraminifera (Fig. 6.3b)

Epifaunal species with elevated habitat such as *Cibicidoides wuellerstorfi* are used for benthic $\delta^{13}C$ records because they are considered to be in equilibrium with the $\delta^{13}DIC$ of ambient bottom waters (Zahn et al., 1986). Epibenthic $\delta^{13}C$ can be used as a proxy of past nutrient concentrations (Broecker and Peng, 1982) and as tracer of the “apparent” O_2 utilization and the deepwater ventilation (that is the intensity of the overturning circulation) (Duplessy et al., 1988). The regional pattern of deep-water $\delta^{13}C$ is affected by changes in bottom water characteristics, mainly the bottom water age, and the overlying local productivity controlling the flux of OM to the seafloor. The epibenthic $\delta^{13}C$ signal is also controlled by the microhabitat effect. For example, in high-productivity areas the values can decrease by up to 0.4‰ (Mackensen et al., 1994;

Sarnthein et al., 1994). However, this effect does not apply to Alboran Sea Site 978 which does not lie in a specific high productive region.

At Site 978, the epibenthic $\delta^{13}C$ record shows a fairly stable range around 0.7–0.8‰ for the interval ~3.6 – 2.7 Ma (as compared to 0.7–0.9‰ for modern DIC; Pierre et al., 1999), except for an increased level near 3.6 Ma and from 3.25 – 3.1 Ma up to values similar to today (~1.1‰) (Voelker et al., 2006) (Fig. 6.3a). In contrast to expectations for high $\delta^{13}C$ values with increased advection of MOW from 3.5 – 3.3 Ma, the $\delta^{13}C$ signal was rather stable oscillating near 0.25–1.0‰ with precessional cycles of ~20 ky. For comparison, the $\delta^{13}C$ running averages of MOW at S. 548 and S. 982 were oscillating between 0.5‰ and 0.8‰ (Fig. 6.4.2).

Earlier studies of Plio-Pleistocene changes in $\delta^{13}C$ of deep waters in the eastern Mediterranean basins (Vergnaud-Grazzini et al., 1990; Thunnel et al., 1987; 1990) showed a stable $\delta^{13}C$ signal near 1‰ for the upper Pliocene (e.g., at Tyrrhenian Sea Site 653; 2820 m w.d.) (Thunnel et al., 1990). This $\delta^{13}C$ level shows that East Mediterranean deep waters, that are West Mediterranean Intermediate waters, are gradually “aging”, that is collecting ^{12}C enriched OM on their way to Gibraltar.

3.3. Conclusions

- The surface waters of the Alboran Sea underwent a period of increasing nutrient supply (lower $\delta^{13}C$) from 3.5 to 3.3 Ma. This period was most likely linked to an increase in the Atlantic inflow of surface waters that compensated for the then enhanced outflow of MOW (section 6.1 and Khélifi et al., 2009).

- Vice versa, a short reduction in MOW from 3.25 – 3.1 Ma was linked to planktic $\delta^{13}C$ maximum that probably documents a short but distinct minimum in MOW flow. In conclusion, we can trace the conjugate signals of the compensating surface water inflow and intermediate water outflow to and from the Mediterranean Sea by the combined planktic and benthic $\delta^{13}C$ records.

- The $\delta^{13}C$ signals of western Mediterranean intermediate and deep waters show a gradual shift by ~0.2 – 0.3‰ from East to West, that records the aging of these waters while flowing to Gibraltar, here forming the source for MOW.

4. Evolution of MOW tongue in the northeast Atlantic over the onset of major Northern Hemisphere Glaciation, 3.0 – 2.6 Ma

4.1. Onset of major Northern Hemisphere Glaciation (as summarized by Sarnthein et al., 2009)

The onset of major Arctic glaciation (~3.15 – 2.73 Ma) was marked by increased/additional poleward transport of heat and moisture via westerlies to northwestern Eurasia following the closure of the last 250–130 m of the Panamanian gateways and the subsequent intensification of the North Atlantic Current (NAC) (Driscoll and Haug, 1998; Lunt et al., 2007). These forcings induced (1) an intensification of North Atlantic Meridional Overturning Circulation (MOC), (2) a little enhanced precipitation over Greenland and North Hemisphere continents (first modeled by Maier-Reimer et al., 1990), and (3) much increased river discharge from Siberia to the Arctic Ocean. The latter forcing partly contributed to more sea ice formation and (5) more Arctic Albedo, sufficient for preconditioning the growth of North Hemisphere ice sheets (Driscoll and Haug, 1998).

A further, perhaps more important forcing following the closure of Panama came from the “pile-up” of freshwater in the subarctic North Pacific (first modeled by Motoi et al., 2005). It resulted in a twofold increase of the Arctic throughflow (ATF) through the Bering Strait in case the sea level was similar as today (modeled by Prange in Sarnthein et al., 2009). Perhaps a 25–35 m higher Pliocene sea level (preliminary estimation of PLIOMAX project; Raymo et al., 2009) may have resulted in a threefold increase in the ATF, which would add further fresh water to the Arctic Ocean and the northern North Atlantic. This increase resulted in more enhanced sea ice accumulation, and in turn, additional albedo in the Arctic Ocean, 3.2 – 3.0 Ma (Sarnthein et al., 2009).

The outlined forcings induced the onset of major Northern Hemisphere Glaciation (NHG) and the gradual intensification of Quaternary-style glaciations in Greenland, Eurasia, and Laurentia, first culminating near MIS G10 (~2.82 Ma) (Bartoli et al., 2005). In particular, the cooling event near 2.95 – 2.82 Ma was marked by an increase in sea surface temperature and salinity of the NAC, which resulted in more convection of deepwater in the Nordic Seas, that is an enhanced North Atlantic MOC. These changes were recorded in the deep ocean by a long-term drop (~2°C) of bottom water temperature (BWT) of NADW at Site 609 (3889 m w. d.) (Bartoli et al.,

2005) and Site 607 (3427 m w. d.) (Sosdian and Rosenthal, 2009), also by increased density (benthic $\delta^{18}O$ values) at Site 610 (2417 m w. d.) (Bartoli et al., 2005).

It was unknown yet to which degree the onset of major NHG may have affected the Mediterranean climate near the cells of Mediterranean deep water convection and the export of MOW. Pioneer studies in the Mediterranean Sea show a trend towards heavier $\delta^{18}O$ values in planktic (Thunell et al., 1990) and benthic (Vergnaud-Grazzini et al., 1990) after 3.0 – 3.1 Ma. These changes were precisely coeval with the onset of pronounced cooling (op. cit.) and Saharan aridification that was recorded in the whole subtropical belt (e.g., Tiedemann et al., 1994). Also, pollen records in the northwestern Mediterranean (e.g., Fauquette et al., 1998) show a minor gradual decrease in subtropical taxa and increase in steppic vegetation after 3.2 Ma ago.

Here, we study the potential effect of the onset of major NHG on (1) western Mediterranean deep-water (WMDW) production (~25% of MOW) by examining bottom water temperature (BWT), salinity (BWS), and density (BWD) records at Site 978 in the Alboran Sea, and (2) the resulting evolution of the MOW tongue in the northeast Atlantic over the onset of major NHG at sites 548 and 982 (Fig. 2.1; Chapter 2). These changes are compared to changes in the properties of the water column after the intensification of NADW formation and to changes in the properties of WMDW (Site 978).

4.2. Evidence for the evolution of MOW tongue in the northeast Atlantic after 3.0 – 2.6 Ma: Major findings

Labrador Sea Water (LSW, equal to Upper NADW) today shows ε_{Nd} values of –14 near its source (Lacan and Jeandel, 2005) and –12 in the Bay of Biscay as a result of admixed Atlantic waters (Rickli et al., 2009). Lower NADW shows ε_{Nd} values of –13.5 in the North Atlantic (Stordal and Wasserburg, 1986) (Fig. 6.1.2).

For comparison, western Mediterranean deep waters at Site 978 show a continuous level of ε_{Nd} values near to the modern level of –9.1 from 3.6 – 2.75 Ma. At northeast Atlantic Site 548 the (low-resolution) Pliocene ε_{Nd} record shows a fairly stable range between –9.8 and –9.1 and no excursion after 3.0 Ma. That is a signal less diluted than the modern-to-Holocene values near –10.5 at this core site (Fig. 6.1.2). The most distal position of MOW at Site 982 shows a fairly stable range between –11.4 and –9.7, that is near to the modern value of –10.9 in the Rockall

Plateau (Scrivner et al., 2008), and thus still a Mediterranean signal. However, before 3.45 Ma (~MIS MG5) the ε_{Nd} reflected a major deviation up to –11.8 from a MOW signal towards the LSW or UNADW level (Fig. 6.1.2). Likewise, near 2.67 Ma (~MIS G4) the ε_{Nd} decreased to –11.4.

Besides these gradual changes in the ε_{Nd} signal from the source at Site 978 up to the most distal Site 982, the MOW tongue shows also changes in BWT, BWS, and BWD (Figs. 6.4.1a,b,c). As described in Chapter 2 today Site 978 is bathed in WMDW that is formed in the northern sector of the western Mediterranean Sea. At a water depth of 1930 m Site 978 records a BWT of ~13°C, a BWS of 38.4 psu, and a BWD of ~29 kg m^{-3}. WMDW contributes from below ~25% and the overlying MIW formed in the eastern Mediterranean basin 75% to MOW before crossing through the Strait of Gibraltar (Pinardi and Masetti, 2000) (Fig. 2.1; Chapter 2).

During the onset of major NHG (~3.0 – 2.7 Ma), BWT at Site 978 show a stable range from 14°–16°C, that is 1°–3°C higher than today, except for short cooling events near 3.05 Ma (MIS G22; 12.2°C), 2.96 Ma (MIS G17; 13.3°C), 2.87 Ma (MIS G13; 13°C), and 2.78 Ma (MIS G9; 13°C). These events may follow a 95-kyr-eccentricity cycle from 3.05 – 2.74 Ma (Fig. 6.4.1a).

Figure 6.4.1. Pliocene changes in (a) bottom water temperature (BWT), (b) salinity (BWS), and (c) density (BWD) of MOW in the northeast Atlantic Sites 548 and 982 as compared to Western Mediterranean Deep Water (WMDW) properties at Site 978. Approximately 40-ka running means (thick lines) highlight long-term trends. Horizontal bars mark modern levels. Mg/Ca-based bottom water temperature (BWT) was obtained from *C. mundulus* at Sites 548 and 982 and from *C. mundulus* and *C. wuellerstorfi* at Site 978.

→

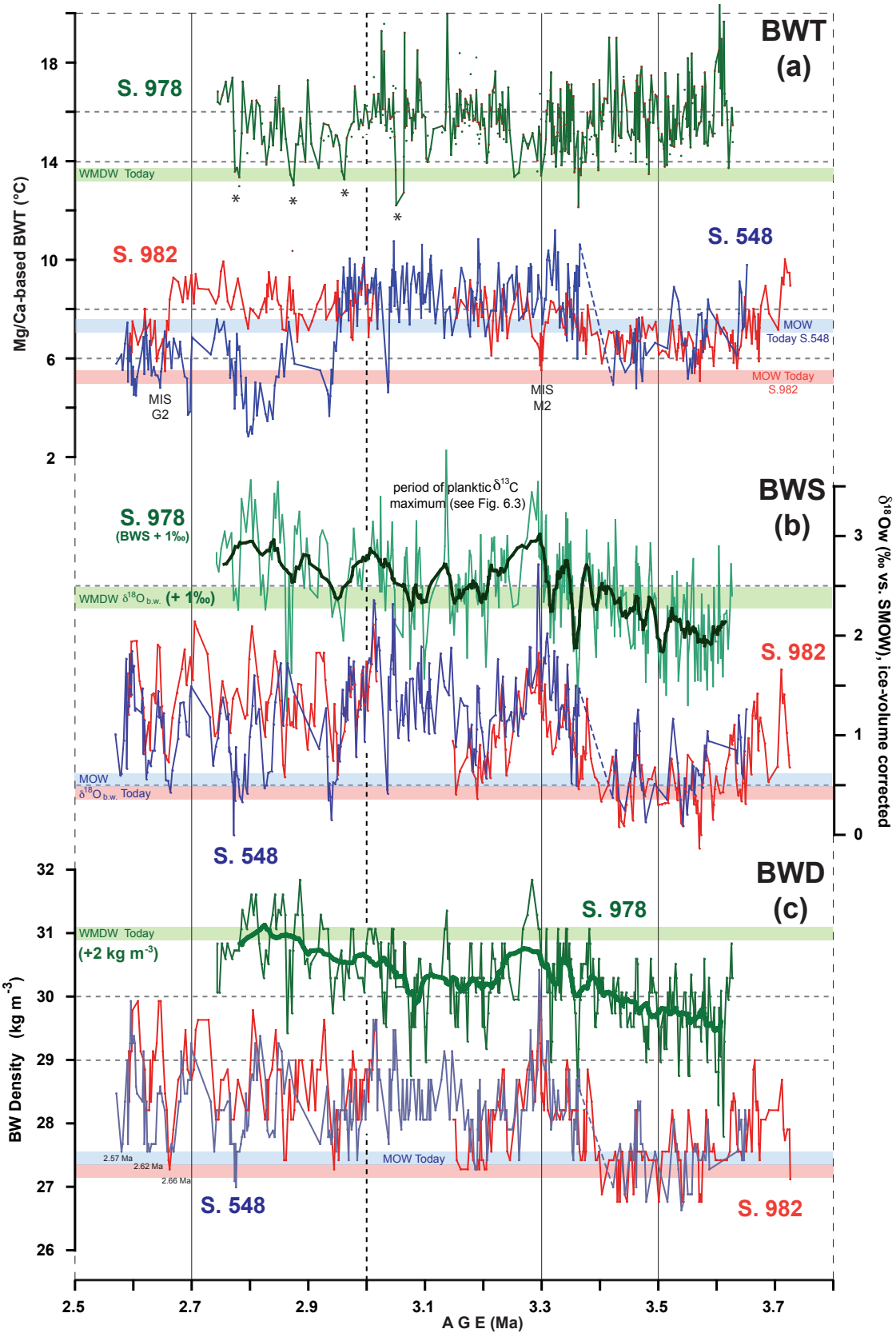
BWT
(a)
S. 978
WMDW Today
S. 982
S. 548
MOW
Today S.548
MOW Today
S.982
MIS
G2
MIS
M2
Mg/Ca-based BWT (°C)
BWS
(b)
period of planktic δ13C
maximum (see Fig. 6.3)
S. 978
(BWS + 1‰)
WMDW δ18Ob.w. (+ 1‰)
S. 982
MOW
δ18Ob.w. Today
S. 548
δ18Ow (‰ vs. SMOW), ice-volume corrected
BWD
(c)
S. 978
WMDW Today
(+2 kg m-3)
MOW Today
2.57 Ma
2.62 Ma
2.66 Ma
S. 548
S. 982
BW Density (kg m-3)
A G E (Ma)

After 2.95 Ma ago, BWS record at Site 978 was marked by a long-term gradual increase by ~1 psu, which was interrupted by three BWS drops of 1–2 psu below modern level during the previously mentioned major interglacials near 2.96 (MIS G17), 2.86 (MIS G13), and 2.825 (MIS G11) Ma (Fig. 6.4.1b). The increase in BWS led to/resulted in a long-term increase in BWD starting near 3.1 Ma ago (MIS K2) from ~28–29 kg m^{-3} up to the modern range of WMDW near ~29 kg m^{-3} after 2.88 Ma (Fig. 6.4.1c).

Today Site 548 (35.5 psu, 7.5°C) is bathed in the lowermost MOW tongue (35.7 psu, 9.5°C in the Gulf of Cadiz) with some NADW admixed (35 psu, 2.5°C) (Fig. 2.1; Chapter 2). The resulting admixture leads to densities of ~27.5 kg m^{-3}. During the onset of major NHG (~3.0–2.7 Ma ago), BWT showed a drop by 2°C to a level lower than today, on this way reaching a NADW pure signal near ~3°C at MIS G10 (2.8 Ma ago) (Fig. 6.4.1a). This event was also marked by a 2-psu long-term decrease in BWS from 2.95 Ma (MIS G17) until 2.82 Ma (MIS G10) (Fig. 6.4.1b). By contrast, BWD showed a stable level of 28–28.5 kg m^{-3}, that was about ~1 density unit higher than today from 3.0 until at least 2.57 Ma (Fig. 6.4.1c). Subsequent to 2.8 Ma, BWT returned to rise near modern level at 5.5–6.5°C, and BWS show a gradual rise of 2 psu reaching modern level near 2.6 Ma. However, BWD continued to oscillate near the level of 28.5 kg m^{-3}, at least until 2.57 Ma (Fig. 6.4.1c).

On the Rockall Plateau, Site 982 (35 psu, 5–6°C) is bathed today by a mixture of most distal MOW (35.7 psu, ~9.5°C in the Gulf of Cadiz) and NADW (35 psu, 2.5°C) (McCartney and Mauritzen, 2001) (Fig. 2.1; Chapter 2). The question is, whether MOW has reached continuously the Rockall Plateau during the Upper Pliocene? Although ε_{Nd} values are pleading for a largely continuous presence of MOW at Site 982 except for the excursion at 2.67 Ma (Fig. 6.1.2), further parameters such as BWT, BWS, and BWD are here employed to define the local properties of MOW and to disentangle the changes in its advection versus changes in the North Atlantic MOC.

Prior to 3.0 Ma, BWT of MOW at Sites 548 and 982 were nearly equal (Fig. 6.4.1a). Over the onset of major NHG (~3.0–2.7 Ma), BWT at Site 982 oscillated at a level of 2°C higher than today (5–7°C), moreover, higher than at the more proximal Site 548. Later, an abrupt decrease by 2–3°C (near modern level 5–6°C) marked S. 982 only at MIS G2 (~2.65 Ma) (Fig. 6.4.1a), the effect of which is also seen in the benthic $\delta^{18}O$ record with a far more positive value than at LRO4 reaching ~3.5‰ (Fig. 4.3; Chapter 4). Subsequently, BWT continued to oscillate near 6.5–7.5°C; that is at the same level as that of Site 548. However, BWS values continued near a

level about 1–1.5 psu higher than today (35 psu) (Fig. 6.4.1b). Also, BWD values were ~1 unit higher than today (~27.4 kg m^{-3}), that is near the level of 28.5 kg m^{-3} such as at Site 548 (Fig. 6.4.1c).

The ventilation record of WMDW at Site 978 as represented by (epi-) benthic $\delta^{13}C$ (Fig. 6.4.2a) showed a stable range of 0.6–0.8‰ after 3.0 Ma. In contrast, benthic $\delta^{13}C$ at S. 548 showed an abrupt increase from 0.6 to 1.0‰ from MIS G10 to G6 (2.82 – 2.74 Ma) up to a high level that may throw some light on the different contributions of WMDW and MIW on the MOW composition (Fig. 6.4.2b). At Site 982 a long-term gradual increase from 0.6 to 1.2‰ already started earlier, after 3.0 Ma (MIS G20) and continued until 2.82 – 2.74 Ma. At MIS G10 (2.82 Ma), an extreme increase in the $\delta^{13}C$ gradient (~0.5‰) was established between Sites 982 and 548, in part the result of several large short-term $\delta^{13}C$ minima (lower of ~1‰ than today, see below) at Site 548 over the onset of major NHG (Fig. 6.4.2c). After ~2.65 Ma (MIS G3), a joint long-term decrease by 0.8‰ started both at Sites 982 and 548. During this time the $\delta^{13}C$ gradient between the two sites remained constant (Figs. 6.4.2). The decrease in MOW ventilation after 2.65 Ma at Site 982 coincides with a coeval major deviation (–11.4) in the ε_{Nd} record from the MOW level up to almost that of modern LSW (–12) or LNADW (–13.5) (horizontal dashed bars in Fig. 6.1.2).

At Site 548, the most extreme negative $\delta^{13}C$ values occurred during cold glacial MIS G12, G10, G8, G4, G2, and 104 (Fig. 6.4.2b). Likewise at Site 982, the decrease in benthic $\delta^{13}C$ values occurred mostly during cold glacial MIS MG10, MG6, MG2, M2, G18, G16, G12, G8, G6, G4, G2, 102, and 100 (Fig. 6.4.2c). In part, these minima in $\delta^{13}C$ values may reflect an evidence for the impact of Upper NADW admixture, in particular different contributions of WMDW and MIW to MOW.

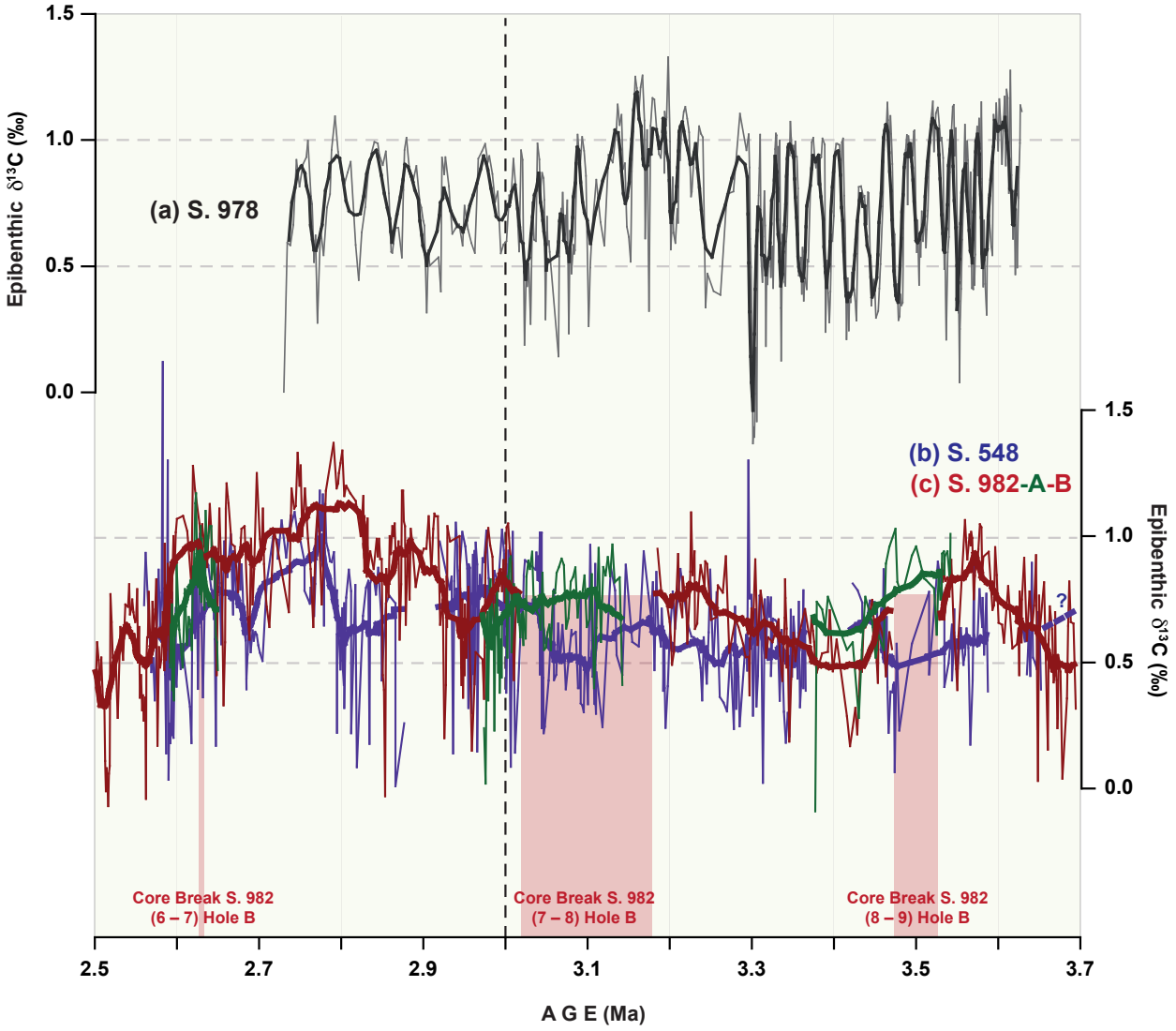

Figure 6.4.2. Pliocene changes in ventilation (epibenthic $\delta^{13}C$) of western Mediterranean Deep Water (WMDW) at Alboran Sea Site 978 (a) and Mediterranean Outflow Water (MOW) at northeast Atlantic Sites 548 (b) and 982 (c). Vertical brownish bars mark potential losses of sediment sections at core breaks in Hole B.

4.3. Discussion

The following models, expectations, and speculations will be tested by means of our data set in this study:

1. Did MOW reach the Rockall Plateau, the most distal position found today for the MOW (McCartney and Mauritzen, 2001), continuously over the onset of major NHG?

2. To what extent did the onset of major NHG influence the climate in the Mediterranean region, in particular near its sources of intermediate and deep-water convection?

3. How did the properties and water depth of the highly warm and saline MOW tongue develop in the northeast Atlantic in relation to changes in both differential MOW advection and NADW formation?

4. To what extent was the $\delta^{18}O$ signal of MOW distinguished from the global $\delta^{18}O$ ice volume signal in northeast Atlantic deep waters after the onset of major ice growth in the North Hemisphere?

5. To what extent/degree did orbital-scale variability influence MOW ventilation in the northeast Atlantic? Can different contributions of (East) MIW and (West) MDW to MOW be deciphered in the MOW ventilation signal?

In parallel to the ε_{Nd} record at Site 978, ε_{Nd} values at sites 548 (–9.8 to –9.1) and 982 (–11.4 to –9.7) that are higher than Atlantic water masses (–12 to –14) show that MOW reached almost continuously the northeast Atlantic continental margin up to the Rockall Plateau after 3.4 Ma to at least 2.7 Ma (Fig. 6.1.2). An exception forms glacial MIS G6–G4 near 2.71–2.67 Ma, when the ε_{Nd} record showed an extreme decrease reaching –11.4, a value that is about 1.5-ε_{Nd} unit lower than the signal of MOW and nearly equal to that of LSW signal in the Bay of Biscay (–12) (Rickli et al., 2009). During that time MOW obviously did not reach the Rockall Plateau for the first time after the onset of major NHG.

On the average, during the whole interval studied the horizontal ε_{Nd} gradient between Sites 978 and 548 amounted to 0.8 units exists. Nearly the same gradient (0.9-ε_{Nd} units) existed between

Sites 548 and 982 (Fig. 6.1.2). These horizontal gradients may indicate the rate of gradual dilution of MOW with Atlantic intermediate water masses along its mixing pathway.

The first step (2.95 – 2.82 Ma) in the onset of major NHG was marked by a 2°–3°C drop in BWT and in BWS (~2 psu), but constant BWD, then still 1 kg m^{-3} higher than today (~27.5 kg m^{-3} at Site 548 near 1250 m w. d.) (Fig. 6.4.1). This period was reflected by an increase in benthic $\delta^{18}O$ values, which exceeded the increase in LR04 by 1.1‰ (Figs. 4.3; Chapter 4), most likely because of the coeval 2–3°C decrease in BWT (Fig. 6.4.1a). In general, this increase in benthic $\delta^{18}O$ (for example, ~0.85‰ at Site 982) is considered to reflect the growth of continental ice volume with the onset of major NHG after 3.0 Ma ago (Lisiecki and Raymo, 2005) (Figs. 4.1; 4.2; Chapter 4).

The changes property of MOW at Site 548 may either indicate vertical (upward?) shift and/or a mixing of the MOW core after 2.95 Ma, following the enhancement of North Atlantic MOC and hence an increased NADW production (Bartoli et al., 2005; Sarnthein et al., 2009). By contrast BWT at the slightly shallower Site 982 (1135 m w. d.) continued to oscillate at a level 3°C higher than today (5°–6°C). BWS values then were 3-psu higher than today (35 psu), and BWD were ~1 kg m^{-3} higher than modern value of ~27.4 kg m^{-3}. In particular, BWD record showed a long-term slight increase and slightly higher level than at Site 548 (Fig. 6.4.1c). Accordingly, it appears that the Rockall Plateau Site at 1135 m w. d. did not move out from the core of MOW, different from Site 548 at its base near 1250 m w. d.

Here a slightly reduced BWD (~28.2 kg m^{-3}), the 3°C drop in BWT and also the long-term ~2-psu decrease in BWS may indicate a slight reduction in MOW flux, possibly resulting in a minor upward shift of the MOW layer on top of the Upper NADW (Fig. 6.4.1). Accordingly, the MOW core might have been either diluted or shifted upward, but not completely lost. In summary, its advection continued at high level up to the Rockall Plateau during the times of major rearrangement of ocean circulation in the northern North Atlantic over the onset of major NHG until ~2.8 Ma.

This conclusion – in part – may be linked to the first step of enhanced Atlantic MOC which was coeval with a massive increase in $\delta^{13}C$ values by ~0.4‰ at both Sites 548 and 982 after 2.95 Ma until 2.8 Ma ago (Fig. 6.4.2). However, this long-term increase in $\delta^{13}C$ may also/more likely reflect a differential/higher contributions of highly ventilated EMIW, because no ventilation change is recorded at S. 978. Thus it may indicate a long-term change in MOW composition (colder, less saline) at a nearly equal density, at least near its lower periphery (near 1250 m w.

d.), a change that resulted from climate changes/variations over the convection zones in the Mediterranean Sea with the onset of NHG. Unfortunately no direct $\delta^{13}C$ record is available from regions near the main cells in the eastern Mediterranean.

Different from ε_{Nd}, $\delta^{13}C$, and BWT the BWS and BWD at S. 978 showed a significant rise by 0.5 psu and 1 kg m^{-3}, respectively, up to levels higher than today. Such as today, these waters were probably admixed from below to the overlying Mediterranean Intermediate Water (MIW) crossing the Strait of Gibraltar (See Chapter 2) (Figs. 2.1; 6.4.1a,b). Accordingly, the increase in $\delta^{13}C$ from 0.6 up to 1.4‰ at northeast Atlantic sites 548 and 982 from 2.95 to 2.76 Ma may reflect indeed a long-term enhanced ventilation of MIW rather than of WMDW.

For comparison, $\delta^{13}C$ of MOW in the Gulf of Cadiz have risen during the LGM up to 1.75‰ (Zahn et al., 1997) or to 1.5‰ (Voelker et al., 2006). The high level may thus reflect a first/early advection of glacial-style MOW to the northeast Atlantic, mainly fed by EMIW sources (short-term, orbital-scale variations in $\delta^{13}C$ records are discussed further below).

Only after 2.7 / 2.65 Ma (MIS G2–G3), the drop in ε_{Nd} to -11.5 (Fig. 6.1.2) suggests a major change in the composition or even a total cease of MOW at the Rockall Plateau, also recorded by a pronounced drop in BWT by 3°C at Site 982 to a level that was sill ~1°C higher than today (in contrast to continuously high oscillations BWS and BWD levels, on the average still ~2 psu and ~2 kg m^{-3} higher than today) (Fig. 6.4.1). Thus MOW advection perhaps persisted also at a high level over the Rockall Plateau after MIS G4, but a transient cease around MIS G3–G4 cannot be excluded being replaced by UNADW.

Also, short-lasting sapropel interval in the West Mediterranean may have increased surface water stratification and switched off MIW formation during that time. Unfortunately, the paleoceanographic data of Site 978 do not extend over that time span to provide a proper reference record from the West Mediterranean Sea.

The evolution of Mediterranean climate may be deduced from the ongoing continuously high salinity (~39–39.25 psu), gradual warming (15°–17°C), and the gain in density from ~30.5 to 31.5 kg m^{-3} of West Mediterranean Deep waters (S. 978) from 3.0 – 2.75 Ma. This evidence may indicate that during the onset of major NHG deep-water convection cells in the northwest Mediterranean were intensified, although the ventilation in the $\delta^{13}C$ record remained low near 0.8‰ (Fig. 6.4.2). By contrast, the $\delta^{13}C$ ventilation record at S. 982 for the first-time approached the LGM $\delta^{13}C$ level as measured by (Zahn et al., 1997; Voelker et al., 2006). This finding is

corroborated by a coeval increase in aridification around the Mediterranean region such as enhanced steppic vegetation near to the Golf of Lion (Fauquette et al., 1998).

Orbital-scale variations in benthic $\delta^{13}C$ at northeast Atlantic sites may have been also controlled by local changes in ^{12}C enriched organic carbon flux and surface water productivity (Fontugne and Duplessy, 1978; Loubere, 1987b; Mackensen et al., 1994). For example the extreme $\delta^{13}C$ values occurring during glacial MIS (e.g., G12, G10, G8, G4, G2, and 104) at Site 982 (Fig. 6.4.2) are paralleled by a short-lasting minima in SSTs (e.g., Mg/Ca and $U^{K'}_{37}$ records in the northeast Atlantic of Bartoli et al., 2005; Lawrence et al., 2009) (Fig. 5.1; Chapter 5). Similar episodes of high flux of carbon linked to high productivity were recorded during the last glacial period off Portugal (Abrantes et al., 2002).

4.4. Conclusions

During the onset of major NHG (~3.0 – 2.7 Ma), MOW reached continuously the northeast Atlantic continental margin until at least the Rockall Plateau (Site 982) as recorded by high ε_{Nd} values. During that time, NADW production in the Nordic Seas strengthened in response to a first step of enhancement in the AMOC from ~2.95 – 2.80 Ma (Bartoli et al., 2005; Sarnthein et al., 2009). The enhanced production of Upper NADW may have diluted and/or rather displaced the MOW tongue upward in the region southwest of Ireland (Site 548) up to a level shallower than 1250 m w. d., as reflected by lower than today BWT and BWS values. By contrast, after 2.7 Ma BWT and ventilation ($\delta^{13}C$) of MOW decreased to a level similar to today at/on the Rockall Plateau (S. 982), whereas BWS and BWD continued to be high. This finding is corroborated by a short lasting reduction of ε_{Nd} values at/on the Rockall Plateau up to the NADW level. Accordingly, the MOW tongue may have disappeared for a short time but reappeared after 2.6 Ma on Rockall Plateau.

5. Potential shifts in vertical position vs. intensity changes of MOW, 3.5–3.3 Ma and 3.0–2.7 Ma

5.1. Introduction/Open Questions

Two major events marked MOW records along the northeast Atlantic continental margin following in harmony with periods of bottom water density displayed at Alboran Sea Site 978 serving as master record (Fig 6.4.1c in section 6.4).

The first event occurred between 3.45 and 3.3 Ma (in part discussed in section 6.1). During that time both the western Mediterranean Site 978 and northeast Atlantic sites 548 and 982 show a unique increase by ~1.5–2 psu in BWS and most important, by ~1 kg m^{-3} in BWD (Fig. 6.4.1b,c). On the other hand a coeval long-term increase of BWT by 3°C at S. 548 and 1°C at S. 982 led to a reduction of the BWD rise (Fig. 6.4.1a,c).

During this time, BWD of WMDW increased by ~1 kg m^{-3}, whereas BWD of MOW did not increase but oscillated around 28.5 kg m^{-3}, that is ~1 kg m^{-3} higher than today (Fig. 6.4.1c). In contrast to BWD, BWS of MOW did not display any distinct second event but a series of oscillations: Average BWS decreased at S. 978 as at Sites 548 and 982 by 1–3 psu from 3.0 to 2.95 Ma and from 2.82 to 2.78 Ma, on the other hand increased by the same amount from 2.9 – 2.82 Ma and (in three steps) from ~2.75–2.7 Ma, with subsequent orbital-scale oscillations until 2.55 Ma, that is with BWS minima during interglacials (Fig. 6.4.1b).

On the basis of these two major events of BWD increase we try to test, whether the MOW tongue (Fig. 2.1) along the northeast Atlantic margin has changed its depth position and/or its inflow intensity over the upper Pliocene (Fig. 6.5.1). Such changes may have depended on:

(1) Different climatic conditions prevailing in the regions of WMDW (Gulf of Lion) and MIW convection (Levantine basin);

(2) Changes in the convection and density of Upper NADW in its zone of formation in the Labrador Sea. The changes control the extent to which NADW density was competing with the density of MOW plumes and eddies (McDowell and Rossby, 1978);

(3) In particular, changes in the water depth of the MOW tongue may depend on the mixing rate of MOW and Upper NADW, which is a product of boundary turbulence being proportional to the strength of advection from the source areas;

(4) Changes in the density of NEAW, which resulted from a delicate balance amongst the mixing rates of various upper intermediate water masses.

Our discussion is making use of the fact that our Atlantic site transect is covering slightly different water depths, with the proximal S. 548 drilled at 1250 m and the distal S. 982 somewhat shallower at 1135 m w. d.. The difference between 1250 m and 1135 m is possibly just sufficient for monitoring slight vertical shifts in the position of MOW “Meddies” (McDowell and Rossby, 1978; Kaese et al., 1985) (Fig. 2.1; Chapter 2).

To trace these goals we employ the following proxy values (modern values summarized in Tab. 6.5.1):

- (Epi-) benthic $\delta^{13}C$ records are used to compare differential trends in ventilation of MOW and Upper NADW (LSW) (Fig. 6.4.2).

- Mg/Ca-based BWT records may help to assess changing mixing rates between Upper NADW (~2°C) and MOW (~9.5°C, in the Gulf of Cadiz) (Fig. 6.4.1a).

- $\delta^{18}O_{b.w.}$ / BWS records indicate the evolution of changes in MOW inherited from the Mediterranean Sea.

- Our main evidence is derived from the evolution/shift of BWD as displayed in temperature–salinity graphs of Fig. 6.5.2.

- **Alboran Sea Site 978 (1930 m w. d.)**

  - ε_{Nd} = -9.5 ± 0.6
  - BWS = 38.4 psu
  - BWT = 13 °C
  - Density = 28.7 kg m^{-3}
  - Benthic $\delta^{18}O$ = 3.3‰ (Martrat et al., 2007)
  - Benthic $\delta^{13}C$ = 1.2‰ (V. Grazzini et al., 1986; Ligurian Sea; 1–1.5 km w.d.)
  - Concentration of dissolved O_2 = 4.55 ml

- **Site 548 in SW Ireland (1250 m w. d.)**

  - ε_{Nd} = -10.5 ± 0.3
  - BWS = 35.4 psu
  - BWT = 7.2 °C
  - Density = 27.4 kg m^{-3}
  - Benthic $\delta^{18}O$ = 2.66‰ (1)
  - Benthic $\delta^{13}C$ = ~ 1.1–1.3‰ (~NADW; Duplessy 1972; Kroopnick, 1980)
  - Concentration of dissolved O_2 = 4.89 ml/l (less than at S. 982)

- **Site 982 in the Rockall Plateau (1135 m. w. d.)**

  - ε_{Nd} = -10.9 (Scrivner et al., 2008)
  - BWS = 35.1 psu
  - BWT = 5.9 °C
  - Density = 27.6 kg m^{-3}
  - Benthic $\delta^{18}O$ = 2.88‰ (2)
  - Benthic $\delta^{13}C$ = 1.01‰ (Venz and Hodell, 2002)
  - Concentration of dissolved O_2 = 5.37 ml/l (> at S. 548, ~ no MOW)

- **Labrador Sea Water (LSW) off Iberia (1500 – 2000 m. w. d.)**

  - ε_{Nd} = -12 (Rickli et al., 2009) (Precise location: Bay of Biscay)
  - BWS = 35.3 psu
  - BWT = 5.8 °C
  - Density = 27.6 kg m^{-3}
  - Benthic $\delta^{18}O$ = 1.5 ‰
  - Benthic $\delta^{13}C$ = 1.75 ‰ (Zahn et al., 1997)
  - Concentration of dissolved O_2 = 4.7 ml/l (see Fig. 6.5.3)

Table 6.5.1. Modern bottom water properties at West Mediterranean Site 978, N. E. Atlantic Sites 548 and 982, and in Labrador Sea Water (LSW) off Iberia (T/S values from Schlitzer, 2007).

Similar total dissolved carbon isotopic values of NADW and MOW (~ 1 to 1.3‰; Duplessy 1972; Kroopnick, 1980) make it difficult to distinguish between those water masses at S. 548 and S. 982.

Outside the MOW tongue, the NADW and LSW have a concentration of dissolved O_2 of about 5.63 ml/l in the N. E. Atlantic (Fig. 6.5.3), as compared to 4.7 ml/l off Iberia.

(1) Measured on *Uvigerina peregrina* (Loubere, 1987) + 0.31 correction to correct for the offset of Loubere data with our data (see Chapter 3).

(2) Including a correction factor of +0.64 to convert $\delta^{18}O$ of *C. wuellerstorfi* into $\delta^{18}O$ of ambient seawater (data from Venz and Hodell, 2002)

(See also Fig. 6.5.3 – O_2 transect over the N.E. Atlantic)

5.2. Evidence for the evolution of MOW tongue in the northeast Atlantic

5.2.1. Nd records

From 3.6 – 2.8 Ma (MIS Gi1–G10), a constant difference of -0.5 marks the ε_{Nd} gradient from S. 548 to S. 982. It may reflect probably a largely constant flow and water depth of MOW. Near ~3.45 Ma, however, the gradient increases up to more than 2-ε_{Nd} units, when S. 982 depicts a 1.5-ε_{Nd} unit decrease down to -11.8, likewise after 2.7 Ma, when the ε_{Nd} signal at S. 982 reached about -11.4. Both events reflect perhaps an advection of “non-MOW” waters, that is LSW, to S. 982 (Fig. 6.1.2), which may imply a short-lasting reduction and possibly a shoaling of the MOW flow.

5.2.2. Carbon isotope records

Carbon isotope records serve as a tracer of the ventilation quality and possibly, also of the intensity of MOW. They show an average gradient of 0.2 ‰ (+0.4/-0.1) from the shallower S. 982 to the deeper S. 548. By contrast, the modern gradient is reversed with ~1.2‰ at S. 548 and ~1.1‰ at S. 982 (see Tab. 6.5.1). Likewise, a reversed $\delta^{13}C$ gradient of 0.15‰ also occurred over short periods in the Pliocene, over ~100-kyr between 3.45 Ma (MG6) and 3.35 Ma (MG 3) and over 4 kyr between 2.98 (MIS G19) and 2.94 Ma (MIS G17) (Fig. 6.4.2).

From 3.75 – 3.55 Ma (MIS Gi8/MG10) an initial massive 0.5‰-$\delta^{13}C$ increase precedes a subsequent drop until 3.45 Ma at Sites 982 and 548.

5.2.3. Sediment records of MOW physical ocean properties

As outlined in the introduction as event one (section 6.5.1), a major rise in BWS and BWD equally marks Sites 548 and 982 from 3.45 – 3.3 Ma, ends with an immense overshot at 3.3 Ma, and is inherited from changes in the Mediterranean (Fig. 6.4.1b,c).

From 3.25 – 3.0 Ma (MIS M2/G20), BWS and BWD remained at a constant oscillation level at all three sites. From 3.0 – 2.6 Ma (MIS G20/103), BWS and BWD of WMDW at S. 978 increased slightly by ~1-psu, initially defined as event 2. By contrast, BWD and BWS of MOW at proximal S. 548 showed a long-term decrease, whereas BWS and BWD of MOW at distal and proximal Sites 982 and 548 show no major change. BWS oscillated around a level that was 1–1.5 psu higher than today (~35.1 psu) (Fig. 6.4.1b). However, it appears significant that BWD of MOW at S. 982 were slightly higher than at S. 548 similar today (Fig. 6.4.1c), suggesting that the “core” of Pliocene MOW occurred approx. 100 m above S. 548, as today.

5.2.4. Major shifts in bottom water density

Long-term shifts in BWD at sites 978, 548, and 982 are summarized for three time slices between 3.7 Ma (MIS Gi5) and 2.6 Ma (MIS 103) (Fig. 6.5.2). During the first period 3.7 – 3.4 Ma (MIS Gi5/MG5), that is prior to the onset of the long-term BWD increase (Fig. 6.4.1c), BWD of WMDW varied between 28 and 28.5 kg m^{-3} near 28 kg m^{-3} and for MOW at sites 548 and 982. From 3.4 – 2.9 Ma (MIS MG5/G15), BWD of 28.5 and 29 kg m^{-3} were common to all three sites. From 2.9 – 2.6 Ma (MIS G15/103), BWD of WMDW at S. 978 increased to 29 and 29.5 kg m^{-3}, whereas BWD of MOW at S. 548 remained constant between 28.5 and 29 kg m^{-3}. By contrast, BWD at Site 982 also increased slightly to ~29 kg m^{-3}, similar to the values at S. 978, as long as this site was bathed in MOW.

At Site 982 the ε_{Nd} record showed a short event at ~2.67 Ma (MIS G4), when MOW was replaced by UNADW (≈ LSW) (Fig. 6.1.2). This conclusion is now fully corroborated by a coeval reduction of BWD by ~1 kg m^{-3}, likewise at S. 548 (Figs. 6.4.1c; 6.5.2).

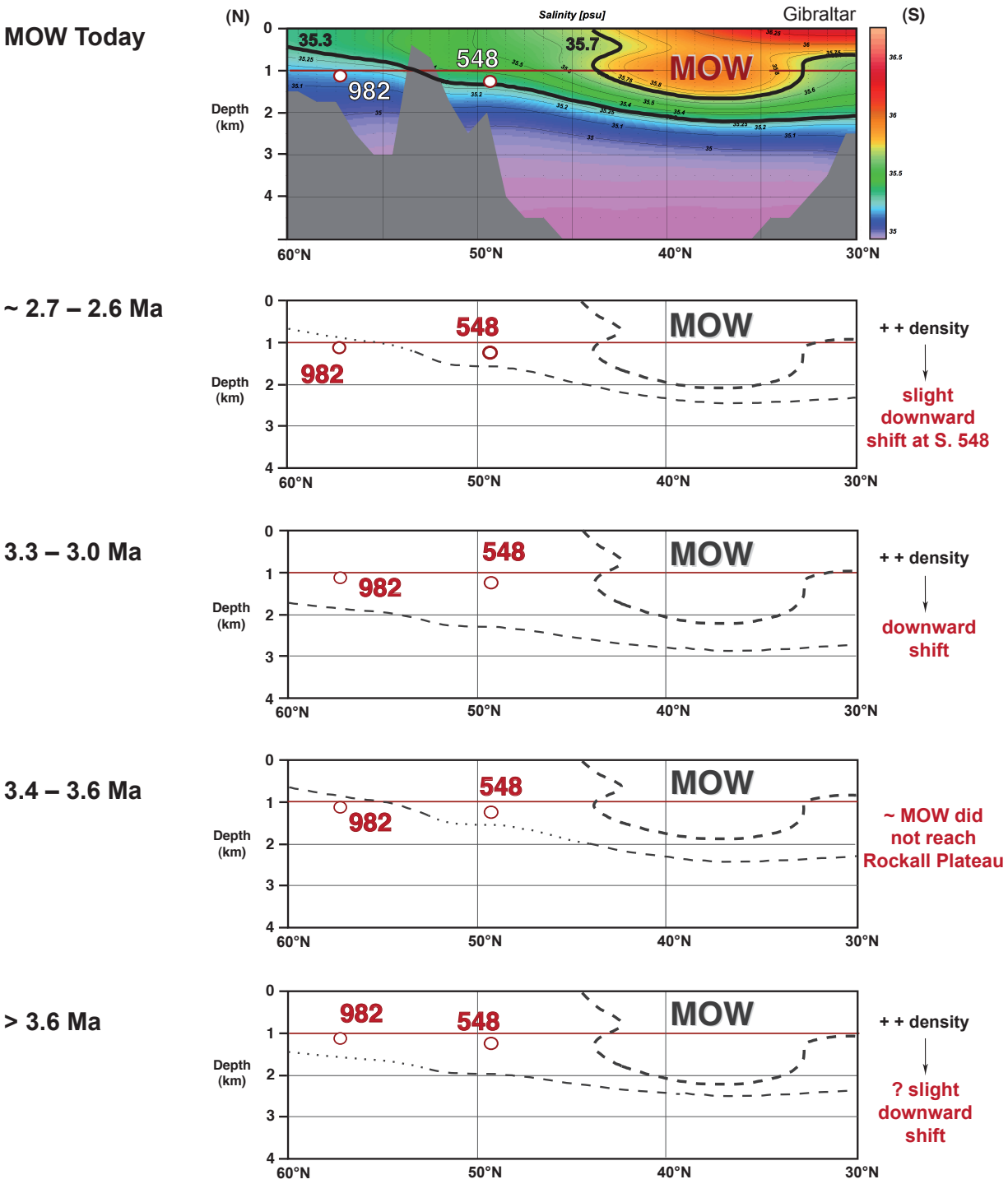

Figure 6.5.1. Scheme of Pliocene changes in the depth position of MOW layer in the northeast Atlantic during 4 time slices as compared to today (Ocean Data View; Schlitzer, 2007). Hypothetical paleosalinity isolines equivalent to modern 35.3 and 35.7 psu values are displayed.

5.3. Discussion of Pliocene depth position vs. flow intensity of MOW in the northeast Atlantic

Besides potential but totally unknown variations in global preformed benthic $\delta^{13}C$ (Duplessy et al., 1988), a ventilation higher than that of UNADW is characteristic of the core of MOW (Zahn et al., 1997). Thus $\delta^{13}C$ at the shallower S. 982 is about ~0.2‰ higher than at S. 548, which today is bathed in waters near to the bottom of the MOW "pipeline" (i.e., ~1250–1500 m w. d.), where somewhat more UNADW is admixed than at S. 982 lying closer to the core of MOW (Fig. 6.4.2b,c).

By contrast, ε_{Nd} records (Fig. 6.1.2) do not directly support this model: About 0.5 higher ε_{Nd} values at S. 548 (i.e., less dilution of MOW) indicate the closer proximity of this site to the MOW source and less admixture of UNADW. However, other sources of evidence such as the BWD records are in harmony with the $\delta^{13}C$ results. For example, BWD after 3.0 Ma were somewhat higher at the shallower S. 982 than at S. 548 (Figs. 6.4.1c; 6.5.2). Accordingly, the density of MOW near 1135 m w. d. (S. 982), that is near the MOW core was higher than ambient to Site 548 (1250 m w. d.). Today the MOW core is centered near 1000 – 1100 m w. d.

5.3.1. Evolution of water depths of the MOW core

Subsequent to a short interval from ~3.6 to ~3.4 Ma, when $\delta^{13}C$ values at S. 982 were as low as 0.8‰ (also recorded at S. 548 near 0.5‰) and ε_{Nd} values near -11.5 to -12, and thus excluded MOW advection (Fig. 6.4.2b) the MOW layer spread to water depths deeper than 1135 m w. d. almost continuously until 2.7 Ma. Subsequent to ~3.62 Ma (MIS Gi1) WMDW at S. 978 shows a short but distinct $\delta^{13}C$ maximum of 0.9–1.1‰ lasting until 3.58 Ma (MIS MG12) (Fig. 6.4.2a). That means that the coeval ventilation maximum of MOW in the northeast Atlantic was possibly origin controlled.

From ~3.60 to 3.45 Ma (MIS Gi6–MG6), MOW was better ventilated at S. 982 (0.7–0.9‰ $\delta^{13}C$ at 1135 m w. d.) than at S. 548 with 0.5–0.6‰ $\delta^{13}C$ at 1250 m w. d.. This $\delta^{13}C$ gradient suggests that the MOW core was closer to S. 982 that is shallower than S. 548 at 1250 m, where the bottom water ventilation was much lower than that in the Alboran Sea source region (0.7–0.9‰ $\delta^{13}C$ at S. 978) (Fig. 6.4.2). During that time BWD was low, with oscillations centered near 27.4 kg m^{-3} at both Atlantic sites (Fig. 6.4.1c). Inside the Mediterranean, BWD values oscillated around a similar level of 27.0 – 28.5 kg m^{-3}, which shows that the core of MOW was not diluted

that much at all in the northeast Atlantic. Likewise, ε_{Nd} values at S. 982 reached almost -10 (close to the level at S. 548) and thus confirm that the core of MOW was little diluted S. 982.

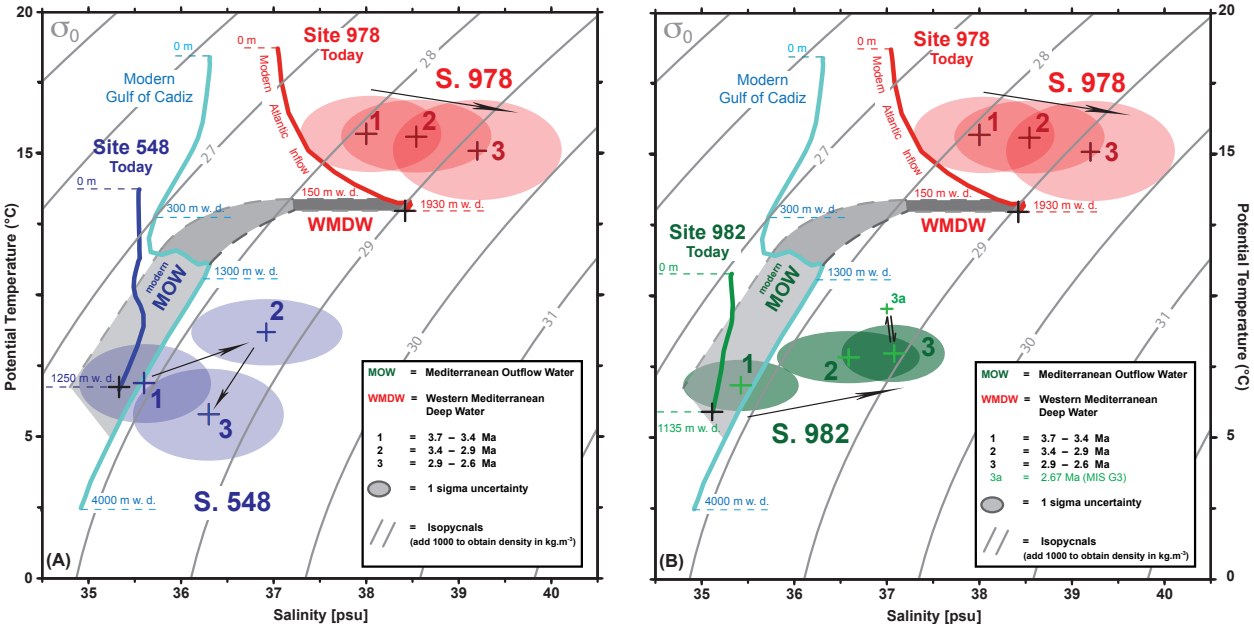

Figure 6.5.2. Temperature/salinity plots of Western Mediterranean Deep Water (WMDW) at Alboran Sea Site 978 and Mediterranean Outflow Water (MOW) at northeast Atlantic Sites 548 and 982. Fine solid lines are lines of equal density. Arrows indicate local variations in the density of MOW over various time slices from 3.7 to 2.6 Ma.

In summary, it appears that the core of MOW occupied a depth level from ~3.60 – 3.45 Ma (MIS Gi5-Gi6/MG6) that was similar to today, that means it was closer to 1135 m than 1250 m w. d.. The modern density level of 27.5–27.8 kg m^{-3} is slightly higher (Ambar et al., 2002). Accordingly, the level of MOW "Meddies" above the Rockall Plateau was probably higher than today.

As previously outlined in sections 6.5.1 and 6.5.2 a dramatic BWD increase ("event no. 1") occurred almost synchronously at all three sites studied from 3.45 – 3.3 Ma (MIS MG6–M2), and ended with a sharp "overshoot" of 30–31 kg m^{-3} in BWD near MIS M2. We interpreted this event by enhanced MOW advection (Fig. 6.4.1b,c and Discussion in section 6.1). During this event and different from preceding and subsequent times, $\delta^{13}C$ values at S. 548 were about equal and/or 0.1‰ higher than at S. 982 (Fig. 6.4.2b,c). In the beginning, event no. 1 was matched by a slight decrease of ε_{Nd} down to -11 at distal S. 982 (Fig. 6.1.2) and by low $\delta^{13}C$

values both in the Alboran Sea (0.7–0.8‰) and at Sites 982B (0.5‰) and probably also at S. 548 (core gap), certainly at 3.35 – 3.25 Ma. At present we are unable to reconcile the opposed trends of strongly increased BWD and low ventilation values and poorly documented, but low ε_{Nd} values in terms of an elevated or lowered position of the MOW layer in the northeast Atlantic.

From 3.3 – 3.0 Ma (MIS M2–G20), the ε_{Nd}-gradient between sites 982 and 548 had reached a minimum of <0.4 (Fig. 6.1.2), except for an enigmatic short-lasting ε_{Nd} excursion at S. 548 near 3.15–3.1 Ma. BWD showed a constant range up to a level ~1 kg m^{-3} higher than today (28.5 kg m^{-3}; Fig. 6.4.1c), with almost no more BWD gradient established between Sites 548 and 982. It appears that the entire water column from 1135 to 1250 m w. d. was uniformly controlled by a high advection of MOW. Possibly this uniformity – at a high density level – implies that the MOW layer was lowered during this time by more than 100 m, that S. 548 moved into the core of the MOW layer.

From 3.0 to 2.8 Ma (MIS G20/103), a decrease in BWS led to a slight decrease in BWD at S. 548 (Fig. 6.4.1b,c), a decrease not seen at S. 982, hence to decreased uniformity of the MOW layer. This differentiation suggests most likely an upward shift of the MOW layer that was reflected by any changes inside the Mediterranean: S. 978 just shows a slight increase in BWD by +0.5 kg m^{-3}. The loss of uniformity of MOW is also recorded by a significant increase in the gradient of ε_{Nd} between Sites 548 and 982. Accordingly, we may indeed conclude on an upward shift of MOW.

Subsequent to 2.8 Ma until 2.5 Ma the ventilation of MOW at sites 548 and 982 likewise decreased significantly from 1.3–1.0 ‰ to 0.5–0.3‰ (Fig. 6.4.2b,c), in contrast to a constant $\delta^{13}C$ level of WMDW at S. 978 (Fig. 6.4.2a). Thus the change in MOW ventilation won't have been controlled by changes in the Mediterranean source region but only by a reduction of the Mediterranean outflow, most likely by the sea level drop that induced a much reduced aperture of the Strait of Gibraltar. The reduced flow of Mediterranean waters in turn finally was subject to enhanced admixture of neighbor Atlantic intermediate waters.

This process was paralleled by a slight decrease of less than 0.5-ε_{Nd}-unit at S. 548 and most prominent but reversible at S. 982 near ~2.67 Ma (MIS G3) (Fig. 6.1.2), when ambient North Atlantic waters dominated at water depths lower than 1135 m w. d., also paralleled by a major, but short-lasting BWD minimum at 2.65 Ma (Fig. 6.4.1c). During that time the depth of the MOW layer had probably shifted to depths of less than 1135 m w. d., possibly due to further sea level induced reductions in the aperture of the Strait of Gibraltar and reduced MOW flow.

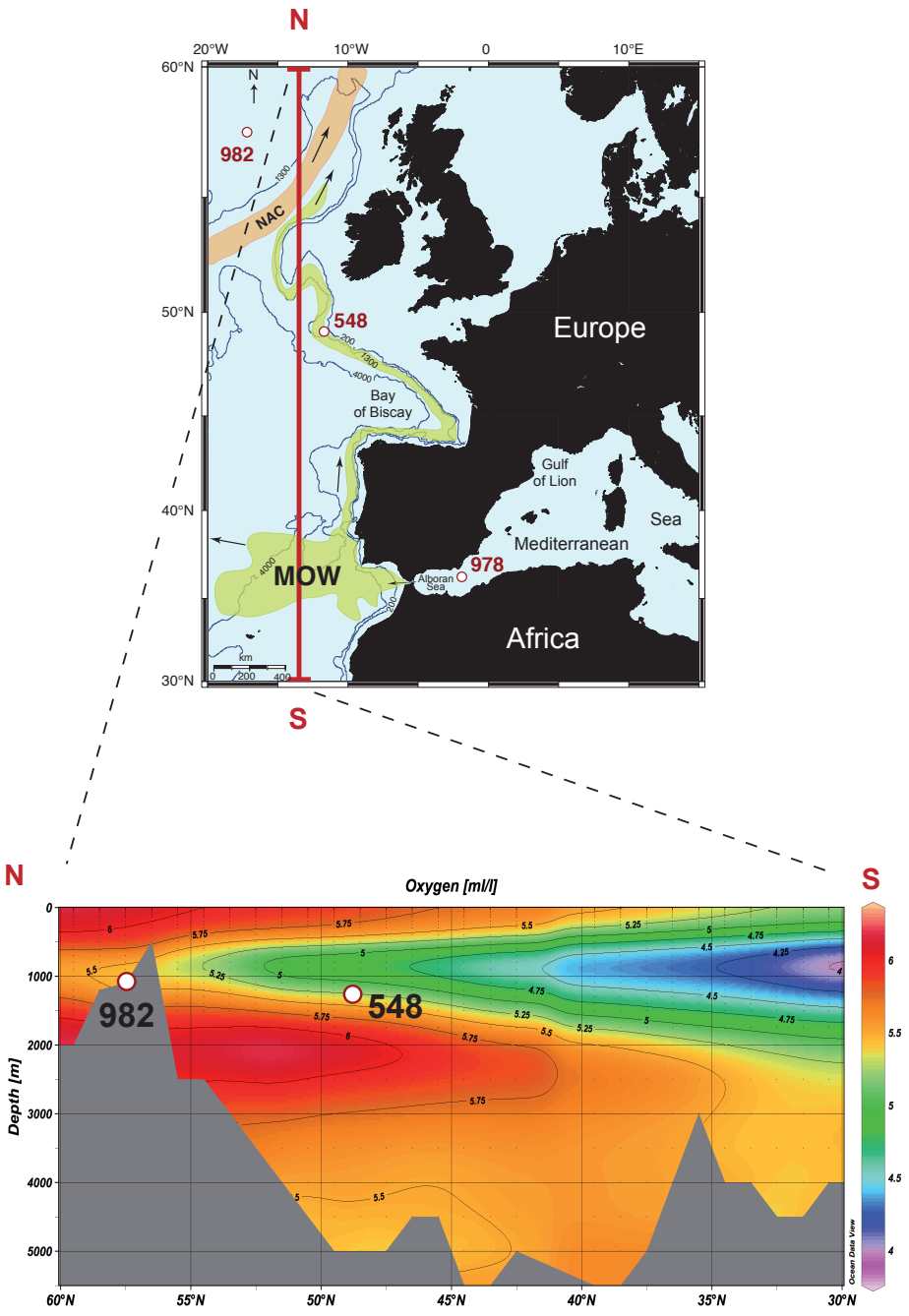

Figure 6.5.3. North – south transect showing the O_2 content of MOW in the northeast Atlantic.

Chapter 7

Potential links between the MOW salt discharge and (Upper) North Atlantic Deep Water formation, 3.5 – 3.3 Ma and 2.8 – 2.5 Ma?

1. Introduction

MOW enters the eastern margin of the subtropical gyre and subsequently flows toward the northeast Atlantic. Finally it may spill into the Nordic seas after mixing from with the North Atlantic Current (NAC) near the Rockall trough (McCartney and Mauritzen, 2001). This is just a weak suspicion, but little substantiated yet by oceanographic data. The NAC maintains the relatively warm climate over western Europe and Scandinavia (Bigg, 1996) by the release of heat during NADW formation (*see* Siedler et al., 2001). This mechanism is salt driven, hence possibly influenced by MOW salt discharge (Reid, 1979).

Enhanced or reduced Mediterranean salt discharge was related to changes in the incursion of MOW during the Pliocene. Thus these variations may have influenced climate changes over northwest Europe. For example, today we calculate that ~3.5 Gt (≈ 1.8 km^3) of salt are exported every day to the Atlantic Intermediate water masses. A 2-psu increase in the salinity of MOW at 30–40 m sea level higher than today near 3.45 Ma (Khélifi et al., 2009) may result in about 4.5 Gt/day of salt export (assuming a sill depth at Gibraltar similar to today), that is 1 Gt/day more than today.

In view of various controversial studies (e.g., Reid, 1979; Rahmstorf, 1998; as discussed below) on the potential influence of MOW salt discharge on North Atlantic MOC, we discuss here the following items:

(1) Whether distinct changes in bottom salinity and density of MOW based on a multi-proxy study at sites 548 and 982 in the northeast Atlantic from 3.5 – 3.3 Ma (Khélifi et al., 2009) may have resulted in coeval changes in the ventilation of NADW in the northeast Atlantic (Kleiven et al., 2002). In particular, we trace changes in the ventilation of distal upper NADW at Caribbean Sea Site 999 (Haug and Tiedemann, 1998) and at sites 704 (Hodell and Venz, 1992) and 1092 (Andersson et al., 2002) in the South Atlantic.

(2) Whether a slight increase (~0.5 kg m^{-3}) in BWD of MOW after 2.9 Ma (following the onset of NHG) was of any influence on NADW formation (Fig. 7.1a,b).

2. Mid-Pliocene changes in North Atlantic Deepwater (NADW) ventilation as potential record of changing strength of deepwater formation

Major events and states of NADW ventilation are compared to five different states of MOW incursion equally displayed at sites 548 and 982 (Fig. 7.1; $\delta^{13}C$ values and trends listed in Tab. 7.1). We start from the expectation that higher salt discharge induce stronger NADW formation and ventilation.

From 3.75 to 3.6 Ma, a time when BWD of MOW were low or decreasing near 28 kg m^{-3}, that is only ~0.5 kg m^{-3} higher than today, $\delta^{13}C$ values show a gradual 0.25‰ increase in the ventilation of distal UNADW at Site 999 (2828 m w. d.) (Haug and Tiedemann, 1998) and Site 704 (2532 m w. d.) (Hodell and Venz, 1992) (Fig. 7.1c,d), however, not S. 1092, where $\delta^{13}C$ shows two extreme minima (Fig. 7.1e). A ~0.25‰ increase also occurs in the ventilation of distal LNADW at Site 607 (3427 m w. d.) (Kleiven et al., 2002) (Fig. 7.1f).

During the extreme minimum of MOW injection near ~3.6 – 3.4 Ma, a low BWD level of MOW was similar to that today (near 27.5 kg m^{-3}) (Fig. 7a,b). The minimum was coeval with a minor ~0.25‰ gradual decrease in the ventilation of both LNADW at Site 607 (3427 m w. d.) (Kleiven et al., 2002) (Fig. 7.1f) and distal UNADW at Site 999 (2828 m w. d.) (Haug and Tiedemann, 1998) (Fig. 7.1c). In contrast, distal UNADW at sites 704 (2532 m w. d.) (Hodell and Venz, 1992) and 1092 (1976 m w. d.) (Andersson et al., 2002) (Fig. 7.1d,e) show an opposite trend that is an initial slight increase by less than 0.2‰ (possibly controlled by a dominant influence of the Antarctic Circumpolar water).

From 3.4 to 2.9 Ma, BWD were generally high, culminating at 3.25 Ma and 3.05 Ma with values up to ~1.5 kg m^{-3} higher than today (near 29 kg m^{-3}) and oscillating around 28.5 kg m^{-3} (Fig. 7a,b). During that time, LNADW ventilation increased by 0.25‰ from 3.25 Ma to 2.9 Ma ago at Site 607 (3427 m w. d.) (Kleiven et al., 2002) (Fig. 7.1f); a trend starting only >200 ky after the rise in BWD of MOW (Fig. 7a,b). However, this trend of increased ventilation does not match any ventilation trends depicted at any other NADW sites. In particular, UNADW ventilation at Site 999 increased slightly by ~0.25‰ and reached a short-lasting maximum of 0.75‰ near 3.4

– 3.2 Ma. Subsequently, $\delta^{13}C$ decreased slightly before oscillating continuously at the high level near 0.75‰ (Fig. 7.1c). The more distal UNADW sites 704 and 1092 (Fig. 7.1d,e) do not show any coherence between bottom water ventilation changes and trends in MOW density during that time (Fig. 7.1a,b). Subsequent to 3.0 Ma, the ventilation of distal UNADW first oscillated toward higher values near 0.5‰, in contrast to slightly decreasing BWD of MOW (Fig. 7.1 a-b).

From 2.9 to 2.7 Ma, BWD oscillations of MOW increased slightly from 28.5 kg m^{-3} (~1 kg m^{-3} higher than today) to almost 29 kg m^{-3} (Fig. 7a,b) possibly linked to an upward shift of the MOW tongue. Both proximal positions of UNADW (Site 999; 2828 m w. d.) and LNADW (Site 607; 3427 m w. d.) just record a 0.25–0.5‰ ventilation decrease, about 120 ky prior to that of distal UNADW (sites 1092 and 704) (Fig. 7c,d).

After 2.7 Ma ago, BWD oscillations of MOW increased slightly from 28.5 to 29 kg m^{-3} (Fig. 7a,b). On the other hand, both sites 999 (2828 m w. d.) and 607 (3427 m w. d.) record a 0.25–0.5‰ decrease. This ventilation decrease was clearly marked by negative excursions and oscillations with large amplitudes at Site 607, perhaps a result of intermittent AABW incursions (Fig. 7c,d). In summary, MOW and NADW records show hardly any coherency.

Site	S. 548 (Fig. 7.1a) BWD	S. 982 (Fig. 7.1b) BWD	S. 999 (Fig. 7.1c) $\delta^{13}C$	S. 704 (Fig. 7.1d) $\delta^{13}C$	S. 1092 (Fig. 7.1e) $\delta^{13}C$	S. 607 (Fig. 7.1f) $\delta^{13}C$
Water depth	1251 m	1134 m	2828 m	2532 m	1976 m	3427 m
Location	Goban Spur	Rockall Plateau	Caribbean Sea	Subpolar SE Atlantic	Subpolar SE Atlantic	Mid-Atlantic Ridge
Water mass	MOW UNADW (Admixed)	MOW UNADW (Admixed)	UNADW (Distal)	UNADW (Distal, SA)	UNADW (Distal, SA)	LNADW (NA)
3.75–3.60 Ma	~0.5 kg m^{-3} decrease	~0.5 kg m^{-3} decrease	0.25‰ increase	0.25‰ increase	Stable near 0.25‰	0.25‰ increase
3.60–3.45 Ma	A level similar to today ~27.5 kg m^{-3}	A level similar to today ~27.5 kg m^{-3}	0.25‰ decrease	Stable near 0.5‰	Stable near 0.5‰	0.25‰ decrease
3.45–2.90 Ma	Distinct culminations in BWD at 3.25 and 3.05 Ma (near 29 kg m^{-3})	Distinct culminations in BWD at 3.25 and 3.05 Ma (near 29 kg m^{-3})	Stable near 0.6‰	Stable near 0.5‰	Stable near 0.5‰	Gradual and long-term 0.25‰ increase after 3.2 Ma
				0.25‰ decrease near 3.0 Ma	0.25‰ decrease near 3.0 Ma	
2.90–2.70 Ma	Slight increase from 28.5 to 29.0 kg m^{-3}	Slight increase from 28.5 to 29.0 kg m^{-3}	0.25‰ decrease	0.35‰ decrease	0.5‰ decrease	0.25‰ decrease
2.70–2.50 Ma	Further increase	Further increase	Slight decrease (~0.16‰)	-	-	0.5‰ decrease

Table 7.1. Comparison of major changes in MOW density with changes in Atlantic deep-water ventilation (reflected in epibenthic $\delta^{13}C$). BWD: Bottom water density. NA: North Atlantic. SA: South Atlantic. MOW: Mediterranean Outflow Water. UNADW: Upper North Atlantic Deep Water. LNADW: Lower North Atlantic Deep Water.

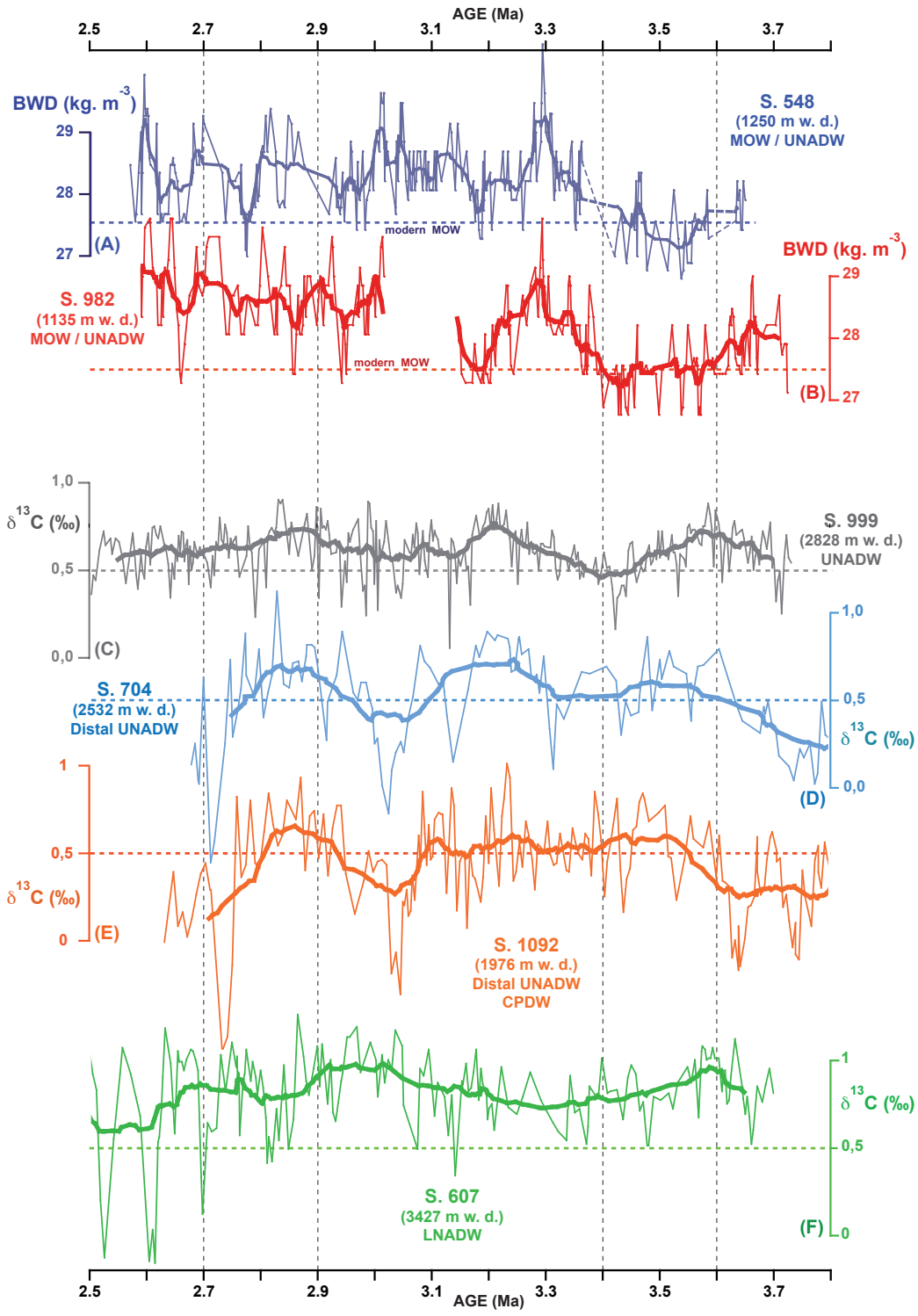

Figure 7.1. Pliocene changes in bottom water density of MOW at northeast Atlantic Site 548 and Site 982 (A and B) as compared to ventilation changes (epibenthic $\delta^{13}C$) of Upper North Atlantic Deep Water (NADW) at Caribbean Sea Site 999 (Haug and Tiedemann, 1998) (C) and Southern Ocean Sites 704 and 1092 (Andersson et al., 2002) (D and E) and Lower NADW at S. 607 (Kleiven et al., 2002) (F).

3. Discussion

As outlined above and discussed in Chapter 6, major changes in Pliocene MOW advection are:

(1) A major and long-term intensification of MOW from 3.45 to 3.25 Ma, which was documented by ~2 psu (BWS) and 1–1.5 kg m^{-3} (BWD) increase at both sites 548 and 982 (Fig. 7.1a,b). As outlined in section 6.1, this event was triggered by an aridification around the Mediterranean region, which resulted in an increase by ~1-psu in BWS and ~1-kg m^{-3} in BWD of WMDW (Fig. 6.4.1b,c). During that time, the advection of salt to the northeast Atlantic is roughly estimated near 4.5 Gt/day (≈ 2.3 km^3/day) that is about 1 Gt higher than today.

(2) With the onset of major NHG (2.95 – 2.8 Ma), a possible upward shift of the MOW tongue to depths shallower than 1250 m w. d. occurred in the northeast Atlantic, as recorded by a 3°C and 2-pu decrease in BWT and BWS at Site 548 (Fig. 6.4.1a,b,c). This event was paralleled by an increase in NADW formation (Bartoli et al., 2005). During that time, BWD of MOW was marked by a slight (~0.5 kg m^{-3}) increase (Fig. 7.1a,b).

Three main questions concern the relationship and linkages between changes in MOW incursion and the rate of NADW formation:

(1) Did the advection of additional MOW salt to northeast Atlantic intermediate waters near 3.45 – 3.3 Ma (rough flux estimate: 1 Gt/day higher than today) contribute to an additional formation of NADW and an intensification of the AMOC?

(2) Did the increased level of MOW salt advection to the northeast Atlantic (continuous discharge of ~4.5 Gt/day) also contribute to the onset of major NHG (~2.95 – 2.8 Ma)?

(3) In turn, did an increase in the formation of NADW lead to a slight shoaling of the MW tongue (by a shift in the relative buoyancy)?

Following (Reid, 1979) the effects of the advection of heat and salt with MOW may be far reaching. His postulate was based on series of observations and speculations that MOW salt advection may precondition the NADW formation (e.g., by adding more salt to the Nordic seas). This may result in enhanced North Atlantic MOC and contribute to the global climate change.

Reid claimed that although the (highly saline) NAC may dominate the pole-ward transport of salt, MOW salt may contribute significantly to the overall salt injection to deep water formation cells in the Nordic Seas. Reid's hypothesis was proposed for modern MOW advection of about 1–2 Sv (roughly 3.5 Gt of salt per day). An increase of MOW salt injection up to 1 Gt/day higher than today near 3.4 Ma may thus be expected to enhance the AMOC and NADW formation.

More cautious and skeptical views on the role of MOW salt discharge were discussed in several studies. For example, based on OCM experiments Rahmstorf (1998) suggests that changes in the Mediterranean salt budget resulting from the Aswan Dam are by far too insignificant to produce the outlined climatic consequences, and thus Johnson's postulate is unfounded. Today, the Mediterranean saltwater outflow has a small effect on the North Atlantic MOC and surface climate by enhancing the formation of NADW by 1-2 Sv, a rate that is near the uncertainty range of the total volume of NADW formed in the North Atlantic (~15±2 Sv) (Ganachaud and Wunsch, 2000).

During times when the Mediterranean salt discharge ceased as result of the Messinian Salinity Crisis (MSC), there is no evidence for any significant change in NADW circulation (Keigwin, 1987). The authors claimed that $\delta^{13}C$ average values of NADW were around 1‰ all over the last 6 Ma as today (Kroopnick et al., 1985; Sarnthein et al., 1994; Curry et al., 1988) as recorded from several DSDP Sites throughout the North Atlantic. Accordingly, it appears that the North Atlantic was permanently bathed in NADW, even during periods of a shutdown of MOW salt discharge prior to ~5.3 Ma.

Likewise, a short-lasting phase of estuarine circulation in the Mediterranean, led probably to a lack of MOW during the earliest Pliocene that was without any influence on NADW formation (Thunnel et al., 1987). Also, the effect of modern MOW salt advection on NADW is still little supported by modern observations (McCartney and Mauritzen, 2001) and modeling studies (Kahana et al., 2007).

Recent reconstructions of MOW changes in the Gulf of Cadiz for the last glacial period show evidence for a strong outflow because of enhanced Mediterranean aridity (Rogerson et al., 2006; Voelker et al., 2006). These authors suggest a MOW salt build-up that might have had a bigger impact on AMOC, at times when NADW formation was weak, in particular during a deglacial state (Rogerson et al., 2006). Also, a modeling study of Bigg and Wadley (2001) points to MOW as a potential trigger for the glacial AMOC. However, further modeling studies on the potential impact of MOW salt advection are needed to verify/refute this hypothesis, in particular

for periods of collapsed AMOC (such as during deglacial Heinrich events; Sarnthein et al., 1994).

Here we discuss the two events that marked BWD of MOW (Figs 7.1a,b) and their potential linkages to changes in the ventilation of lower and upper NADW as outlined above (Table 7.1).

– (1) Event 1 (3.45 – 3.25 Ma): The enhanced NADW production did not translate into trends of better ventilation at any of the sites studied. For example, the LNADW ventilation record at S. 607 (3427 m w. d.) (Kleiven et al., 2002) shows a long-term increase of 0.25‰ only after 3.2 Ma, reaching 1‰ (modern level: 1.1‰; Curry et al., 1988) near 2.9 Ma. However, the ventilation decreases subsequently by 0.25‰ from 2.9 to 2.7 Ma, different from the increase in BWD of MOW (Fig. 7.1f). The increase in MOW density from 3.45 – 3.25 Ma was only accompanied by a coeval 0.25‰ increase of (distal) UNADW ventilation at S. 999 (2828 m w. d.) up to a level near 0.75‰, which continued until approx. 2.8 Ma (Haug and Tiedemann, 1998) (Fig. 7.1c). This is obviously the only linkage to be observed between a rise in MOW density and enhanced (U) NADW ventilation, in case no other, still unknown factors have resulted in the slight $\delta^{13}C$ rise at S. 999. However, UNADW did not show any ventilation increase such at S. 999 at the more distal positions in the southern Atlantic Ocean (S. 704 and S. 1092) (Fig. 7.1e,d) (Table 7.1).

In summary it appears that the increased advection of salt with MOW from 3.45 – 3.25 Ma (~1 Gt/day higher than today) was hardly matched by any change in NADW formation, as was suggested by the salt discharge hypothesis.

This conclusion does not totally exclude the role of MOW salt advection in the NADW formation for preconditioning MOC, especially during periods of decreased AMOC (Rahmstorf, 1998; Bigg et al., 2003). In total, a 2-psu rise in MOW salinity from 3.45 – 3.25 Ma (1 Gt/day higher than today) may possibly have been sufficient to strengthen the ventilation of the UNADW as depicted at S. 999. Middle and lower NADW remained unaffected.

– (2) Event 2 (2.9 – 2.6 Ma): The second case to be tested concerns the increase in BWD of MOW by 0.25–0.5 kg m^{-3} after 2.9 Ma. In contrast to the slight rise in MOW BWD, we find a gradual decrease in benthic ventilation (up to -0.5‰) at all four Atlantic sites studied, in particular during glacial stages after ~2.8 Ma (Figs 7.1c,f). This may reflect an oscillating decrease in the relative flux of NADW with an increasing number of glacial and meltwater scenarios in the North Atlantic (Hodell and Venz, 1992; Raymo et al., 1992).

By contrast, Bartoli et al. (2005) show a major long-term drop in BWT and rise in benthic $\delta^{18}O$ that reflect higher NADW salinity and density. Thus they conclude on a long-term enhanced AMOC during that time (e.g., over the first step of the onset of major NHG; 2.95 – 2.8 Ma). It is not clear (at least based on these records) how to reconcile the long-term increase in NADW density with the decrease in $\delta^{13}C$ ventilation over the onset of major NHG.

In summary, the distinct change in MOW advection and salt injection after 2.9 Ma was not linked to any coeval change in the ventilation of NADW. Since the first event (3.45 – 3.25 Ma) only matches a single potential response of (distal Upper) NADW, we may conclude that in total the influence of MOW salt injections into the North Atlantic MOC may be too small to produce significant effects. That means that the speculations of Reid (1979) cannot be corroborated yet by paleoceanographic evidence.

Chapter 8
Conclusions

Largely continuous paleooceanographic records of bottom water origin and ventilation, SST, BWT, BWS and BWD were generated with millennial-scale resolution from three ODP/DSDP Sites in the Alboran Sea (S. 978; 1930 m w.d.) and along the northeast Atlantic continental margin at Sites 548 (1250 m w.d.) and 982 (1135 m w.d.). The aim was to study variations in MOW and its salt discharge as compared to Pliocene changes in North Atlantic thermohaline circulation prior and during the onset of major NHG, 3.7 – 2.6 Ma.

High ε_{Nd} values of –11 to –9 show that MOW was advected continuously to the northeast Atlantic throughout the Upper Pliocene and reached up to the Rockall Plateau from 3.4 until 2.7 Ma and after 2.55 Ma. We find clear evidence for a major and long-term Pliocene intensification of MOW from 3.5 – 3.3 Ma. During that time, northeast Atlantic Sites 548 and 982 showed a singular and persistent increase in bottom water salinities (BWS) by ~2 psu and in densities (BWD) by 1 kg m^{-3}, which was matched by an ~1°–3°C increase in BWT. This event was coeval with a unique rise in bottom water salinities by 0.75–1 psu and in densities by ~1 kg m^{-3} of MOW near its West Mediterranean source at Site 978.

This event suggests that the onset of strongly enhanced deep-water convection in the Mediterranean Sea and the related increase in MOW flow (roughly estimated ~1 Gt/day higher than today) were a result of major aridification in the Mediterranean source region (Fauquette et al., 1998). The change in Mediterranean hydrology most likely originated from key changes in the African monsoon system, as shown by increasingly dry conditions depicted in terrestrial records from East Africa near that time (Trauth et al., 2005; 2007).

Precisely at that time, the surface waters of the Alboran Sea underwent a period of increasing nutrient contents (lower planktic $\delta^{13}C$) from 3.5 to 3.3 Ma. This increase was most likely linked to an enhanced Atlantic inflow of nutrient enriched surface waters that compensated for the then enhanced outflow of MOW (as modeled by Alhammoud et al., in press).

Following model suggestions (e.g., Reid, 1979; Rahmstorf, 1998; Bigg et al., 2003), the enhanced MOW flow from 3.5 – 3.3 Ma might have induced an intensification of Upper NADW formation. By contrast, the increased advection of salt with MOW did not translate into any

trends of better ventilation ($\delta^{13}C$) of Lower NADW at S. 607 (Kleiven et al., 2002) and Upper NADW at southern Atlantic Sites 704 (Hodell and Venz, 1992) and 1092 (Andersson et al., 2002). The only linkage is observed at Caribbean Sea S. 999 with a slight $\delta^{13}C$ rise (Haug and Tiedemann, 1998), in case no other, still unknown factors have resulted in this ameliorated ventilation.

Over the onset of major NHG from ~3.0 – 2.7 Ma, the long-term average BWT at S. 548 decreased by 2–3°C below modern level (~7°C) and BWS by 2 psu until 2.82 Ma (MIS G10). However, BWT and BWS at S. 982 continued to oscillate at a level that was 3°C and 1.5-psu higher than today, respectively. Generally, BWD were slightly higher at the shallower S. 982 than at S. 548. Accordingly, it appears that the first step of enhanced production of UNADW, that is of North Atlantic MOC from ~2.95 – 2.80 Ma (Bartoli et al., 2005) may have diluted and/or rather displaced the MOW tongue upward in the region southwest of Ireland (S. 548) up to a level shallower than 1250 m w. d.. However, the lowering of BWD at S. 548 apparently was not sufficient to shift the MOW core upward completely beyond the depth of S. 548 because BWD still was about 0.5-kg m^{-3} higher than today.

By contrast, after 2.7 Ma BWT and ventilation of MOW over the Rockall Plateau (S. 982) decreased to a level similar to today, whereas BWS and BWD continued to be high. This finding is corroborated by a short lasting significant reduction of ε_{Nd} values over the Rockall Plateau down to the NADW level. Accordingly, the MOW tongue may have disappeared for a short interval but reappeared after ~2.6 Ma on Rockall Plateau.

The distinct change in MOW advection and salt injection after 2.9 Ma was not linked to any coeval change in the ventilation of NADW. Since the previous event (~3.5 – 3.3 Ma) of increase in MOW advection only matches a single and potential response of (distal Upper) NADW at S. 999, we may conclude that the influence of MOW salt injections into the North Atlantic MOC may be too small to produce any significant effects. That means that the postulate of Reid (1979) and others cannot be corroborated yet by paleoceanographic evidence.

References

A

Abrantes, F., H. Megers, S. Nave, et al., 2002: Fluxes of micro-organisms along a productivity gradient in the Canary Islands region (29°N): Implications for paleoreconstructions: Deep-Sea Research. Part II, Topical Studies in Oceanography, 49, pp. 3599–3629, doi: 10.1016/S0967-0645(02)00100-5.

Alhammoud, B., P. Th. Meijer, and H. A. Dijkstra, 2010: Sensitivity of Mediterranean thermohaline circulation to gateway depth: A model investigation, Paleoceanography, doi:10.1029/2009PA001823, in press.

Ambar, I., N. Serra, M. J. Brogueira, et al., 2002: Physical, chemical and sedimentological aspects of the Mediterranean outflow off Iberia, Deep-Sea Research II, 49, pp. 4163–4177.

Anand, P., H. Elderfield, M.H. Conte, 2003: Calibration of Mg/Ca thermometry in planktonic foraminifera from a sediment trap time series, Paleoceanography, 18 (2), P1050.

Andersson, C., D. A. Wanke, J. E. T. Channell, et al., 2002: The Mid-Pliocene (3.6–2.6 Ma) benthic stable isotope record of the Southern Ocean: ODP Sites 1092 and 704, Meteor Rise, Palaeogeogr. Palaeoclimatol. Palaeoecol., S0031-0182(01)00494-1.

Armi, L., W. Zenk, 1984: Large lenses of highly saline Mediterranean Water, J. Phys. Oceanogr., 14, pp. 1560–1576.

B

Bard, E., 2001: Comparison of alkenone estimates with other paleotemperature proxies, Geochem. Geophys. Geosyst., 2, 1002, doi:10.1029/2000GC000050.

Baringer, M. O'Neil, J. F. Price, 1997: Mixing and spreading of the Mediterranean outflow, Journal of Physical Oceanography, 27 (8), 1654-1677.

Barker, S., M. Greaves, H. Elderfield, 2003: A study of cleaning procedures used for foraminiferal Mg/Ca paleothermometry, Geochemistry, Geophysics, Geosystems, 4, pp. 8407, doi: 10.1029/2003GC000559.

Bartoli, G., M. Sarnthein, M. Weinelt 2006: Late Pliocene millennial-scale climate variability in the northern North Atlantic prior to and after the onset of Northern Hemisphere glaciation, Paleoceanography, 21, PA4205, doi:10.1029/2005PA001185.

Bartoli, G., Sarnthein, M., Weinelt, M., Erlenkeuser, H., Garbe-Schönberg, D., and Lea, D.W., 2005: Final closure of Panama and the onset of northern hemisphere glaciation: Earth and Planetary Science Letters, 237, p. 33–44, doi: 10.1016/j.epsl.2005.06.020.

Bemis, B.E., H. J. Spero, J. Bijma, et al., 1998: Reevaluation of the oxygen isotopic composition of planktonic foraminifera: experimental results and revised paleotemperature equations, Paleoceanography, 13, pp. 150-160.

Benthien, A., P. J. Müller, 2000: Anomalously low alkenone temperatures caused by lateral particle and sediment transport in the Malvinas Current region, western Argentine Basin, Deep-Sea Res., 47, pp. 2369-2393.

Berger, W. H., E. L. Winterer, 1974: Plate stratigraphy and the fluctuating carbonate line, Spec. Publ. Int. Assoc. Sedimentol., 1, pp. 11–48.

Berggren, W.A., 1972: Late Pliocene-Pleistocene glaciation: in Laughton, A.S., Berggren, W.A., et al., Init. Repts. DSDP, 12: Washington (U.S. Govt. Printing Office), pp. 953–963, doi: 10.2973/dsdp.proc.12.113.

Béthoux, J.-P., C. Pierre, 1999: Mediterranean functioning and sapropel formation: respective influences of climate and hydrological changes in the Atlantic and the Mediterranean: Marine Geology, 153, pp. 29–39, doi: 10.1016/S0025-3227(98) 00091-7.

Bethoux, J.-P., 1979: Budgets of the Mediterranean Sea: their dependence on the local climate and on the characteristics of the Atlantic waters, Ocean. Acta 2, pp. 157–163.
Betzler, C., J. C. Braga, J. M. Martin, I. M. Sánchez-Almazo, S. Lindhorst, 2006: Closure of a seaway: stratigraphic record and facies (Guadix basin, Southern Spain), Int J. Earth Sci. (Geol Rundsch), 95, 903–910, DOI 10.1007/s00531-006-0073-y.
Bigg, G. R., 1996: The Oceans and Climate: Cambridge, Cambridge University Press, p. 266.
Bigg, G. R., M. R. Wadley, 2001: Millennial-scale variability in the oceans: an ocean modelling view, Journal of Quaternary Science, 16, pp. 309–319.
Bigg, G.R., Jickells, T.D., Liss, P.S., and Osborn, T.J., 2003: The role of the oceans in climate: International Journal of Climatology, 23, pp. 1127–1159, doi: 10.1002/joc.926.
Bizon, G., C. Müller, 1978: Remarks on the determination of the Pliocene-Pleistocene boundary in the Mediterranean, Initial Reports of the Deep Sea Drilling Project, 42, pp. 847-853.
Blanc, P. L., 2002: The opening of the Plio-Quaternary Gibraltar Strait: assessing the size of a cataclysm, Geodinamica Acta, 15, pp. 303-317.
Boyle, E.A., 1981: Cadmium, zinc, copper and barium in foraminifera tests, Earth and Planet. Sci. Lett., 53, pp. 11-35.
Brassell, S. C., 1993: Applications of biomarkers for delineating marine palaeoclimatic fluctuations during the Pleistocene, Organic Geochemistry: Principles and Applications, pp. 699-738.
Brassell, S. C., G. Eglinton, 1984: Lipid indicators of microbial activity in marine sediments, in Heterotrophic Activity in the Sea, pp. 481-503.
Brassell, S. C., G. Eglinton, I. T. Marlowe, et al., 1986: Molecular stratigraphy: a new tool for climate assessment, Nature, 320, 129-133.
Broeker, W. S., T. H. Peng, 1982: Tracers in the Sea, Lamont-Doherty Geological Observatory Publications, 690 p.
Brown, S. J., H. Elderfield, 1996: Variations in Mg/Ca and Sr/Ca ratios of planktonic foraminifera caused by postdepositional dissolution: evidence of shallow Mg-dependent dissolution, Paleoceanography, 11, pp. 543–551.
Bryden, H. L., T. H. Kinder, 1991: Steady two-layer exchange through the Strait of Gibraltar, Deep-Sea Research, 38, pp. 445-463.

C

Cacho, I., Shackleton, N., Elderfield, H., Sierro, F.J., and Grimalt, J.O., 2006: Glacial rapid variability in deep-water temperature and $\delta^{18}O$ from the Western Mediterranean Sea: Quaternary Science Reviews, v. 25, p. 3294–3311, doi: 10.1016/j.quascirev. 2006.10.004.
Candela, J., 2001: Mediterranean water and global circulation, in Siedler, G., Church, J., and Gould, J., ed., Ocean Circulation and Climate: Observing and Modelling the Global Ocean: International Geophysics Series, v. 77, 715 p., Academic Press: San Diego, CA (USA), ISBN 0-12-641351-7. xix.
Cane, M., P. Molnar, 2001: Closing of the Indonesian seaway as a precursor to east African aridification around 3-4 million years ago, Nature, 411, pp. 157-162.
Channell, J.E.T., B. Lehman, 1999: Magnetic stratigraphy of North Atlantic Sites 980–984. In Raymo, M.E., Jansen, E., Blum, P., and Herbert, T.D. (Eds.), Proc. ODP, Sci. Results, 162: College Station, TX (Ocean Drilling Program), pp. 113–130. doi:10.2973/ odp.proc.sr.162.002.1999.
Cohen, A. S., R. K. O'Nions, R. Siegenthaler, et al., 1988: Chronology of the pressure-temperature history recorded by a granulite terrain: Contributions to Mineralogy and Petrology, 98, pp. 303–311.
Conte, M. H., M. A. Sicre, C. Rühlemann, et al., 2006: Global temperature calibration of the

alkenone unsaturation index (Uk'37) in surface waters and comparison with surface sediments, Geochemistry, Geophysics, Geosystems, 7, pp. Q02005, doi: 10.1029/2005GC001054.
Craig, H., L. I. Gordon, 1965: Deuterium and oxygen-18 variations in the ocean and the marine atmosphere, in E. Tongiorgi, ed, Proceedings of a Conference on Stable Isotopes in Oceanographic Studies and Paleotemperatures, Spoleto, pp. 9-130.
Cronin, T. M., 1991: Pliocene shallow water paleoceanography of the North Atlantic ocean based on marine ostracodes, Quaternary Science Reviews, 10, pp. 175-188.
Crowley, T. J., 1991: Modeling pliocene warmth, Quaternary Science Reviews, 10, pp. 275-282, doi:10.1016/0277-3791(91)90025-P.
Curry, W. B., J.-C. Duplessy, L. Labeyrie, et al., 1988: Changes in the distribution of $\delta^{13}C$ of deep water sum CO_2 between the last glaciation and the Holocene, Paleoceanography, 3, pp. 317–341.

D

de Villiers, S., M. Greaves, H. Elderfield, 2002: An intensity ratio calibration method for the accurate determination of Mg/Ca and Sr/Ca of marine carbonates by ICP-AES, Geochemistry, Geophysics, Geosystems, 3, pp. 1001, doi:10.129/2001GC000169.
Dekens, P.S., A.C. Ravelo, M.D. McCarthy, et al., 2008: A 5 million year comparison of Mg/Ca and alkenone paleothermometers, Geochemistry Geophysics Geosystems, 9, Q10001, doi: 10.1029/2007GC001931.
DeMenocal, P. B., 1995: Plio-Pleistoeene african elimate, Science, 270, pp. 53-59.
Dowsett, H. J., J. A. Barron, R. Z. Poore, R. S. Thompson, T. M. Cronin, S. E. Ishman, D. A. Willard, 1999: Middle Pliocene Paleoenvironmental Reconstruction: PRISM2, U.S. Geol. Surv. Open File Rep., pp. 99–535.
Dowsett, H. J., M. M. Robinson, K. M. Foley, 2009b: Pliocene three-dimensional global ocean temperature reconstruction, Climate of the Past, 5 (4), pp. 769-783.
Dowsett, H. J., R. Z. Poore, 1990: A new planktic foraminifer transfer function for estimating Pliocene-Holocene paleoceanographic conditions in the North Atlantic, Marine Micropaleontology, 16, pp. 1-23.
Dowsett, H., J. Barron, R. Poore, 1996: Middle Pliocene sea surface temperatures: A global reconstruction, Marine Micropaleontol, 27, pp. 13–25.
Dowsett, H.J., T.M. Cronin, 1990: High eustatic sea level during the middle Pliocene: evidence from southeastern U.S. Atlantic coastal plain, Geology, 18, pp. 435-438.
Draut, A. E., M. E. Raymo, J. F. McManus, D. W. Oppo, 2003: Climate stability during the Pliocene warm period, Paleoceanography, 18(4), 1078, doi:10.1029/2003PA000889.
Driscoll, N. W., G. H. Haug, 1998: A short circuit in thermohaline circulation: a cause for northern hemisphere glaciation?, Science, 282, pp. 436–438.
Duggen, S., K. Hoernie, P. van den Bogaard, L. Rupke, J. Phipps Morgan, 2003: Deep roots of the Messinian salinity crisis, Nature, 422, pp. 602-605.
Dünkeloh, A., J. Jacobeit, 2003: Circulation dynamics of Mediterranean precipitation variability 1948–98, Int. J. Climatol, 23, pp. 1843–1866.
Duplessy, J. C., 1972: La Geochimie des isotopes stables du carbone dans la mer, Ph.D. Thesis, p. 196.
Duplessy, J. C., N. J. Shackleton, R. K. Matthews, et al., 1984: ^{13}C Record of benthic foraminifera in the last interglacial ocean: Implications for the carbon cycle and the global deep water circulation, Quaternary Research, 21, pp. 225-243.
Duplessy, J.-C., Shackleton N.J., Fairbanks R.G., Labeyrie L.D., Oppo D., Kallel N., 1988: Deep water source variations during the last climatic cycle and their impact on the global deep water circulation, Paleoceanography, 3, pp. 343–360.
Dwyer, G. S., M. A. Chandler, 2009: Mid-Pliocene sea level and continental ice volume based on coupled benthic Mg/Ca palaeotemperatures and oxygen isotopes, Phil.

Trans. Royal Soc. A, 367, pp. 157-168, doi:10.1098/rsta.2008.0222.
Dwyer, G. S., T. M. P. Cronin, A. Baker, et al., 1995: North-Atlantic deep-water temperature-change during late pliocene and late quaternary climatic cycles, Science, 270, pp. 1347–1351.

E

Elderfield, H., G. Ganssen, 2000: Past temperature and $\delta^{18}O$ of surface ocean waters inferred from foraminiferal Mg/Ca ratios, Nature, 405, pp. 442-445.
Elderfield, H., J. Yu, P. Anand, et al., 2006: Calibrations for benthic foraminiferal Mg/Ca paleothermometry and the carbonate ion hypothesis, Earth and Planetary Science Letters, 250, pp. 633–649, doi: 10.1016/j.epsl.2006.07.041.
Eshel, G., 2002: Mediterranean climates, Israel J. Earth Sci., 51, pp. 157-168.
Etourneau, J., 2009: Pliocene-Pleistocene variability of upwelling activity, productivity and nutrient cycle in the Benguela Upwelling System and the Eastern Equatorial Pacific, Kiel University, 164 p.

F

Fauquette, S., Guiot, J., and Suc J.-P., 1998: A method for climatic reconstruction of the Mediterranean Piocene using pollen data, Palaeogeography, Palaeoclimatology, Palaeoecology, 144, p. 183–201, doi: 10.1016/S0031-0182(98)00083-2.
Fedorov, A. V., C. M. Brierley, K. Emanuel, 2010: Tropical cyclones and permanent El Niño in the early Pliocene epoch, Nature, 463, 1066, doi:10.1038/nature08831.
Ferguson, J.E., G. M. Henderson, M. Kucera, et al., 2008: Systematic change of foraminiferal Mg/Ca ratios across a strong salinity gradient, Earth Planet. Sci. Lett., 265, pp. 153-166.
Fofonoff, N. P., R. C. Jr. Millard, 1983: Algorithms for computation of fundamental properties of seawater (UNESCO Tech. Papers in Marine Science 44), Division of Marine Science.
Fontugne, M. R., J. C. Duplessy, 1978: Carbon isotope ratio of marine plankton related to water masses, Earth Planet. Sci. Lett., 41, pp. 365–371.
Frank, M., 2002: Radiogenic isotopes: tracers of past ocean circulation and erosional input: Reviews of Geophysics, 40/1, 1001, doi: 10.1029/2000RG00094.
Freeman, K.H., S. G. Wakeham, 1992: Variations in the distributions and isotopic compositions of alkenones in Black Sea particles and sediments, Org. Geochem., 19, pp. 277-285.

G

Ganachaud, A., C. Wunsch, 2000: Improved estimates of global ocean circulation, heat transport and mixing from hydrographic data, Nature, 408, pp.453–457.
Ganssen, 1983: Dokumentation von küstennahem Auftrieb anhand stabiler Isotope in rezenten Foraminiferen vor Nordwest-Afrika, “Meteor” Forschungsergeb. 37 (1983), pp. 1–46 Reihe C.
Garcia-Castellanos, D., F. Estrada, I. Jiménez-Munt, et al., 2009: Catastrophic flood of the Mediterranean after the Messinian Crisis, Nature, 462, pp. 778-781, doi:10.1038/nature08555.
Garrett, C., 1994: The Mediterranean Sea as a climate test basin, Ocean Processes in Climate Dynamics: Global and Mediterranean Examples, pp. 227-237.
Gebhardt, H., M. Sarnthein, P. M. Grootes, T. Kiefer, et al., 2008: Paleonutrient and productivity records from the subarctic North Pacific for Pleistocene glacial terminations I to V, Paleoceanography, 23.

Gilman, C., C. Garrett, 1994: Heat Flux parameterizations for the Mediterranean Sea: The role of atmospheric aerosols and constraints from the water budget, J. Geophys. Res., 99, pp. 5119–5134.
Graciansky, P.C. de, Poag, C.W., and 29 others (Editors), 1985: Initial Reports DSDP, 80, U.S. Government Printing Office, Washington, DC, doi: 10.2973/dsdp.proc. 80.117.1985.
Greaves M., S. Barker, C. Daunt, et al. 2005: Accuracy, standardization, and interlaboratory calibration standards for foraminiferal Mg/Ca thermometry, Geochemistry Geophysics Geosystems, 6, doi: 10.1029/2004GC000790.
Greaves, M., N. Caillon, H. Rebauier, 2008: Interlaboratory comparison study of calibration standards for foraminiferal Mg/Ca thermometry, Geochem. Geophys. Geosys., 9, doi: 10.1029/2008GC001974.
Groeneveld, J., D. Nürnberg, R. Tiedemann, et al., 2008: Foraminiferal Mg/Ca increase in the Caribbean during the Pliocene: Western Atlantic Warm Pool formation, salinity influence, or diagenetic overprint?, Geochem. Geophys. Geosys., 9, doi: 10.1029/2006GC001564.
Gutjahr, M., M. Frank, C. H. Stirling, et al., 2007: Reliable extraction of a deepwater trace metal isotope signal from Fe-Mn oxyhydroxide coatings of marine sediments, Chemical Geology, 242, pp. 351–370.

H

Haug, G. H., R. Tiedemann, 1998: Effect of the formation of the Isthmus of Panama on Atlantic Ocean thermohaline circulation, Nature, 393, pp. 673–676.
Haywood, A. M., B.W. Sellwood, P.J. Valdes, 2000: Regional warming: Pliocene (3 Ma) paleoclimate of Europe and the Mediterranean, Geology, 28, pp. 1063-1066, doi: 10.1130/0091-7613(2000)28<1063:RWPMPO>2.0.CO;2.
Healey, S. L., R. C. Thunell, B. H. Corliss, 2008: The Mg/Ca-temperature relationship of benthic foraminiferal calcite: New core-top calibrations in the <4 °C temperature range, Earth and Planetary Science Letters, 272, pp. 523–530, doi:10.1016/j.epsl. 2008.05.023.
Heburn, G. W., and P. E. La Violette, 1990: Variations in the structure of the anticyclonic gyres found in the Alboran Sea, Journal of Geophysical Research, 92, 2901-2906.
Herbert, T.D., J.D. Schuffert, 1998: Alkenone unsaturation estimates of Late Miocene through Late Pliocene sea-surface temperatures at Site 958, Proceedings of the Ocean Drilling Program Scientific Results, 159, College Station, Tex.
Hodell, D.A., K. Venz, 1992: Toward a high-resolution stable isotopic record of the Southern Ocean during the Pliocene–Pleistocene (4.8 to 0.8 Ma), In: Kennett, J.D., D. A.Warnke: The Antarctic Paleoenvironment: A Perspective on Global Change, Antarct. Res. Ser., 56, pp. 265–310.
Holbourn, A.E., A. Henderson, 2002: Re-illustration and revised taxonomy for selected deep-sea benthic foraminifers, Paleontologia Electronica 4, pp. 0–34.

I

ISSC, 2009: International Subcommission on Stratigraphic Classification ISSC, Newsletter no. 15, Edited by M.R. Petrizzo. http://users.unimi.it/issc.

J

Jacobsen, S. B.,G.. J. Wasserburg, 1980: Sm-Nd isotopic evolution of chondrites, Earth and Planetary Science Letters, 50, pp. 139-155.

Jansen, E., J. Overpeck, K. R. Briffa, et al., 2007: Palaeoclimate, In Climate Change 2007: The Physical Science Basis. Contribution of Working Group I to the Fourth Assessment Report of the Intergovernmental Panel on Climate Change, S. Solomon, D. Qin, M. Manning, et al., Eds., Cambridge University Press, pp. 433-497.

Jochum, M., B. Fox-Kemper, P. H. Molnar, C. Shields, 2009: Differences in the Indonesian seaway in a coupled climate model and their relevance to Pliocene climate and El Niño, Paleoceanography, 24, PA1212, doi:10.1029/2008PA001678.

Jonkers, L., G.-J. A. Brummer, F. J. C. Peeters, H. M. van Aken, M. F. De Jong, (in press): Seasonal stratification, shell flux and oxygen isotope dynamics of left-coiling N. pachyderma and T. quinqueloba in the western sub-polar North Atlantic, Paleoceanography, in press.

K

Kahana, R., Bigg, G.R., and Wadley, M.R., 2007: Modeling the effect of large climatic changes over the Mediterranean on the Atlantic Circulation, Geophysical Research Abstracts, 9, EGU2007-A-07834.

Karas, C., D. Nurnberg, A. Gupta, et al., 2009: Mid-Pliocene climate change amplified by a switch in Indonesian subsurface throughflow, Nat. Geosci., 2, pp. 434–438.

Käse, R. H., W. Zenk, 1987: Reconstructed Mediterranean salt lens trajectories, J. Phys. Oceanogr., 17, pp. 158-163.

Keigwin, L. D., 1987: Pliocene Stable-Isotope Record of Deep Sea Drilling Project Site 606: Sequential Events of ^{18}O Enrichment Beginning at 3.1 Ma, Initial Rep. Deep Sea Drill. Pro., 94, 911-920, doi:10.2973/dsdp.proc.94.127.1987.

Keigwin, L. D., R. C. Thunell, 1979: Middle Pliocene climatic change in the western Mediterranean from faunal and oxygen isotopic trends. Nature, 282, p. 294-296.

Khélifi N., Sarnthein M., Andersen N., Blanz T., Frank M., Garbe-Schönberg D., Haley B.A., Stumpf R., Weinelt M., 2009: A major and long-term Pliocene intensification of the Mediterranean Outflow, 3.5–3.3 Ma ago, Geology, 37, 9, p. 811-814; DOI: 10.1130/G30058A.1.

Khélifi, N., M. Sarnthein (in prep.): Major shifts in age control at ODP Site 982 near the Pliocene onset of Northern Hemisphere Glaciation – Composite depths and $\delta^{18}O$ stratigraphy revisited.

Kisakürek, B., A. Eisenhauer, F. Böhm, 2008: Controls on shell Mg/Ca and Sr/Ca in cultured planktonic foraminiferan, Globigerinoides ruber (white), Earth Planet. Sci. Lett., 273, doi: 10.1016/j.epsl.2008.06.026.

Kleiven, H.F., Jansen, E., Fronval, T., and Smith, T.M., 2002: Intensification of Northern Hemisphere glaciations in the circum Atlantic region (3.5–2.4 Ma), ice-rafted detritus evidence, Palaeogeography, Palaeoclimatology, Palaeoecology, v. 184, p. 213–223, doi: 10.1016/S0031-0182(01)00407-2.

Krijgsman, W., F. J. Hilgen, I. Raffi, F.J. Sierro, D. S. Wilson, 1999: Chronology, causes and progression of the Messinian salinity crisis, Nature, 400, 652–655.

Kroopnick, P. M., 1980: The distribution of ^{13}C in the Atlantic Ocean, Earth Planet. Sci. Lett., 49, pp. 469–484.

Kroopnick, P.M., 1985: The distribution of CO_2 in the world oceans, Deep-Sea Research 32, pp. 57–84.

Kröpelin, S., 1987: Paleoclimatic Evidence from Early to Mid-Holocene Playas in the Gilf-Kebir (South-West Egypt), Paleoecol. Africa, 18, pp.189-208.

L

Lacan, F., Jeandel, C., 2005: Neodymium isotopes as a new tool for quantifying exchange fluxes at the continent–ocean interface, Earth and Planetary Science Letters, 232, p. 245–257, doi: 10.1016/j.epsl.2005.01.004.

Lawrence, K. T., T. D. Herbert, C. M. Brown, M. E. Raymo, A. M. Haywood, 2009: High-amplitude variations in North Atlantic sea surface temperature during the early Pliocene warm period, Paleoceanography, 24, PA2218, doi:10.1029/2008PA001669.

Lea, D. W., 2003: Elemental and Isotopic Proxies of Past Ocean Temperatures, Treatise on Geochemistry, 6, Editor: Henry Elderfield. Executive Editors: Heinrich D. Holland and Karl K. Turekian, pp. 625. ISBN 0-08-043751-6. Elsevier, pp. 365-390.

Lea, D. W., T. A. Mashiotta, H. J. Spero, 1999: Controls on magnesium and strontium uptake in planktonic foraminifera determined by live culturing, Geochim. Cosmochim. Acta, 63, pp. 2369–2379.

Leaman, K.D, F.A. Schott, 1991: Hydrographic structure of the convective regime in the Gulf of Lions: winter 1987, J. Phys. Oceanogr., 21, 4, 575-598.

Lear, C. H., Y. Rosenthal, N. Slowey, 2002: Benthic foraminiferal Mg/Ca-paleothermometry: A revised core-top calibration, Geochim. Cosmochim. Acta, 66, pp. 3375-3387.

Lear, C.H., P. A. Wilson, N. J. Shackleton, et al., 2000: Palaeotemperature and ocean chemistry records for the Palaeogene from Mg/Ca and Sr/Ca in benthic foraminiferal calcite, GFF, 122, pp. 93-93.

Leduc, G., R. Schneider, J.-H. Kim, G. Lohmann, 2010: Holocene and Eemian sea surface temperature trends as revealed by alkenone and Mg/Ca paleothermometry, Quaternary Science Reviews, 29(7-8), pp. 989-1004. doi:10.1016/j.quascirev. 2010.01.004.

Levin, N., J. Quade, S. W. Simpson, et al., 2004: Isotopic evidence for Plio-Pleistocene environmental change at Gona, Ethiopia, Earth and Planetary Science Letters, 219, pp. 93–110.

Levitus, S., T. P. Boyer, 1994: World Ocean Atlas, Temperature, NOAA Atlas NESDIS 4. U.S. Government Printing Office, Washington, D.C., 4, p. 117.

Lionello, P., P. Malanotte-Rizzoli, R. Boscolo (Eds), 2006: The Mediterranean climate: an overview of the main characteristics and issues, Elsevier, pp. 438.

Lisiecki, L. E., M. E. Raymo, 2005: A Pliocene-Pleistocene stack of 57 globally distributed benthic $d^{18}O$ records, Paleoceanography, 20, PA1003, doi:10.1029/2004PA001071.

Lolis, C. J., A. Bartzokas,B. D. Katsoulis, 2002: Spatial and temporal 850 hPa air temperature and sea-surface temperature covariances in the Mediterranean region and their connection to atmospheric circulation, International Journal of Climatology, 22, pp. 663–676.

Loubere, P., 1987a: Late Pliocene variations in the carbon isotope values of North Atlantic benthic Foraminifera: Biotic control of the isotopic record?, Marine Geology, 76, pp. 45-56.

Loubere, P., 1987b: Changes in mid-depth North Atlantic and Mediterranean circulation during the Late Pliocene — Isotopic and sedimentological evidence, Marine Geology, 77, pp. 15-38, doi: 10.1016/0025-3227(87)90081-8.

Loubere, P., 1988: Gradual late pliocene onset of glaciation: A deep-sea record from the Northeast Atlantic: Palaeogeography, Palaeoclimatology, Palaeoecology, v. 63, p. 327–334, doi: 10.1016/0031-0182(88)90103-4.

Lourens, L. J., F. J. Hilgen, J. Laskar, et al., 2004: The Neogene Period, A Geologic Time Scale, pp. 409-440.

Lourens, L.J., Hilgen, F.J., Raffi, I., and Vergnaud-Grazzini, C., 1996: Early Pleistocene chronology of the Vrica section (Calabria, Italy), Paleoceanography, 11/6, p. 797–812, doi: 10.1029/96PA02691.

Lowrie, W., W. Alvarez, 1981: One hundred million years of geomagnetic polarity history, Geology, 9, pp. 392–397.
Lunt, D. J., P. J. Valdes, A. M. Haywood, I. C. Rutt, 2007: Closure of the Panama Seaway during the Pliocene: implications for climate and Northern Hemisphere glaciation, Clim. Dynam., 1–18, doi:10.1007/s00382-0070265-6, 2007.

M

Mackensen, A., H. Grobe, H. W. Hubberten, et al., 1994: Benthic foraminiferal assemblages and the $\delta^{13}C$-signal in the Atlantic sector of the Southern Ocean: Glacial-to-interglacial Contrasts, Carbon cycling in the glacial ocean: Constraints on the ocean's role in global change, 17, pp. 105-144.
Maheras, P., E. Xoplaki, T. Davies, et al., 1999: Warm and cold monthly anomalies across the Mediterranean basin and their relationship to circulation, Int J. Climatol, 19, pp. 1697–1715.
Maier-Reimer, E., U. Mikolajewicz, T. Crowley, 1990: Ocean General Circulation Model Sensitivity Experiment with an open Central American Isthmus, Paleoceanography, 5, pp. 349–366.
Marino, G., 2008: Paleoceanography of the interglacial eastern Mediterranean Sea, PhD Thesis, Utrecht University, 145 p.
Marlowe, I. T., S. C. Brassell, G. Eglinton, J.C. Green, 1990: Long-chain alkenones and alkyl alkenoates and the fossil coccolith record of marine sediments, Chemical Geology, 88, pp. 349-375.
Martin, P.A., D. W. Lea, 2002: A simple evaluation of cleaning procedures on fossil benthic foraminiferal Mg/Ca, Geochemistry, Geophysics, Geosystems, 3, pp. 8401, doi: 10.1029/2001GC000280.
Martrat, B., J. O. Grimalt, N. J. Shackleton, et al., 2007: Four climate cycles of recurring deep and surface water destabilizations on the Iberian Margin, Science, 317, pp. 502–507.
Maslin, M.A., M.H. Trauth, 2009: Plio-Pleistocene East African Pulsed Climate Variability and its influence on early human evolution, in "The First Humans - Origins of the Genus Homo" (editors F. E. Grine, R. E. Leakey and J. G. Fleagle), Springer Verlag, Vertebrate Paleobiology and Paleoanthropology Series, 151-158.
Mazzei, R., I. Raffi, D. Rio, et al., 1979: Calibration of Late Neogene calcareous plankton datum planes with the paleomagnetic record of Site 397 and correlation with Moroccan and Mediterranean sections, Init. Repts: DSDP, 47, pp. 375-389.
McCartney, M.S., C. Mauritzen, 2001: On the origin of the warm inflow to the Nordic Seas, Progress In Oceanography, v. 51, p. 125–214, doi: 10.1016/S0079-278 6611(01) 00084-2.
McDowell, S. E., H. T. Rossby, 1978: Mediterranean Water: An intense mesoscale eddy off the Bahamas, Science, 202, pp. 1085–1087.
McKenzie, J. A., 1999: From desert to deluge in the Mediterranean, Nature, 400, 6745, pp.
MEDATLAS, 1997: Mediterranean Hydrographic Atlas (Mast Supporting Initiative; MAS2-CT93-0074): CD-ROM.
MEDOC group, 1970: Observation of formation of deep water in the Mediterranean Sea, Nature, 277, pp. 1037-1040.
Mollenhauer, G., M. Kienast, F. Lamy, et al., 2005: An evaluation of ^{14}C age relationships between co-occurring foraminifera, alkenones, 6 and total organic carbon in continental margin sediments, Paleoceanography, 20, PA1016.
Motoi, T., W.-L. Chan, S. Minobe, et al., 2005: North Pacific halocline and cold climate induced by Panamanian Gateway closure in a coupled ocean-atmosphere GCM, Geophys. Res. Lett., 32, pp.L10618, doi: 10.1029/2005GL022844.
Muiños, S.B., Frank, M., Maden, C., Hein, J.R., van de Flierdt, T., Lebreiro, S.M., Gaspar, L.,

Monteiro, J.H., and Halliday, A.N., 2008: New constraints on the Pb and Nd isotopic evolution of NE Atlantic water masses: Geochemistry, Geophysics, Geosystems, 9, p. Q02007, doi: 10.1029/2007GC001766.
Müller, C., 1985: Biostratigraphic and paleoenvironmental interpretation of the Goban Spur region based on a study of calcareous nannoplankton: In de Gracinsky, P.C., and Poag, C.W., et al., Editors, Init. Repts. DSDP, 80, U.S. Government Printing Office, Washington, DC (1985), pp. 573–599, doi: 10.2973/dsdp.proc.80.117.1985.
Müller, P.J., G. Kirst, G. Ruhland, I. von Storch, A. Rosell-Melé, 1998: Calibration of the alkenone paleotemperature index Uk´37 based on core-tops from the eastern South Atlantic and the global ocean (60°N-60°S), Geochimica et Cosmochimica Acta, 62, pp. 1757-1772.

N

Naafs, B. D., R. Stein, N. Khélifi, G. H. Haug, (in prep.): Late Pliocene variations in the North Atlantic Current and subsequent northward heat transport.
Naish, T. R., G. S. Wilson, 2009: Constraints on the amplitude of Mid-Pliocene (3.6-2.4?Ma) eustatic sea-level fluctuations from the New Zealand shallow-marine sediment record, Phil. Trans. R. Soc. A., 367, pp. 169-187.
Nürnberg, D., 1995: Magnesium in tests of Neogloboquadrina pachyderma (sinistral) from high northern and southern latitudes, Journal of Foraminiferal Research, 25, pp. 350–368.
Nürnberg, D., J. Bijma, C. Hemleben, 1996: Assessing the reliability of magnesium in foraminiferal calcite as a proxy for water mass temperatures, Geochimica et Cosmochimica Acta, 60, pp. 803–814.

O

O'Nions, R.K., Frank, M., von Blanckenburg, F., Ling, H.-F., 1998: Secular variation of Nd and Pb-isotopes in ferromanganese crusts from the Atlantic, Indian and Pacific Oceans, Earth and Planetary Science Letters, v. 155, p. 15–28, doi: 10.1016/S0012-821X(97)00207-0.
Ohkouchi, N., T. I. Eglinton, L. D. Keigwin, et al., 2002: Spatial and temporal offsets between proxy records in a Sediment Drift, Science, 298, pp. 1224–1227.
Osborne, A. H., D. Vance, E. J. Rohling, et al., 2008: A humid corridor across the Sahara for the migration of early modern humans out of Africa 120,000 years ago, Proceedings of the National Academy of Sciences, 105, pp. 16444–16447.
Ostermann, D.R., W. B. Curry, 2000: Calibration of stable isotopic data: An enriched $\delta^{18}O$ standard used for source gas mixing detection and correction, Paleoceanography, 15, pp. 353–360.

P

Pachur, H. D., S. Kröpelin, W. Howar, 1987: Paleoclimatic evidence from an extinct river system in the southeastern Sahara, Science, 237, pp. 298–300.
Pachur, H. J., N. Altmann, 2006: Die Ostsahara im Spätquartär, pp. 662.
Paillard, D., L. Labeyrie, P. Yiou, 1996: Macintosh program performs time-series analysis, EOS Trans, AGU, 77, p. 379.
Petit-Maire N., 1985: La Néolithisation au Sahara. Cahiers ORSTOM, Géologie, 4, pp. 189–212.
Pflaumann, U., M. Sarnthein, M. R. Chapman, 2003: Glacial North Atlantic: Sea-surface conditions reconstructed by GLAMAP 2000. Paleoceanography, 18(3), p. 1065, doi: 10.1029/2002PA000774.

Pierre, C., 1999: The oxygen and carbon isotope distribution in the Mediterranean water masses, Marine Geology, 153 (1999), pp. 41–55.
Pinardi, N., E. Masetti, 2000: Variability of the large scale general circulation of the Mediterranean Sea from observations and modelling: a review, Palaeogeography, Palaeoclimatology, Palaeoecology, 158, pp. 153–173.
POEM group, 1992: General circulation of the eastern Mediterranean Sea, Earth-Science Reviews, 32, pp. 285-308.
Prahl, F. G., G. J. de Lange, M. Lyle, et al., 1989: Post-depositional stability of long-chain alkenones under contrasting redox conditions, Nature, 341, pp. 434-437.
Prahl, F. G., L. A. Muehlhausen, D. L. Zahnle, 1988: Further evaluation of long-chain alkenones as indicators of paleoceanographic conditions, Geoehimica et Cosmochimica Acta, 52, pp. 2303-2310.
Prahl, F.G., S. G. Wakeham, 1987: Calibration of unsaturation patterns in long-chain ketone compositions for paleotemperature assessment, Nature, 330, pp. 367-369.
Price, J. F., M. O'Neil Baringer, R. G. Lueck, et al., 1993: Mediterranean outflow mixing and dynamics, Science, 259, pp. 1277-1282.
Pujol, C., C. Vergnaud Grazzini, 1989: Palaeoceanography of the last deglaciation in the Alboran Sea (western Mediterranean). Stable isotopes and planktonic foraminiferal records, Marine Micropaleontology, 15, pp. 153-179.

R

Rahmstorf, S., 1998: Influence of Mediterranean outflow on climate: EOS, Transactions American Geophysical Union, 79, p. 281–282, doi: 10.1029/98EO00208.
Ravelo, A.C., and Andreasen, D.H., 2000: Enhanced circulation during a warm period: Geophysical Research Letters, 27, p. 1001–1004.
Raymo, M. E., D. Hodell, E. Jansen, 1992: Response of deep ocean circulation to initiation of Northern Hemisphere glaciation (3–2 MA), Paleoceanography, 7, pp. 645– 672.
Raymo, M. E., P. Hearty, R. De Conto, et al., 2009: PLIOMAX: Pliocene maximum sea level project, PAGES News, 17, pp. 58–59.
Regenberg, M., D. Nürnberg, S. Steph, et al., 2006: Assessing the dissolution effect on planktonic foraminiferal Mg/Ca ratios: Evidence from Caribbean core-tops, Geochem. Geophys. Geosys., 7, doi:10.1029/2005GC001019, 2006a.
Regenberg, M., S. Steph, D. Nürnberg, R. Tiedemann, D. Garbe-Schönberg 2009: Calibrating Mg/Ca ratios of Multiple Planktonic Foraminiferal Species with ∂^{18}O-Calcification Temperatures: Paleothermometry for the Upper Water Column., Earth and Planetary Science Letters, 278(3-4), 324-336. doi:10.1016/j.epsl.2008.12.019.
Reid, J.L., 1979: On the contribution of the Mediterranean Sea outflow to the Norwegian-Greenland Sea: Deep Sea Research Part A., Oceanographic Research Papers, 26, p. 1199–1223, doi: 10.1016/0198-0149(79)90064-5.
Rickli, J., Frank, M., A.N. Halliday, 2009: The hafnium–neodymium isotopic composition of Atlantic seawater: Earth and Planetary Science Letters, 280, p. 118–127, doi: 10.1016/j.epsl.2009.01.026.
Robinson, A.R., W.G. Leslie, A. Theocharis, A. Lascaratos, 2001: Mediterranean Sea Circulation Encyclopedia of Ocean Sciences, Academic Press, 1689-1706.
Robinson, M. M., H. J. Dowsett, G. S. Dwyer, et al., 2008: Reevaluation of mid-Pliocene North Atlantic sea surface temperatures, Paleoceanography, 23, PA3213, doi: 10.1029/2008PA001608, 2008.
Rodgers, K. B., M. Latif, S. Legutke, 2000: Sensitivity of equatorial Pacific and Indian Ocean watermasses to the position of the Indonesian throughflow, Geophys. Res. Lett, 27, pp. 2941-2944.
Rogerson, M., E.J. Rohling, P.P.E. Weaver, 2006: Promotion of meridional overturning by Mediterranean-derived salt during the last deglaciation, Paleoceanography, 21, p.

10.1029/2006PA001306.
Rohling, E. J., A. Hayes, S. De Rijk, D. Kroon, W. J. Zachariasse, D. Eisma, 1998b: Abrupt cold spells in the northwest Mediterranean, Paleoceanography, 13, pp. 316-322.
Rohling, E. J., H. L. Bryden, 1992: Man-induced salinity and temperature increases in western Mediterranean deep water, Journal of Geophysical Research, 97, pp. 11191–11198.
Rohling, E. J., M. Den Dulk, C. Pujol, et al., 1995: Abrupt hydrographic change in the Alboran Sea (western Mediterranean) around 8000 yrs BP, Deep-Sea Research, 42, pp. 1609-1619.
Rohling, E. J., T. R. Cane, S. Cooke, et al., 2002b: African monsoon variability during the previous interglacial maximum, Earth and Planetary Science Letters, 202, pp. 61-75.
Rohling, E.J., R.H. Abu-Zied, J.S.L. Casford, A. Hayes, B.A.A. Hoogakker, 2008a: The Mediterranean Sea: present and past. In: J.C. Woodward, Editor, The Physical Geography of the Mediterranean, Oxford University Press, Oxford, UK.
Rosenthal, Y., C.H. Lear, D.W. Oppo, et al., 2006: Temperature and carbonate ion effect on Mg/Ca and Sr/Ca ratios in benthic foraminifera: Aragonitic species Hoeglundina elegans, Paleoceanography, 21, PA1007 10.1029/2005PA001158.
Rosenthal, Y., E. Boyle, 1993: Factors controlling the fluoride content of planktonic foraminifera: an evaluation of its paleoceanographic applicability, Geochim. Cosmochim. Acta., 57, pp. 335-346.
Rosenthal, Y., E.A. Boyle, N. Slowey, 1997: Environmental controls on the incorporation of Mg, Sr, F and Cd into benthic foraminiferal shells from Little Bahama Bank: Prospects for thermocline paleoceanography, Geochim. Cosmochim. Acta, 61, pp. 3633–3643.
Rosenthal, Y., S. Perron-Cashman, C. H. Lear, et al., 2004: Laboratory inter-comparison study of Mg/Ca and Sr/Ca measurements in planktonic foraminifera for paleoceanographic research, Geochemistry Geophysics Geosystems, doi: 10.1029/2003GC000650.
Rossignol-Strick, M., 1983: African monsoons, an immediate climate response to orbital insolation: Nature, v. 304p. 46-49.
Rossignol-Strick, M., 1985: Mediterranean Quaternary sapropels, an immediate response of the African monsoon to variation of insolation, Palaeogeography, Palaeoclimatology, Palaeoecology, 49, pp. 237-263.
Russell, A. D., B. Hönisch, H. J. Spero, et al., 2004: Effects of seawater carbonate ion concentration and temperature on shell U, Mg, and Sr in cultured planktonic foraminifera, Geochim. Cosmochim. Ac., 68, pp. 4347–4361.

S

Saaroni, H., B. Ziv, J. Edelson, et al., 2003: Long-term variations in summer temperatures over the eastern Mediterranean, Geophysical Research Letters, 30(18), doi: 10.1029/2003GL017742.
Salzmann, U., A. M. Haywood, D. J. Lunt, 2009: The past is a guide to the future? Comparing Middle Pliocene vegetation with predicted biome distributions for the twenty-first century, PHILOS T R SOC A, 367(1886), pp.189-204.
Sarnthein, M., G. Bartoli, M. Prange, et al., 2009: Mid-Pliocene shifts in ocean overturning circulation and the onset of Quaternary-style climates, Climates of the Past, 5, pp. 269–283.
Sarnthein, M., K. Winn, et al., 1994: Changes in East Atlantic Deepwater Circulation Over the Last 30,000 years: Eight Time Slice Reconstructions, Paleoceanography, 9(2), pp. 209–267.
Schiebel, R., S. Barker, R. Lendt, et al., 2007: Planktic foraminiferal dissolution in the twilight zone, Deep Sea Res. II, 54, pp. 670–686.
Schlitzer, R., 2007: Ocean Data View, http://odv.awi.de.

Schmidt, M.W., H.J. Spero, D.W. Lea, 2004: Links between salinity variation in the Caribbean and North Atlantic thermohaline circulation, Nature, 428, pp. 160-163.
Schönfeld, J., and Zahn, R., 2000: Late Glacial to Holocene history of the Mediterranean Outflow. Evidence from benthic foraminiferal assemblages and stable isotopes at the Portuguese margin, Palaeogeography, Palaeoclimatology, Palaeoecology, v. 159, p. 85–111, doi: 10.1016/S0031-0182(00)00035-3.
Schott, F. A., Dengler, M., Schoenefeld, R., 2002: The shallow overturning circulation of the Indian Ocean, Prog. Oceanogr., 53, pp. 57-103.
Scrivner, A. E., D. Vance, E. J. Rohling, 2004: New neodymium isotope data quantify Nile involvement in Mediterranean anoxic episodes, Geology, 32, pp. 565–568.
Scrivner, A.E., A.M. Piotrowski, A.C. Elmore, J.D. Wright, 2008: Reconstructing past surface and deep water neodymium isotope compositions in the North Atlantic, EGU2008-A-03943, CL39-1MO5P-0265.
Sepulchre, P., G. Ramstein, R. Fluteau, et al., 2006: Tectonic Uplift and Eastern Africa Aridification, Science, 313, pp.1419-1423.
Shackleton, N. J., M. A. Hall, 1984: Carbon isotope Data from Leg 74 sediments, Initial Rep. Deep Sea Drill. Proj., 74, pp. 613-619.
Shackleton, N. J., N. D. Opdyke, 1973: Oxygen isotope and palaeomagnetic stratigraphy of Equatorial Pacific core V28-238: Oxygen isotope temperatures and ice volumes on a 105 year and 106 year scale, Quaternary Research, 3, pp. 39-55.
Shackleton, N.J., 1974: Attainment of isotopic equilibrium between ocean water and the benthonic foraminifera genus Uvigerina: isotopic changes in the ocean during the last glacial, Colloques Internationaux du Centre National du Recherche Scientifique, 219, pp. 203–210.
Shipboard Scientific Party, 1985: Initial Rep. Deep Sea Drill. Proj., 82, Washington (U.S. Govt. Printing Office). doi:10.2973/dsdp.proc.85.1985.
Shipboard Scientific Party, 1996a: Site 978, in Comas: M.C., Zahn, R., Klaus, A., and 25 others: Proceedings of the Ocean Drilling Program (ODP), Initial Reports, 161, College Station, TX (Ocean Drilling Program), pp. 355–388. doi:10.2973/odp.proc.ir.161.108.1996.
Shipboard Scientific Party, 1996b: Shipboard Scientific Party, Site 982, in: E. Jansen, M. Raymo and P. Blum et al., Editors, Proceedings of Ocean Drilling Program, Initial Reports, 162, College Station, Texas (1996), pp. 91–138.
Sicre, M. A., Y. Ternois, J. C. Mique, et al., 1999: Alkenones in the northwestern Mediterranean Sea: interannual variability and vertical transfer, Geophys. Res. Lett., 26, pp. 1735-1738.
Siedler, G., J. Church, J. Gould, 2001: Ocean Circulation and Climate: Observing and Modelling the Global Ocean., Academic Press, San Diego, USA.
Sikes, E.L., J.W. Farrington, L.D. Keigwin, 1991: Use of the alkenone unsaturation ratio Uk'37, to determine past sea surface temperatures: core-top SST calibrations and methodology considerations, Earth and Planetary Science Letters, 104, pp. 36–47.
Simstich, J., M. Sarnthein, H. Erlenkeuser, 2002: Paired $\delta^{18}O$ signals of N. pachyderma (s) and T. quinqueloba show thermal stratification structure in the Nordic Seas, Marine Micropaleontology, 48, pp. 107–125.
Sosdian, S., Y. Rosenthal, 2009: Deep-sea temperature and ice volume changes across the Pliocene–Pleistocene climate transitions, Science, 325, pp. 306–310.
Spezzaferri, S., F. Tamburini, 2007: Paleodepth variations on the Eratosthenes Seamount (Eastern Mediterranean): sea-level changes or subsidence?, eEarth Discuss., 2, 115–132.
Stommel, H., H. Bryden, P. Mangelsdorf, 1973: Does some of the Mediterranean outflow come from great depth?, Pure and Applied Geophysics, 105, pp. 879-889.
Stordal, M. C., G. J. Wasserburg, 1986: Neodymium isotopic study of Baffin Bay water: sources of REE from very old terranes, Earth Planet. Sci. Lett., 77, pp. 259–272.
Suc, J. P. 1984: Origin and evolution of the Mediterranean vegetation and climate in Europe,

Nature, 307, pp. 429-432.

T

Tachikawa, K., Roy-Barman, M., Michard, A., Thouron, D., Yeghicheyan, D., and Jeandel, C., 2004: Neodymium isotopes in the Mediterranean Sea: Comparison between seawater and sediment signals: Geochimica et Cosmochimica Acta, 68, 14, p. 3095–3106, doi: 10.1016/j.gca.2004.01.024.

Talley, L.D., M.S. McCartney, 1982: Distribution and circulation of Labrador Sea Water. J. Phys. Oceanogr., 12, pp. 1189-1205.

Tanaka, T., S. Togashi, H. Kamioka, et al., 2000: JNdi-1: a neodymium isotopic reference in consistency with LaJolla neodymium, Chemical Geology, 168, pp. 279–281.

Ternois, Y., M. A. Sicre, A. Boireau, et al., 1997: Evaluation of long-chain alkenones as paleo-temperature indicators in the Mediterranean Sea, Deep-Sea Res., 44, pp. 271-286.

Thunell, R. C., D. F. Williams, M. Howell, 1987: Atlantic-Mediterranean water exchange during the late Neogene, Paleoceanography, 2 (6), pp. 661-678.

Thunell, R., D. Rio, R. Sprovieri, C. Vergnaud-Grazzini, 1991: An overview of the post-Messinian paleoenvironmental history of the Western Mediterranean. Paleoceanography, 6, 143-164.

Thunell, R.C., D.F. Williams, M. Howell, 1987: Atlantic-Mediterranean water exchange during the late Neogene. Paleoceanography, 2, 661-678.

Thunnel, R. T., D. Williams, E. Tappa, et al., 1990: Plio-Pleistocene stable isotope record for ocean drilling program Site 653, Tyrrhenian Basin: implications for the paleoenvironmental history of the Mediterranean Sea, Proc.of the Oc. Drill. Progr. Sci. Res., 107, pp. 387-399.

Tiedemann, R., Sarnthein, M., Shackleton, N., 1994: Astronomical timescale for Pliocene Atlantic $\delta^{18}O$ and dust flux records of Ocean Drilling Program Site 659, Paleoceanography, 9, pp. 619–638.

Townsend, H. A., 1985: The paleomagnetism of sediments acquired from the Goban Spur on DSDP Leg 80, Deep Sea Drilling Project, Initial reports, 80, pp. 389– 414.

Trauth, M. H., M. A. Maslin, A. Deino, et al., 2005: Late Cenozoic moisture history of East Africa, Science, 309, pp. 2051–2053.

Trauth, M. H., M. A. Maslin, A. Deino, et al., 2007: High- and low-latitude forcing of Plio-Pleistocene East African climate and human evolution, Journal of Human Evolution, 53, pp. 475–486.

V

Van Gorsel, J. T., S. R. Troelstra, 1980: Géol. Méditerr., 7, pp. 127-134.

Van Harten, D., 1984: A model of estuarine circulation in the Pliocene Mediterranean based on new ostracod evidence, Nature 312, pp. 359–361, doi:10.1038/312359a0.

van Morkhoven, F. P. C. M., W. A. Berggren, A. S. Edwards, 1986: Cenozoic Cosmopolitan Deep-Water Benthic Foraminifera, Bull. Cent. Rech. Explor.—Prod. Elf-Aquitaine, Mem. 11.

Venz, K. A., D. A. Hodell, 2002: New evidence for changes in Plio–Pleistocene deep water circulation from Southern Ocean ODP Leg 177 Site 1090, Palaeogeography, Palaeoclimatology, Palaeoecology, 182, pp. 197-220.

Venz, K. A., D. A. Hodell, C. Stanton, et al., 1999: A 1.0 Myr record of glacial north Atlantic intermediate water variability from ODP site 982 in the northeast Atlantic, Paleoceanography, 14, pp. 42–52.

Vergnaud Grazzini, C., J.-F. Saliège, M.-J. Urrutiaguer, et al., 1990: Oxygen and carbon isotope stratigraphy of ODP Hole 653A and Site 654: the Pliocene-Pleistocene glacial

history recorded in the Tyrrhenian basin (West Mediterranean), ODP Leg 107B Proceedings of the Ocean Drilling Program, 107, pp. 361–386.
Vergnaud Grazzini, C., M. Devaux, J. Znaidi, 1986: Stable isotope “Anomalies” in Mediterranean Pleistocene records, Mar. Micropaleontol., 10, pp. 35–69.
Vergnaud-Grazzini, C., 1985: Mediterranean late Cenozoic stable isotope record: stratigraphic and paleoclimatic implications. In Stanley, D.J., and Wezel, F-C. (Eds.), Geological Evolution of the Mediterranean Basin: New York (Springer-Verlag), pp. 413-451.
Vergnaud-Grazzini, C., A. M. Borsetti, F. Cati, et al., 1988: Palaeoceanographic record of the last deglaciation in the Strait of Sicily, Marine Micropaleontology, 13, 1-21.
Voelker, A.H.L., Lebreiro, S.M., Schönfeld, J., Cacho, I., Erlenkeuser, H., and Abrantes, F., 2006: Mediterranean outflow strengthening during Northern Hemisphere coolings: A salt source for the glacial Atlantic?, Earth and Planetary Science Letters, v. 245, p. 39–55, doi: 10.1016/j.epsl.2006.03.014.
Volkman, J. K., G. Eglinton, E. D. S. Corner, et al., 1980: Long chain alkenes and alkenones in the marine coccollithophorid Emiliana huxleyi, Phytochemistry, 19, pp. 2619-2622.

W

Wang, L., M. Sarnthein, H. Erlenkeuser, J. Grimalt, P. Grootes, S. Heilig, E. Ivanova, M. Kienast, C. Pelejero, U. Pflaumann, 1999: East Asian monsoon climate during the late Pleistocene: high-resolution sediment records from the South China Sea, Marine Geology, 156, pp. 245–284.
Weaver, P. P. E., M. R. Chapman, G. Eglinton, M. Zhao, D. Rutledge, G. Read, 1999: Combined coccolith, foraminiferal, and biomarker reconstruction of paleoceanographic conditions over the past 120 kyr in the northern North Atlantic (59°N, 23°W), Paleoceanography, 14(3), pp. 336-349.
Weinelt, M., et al., 2001: Paleoceanographic proxies in the northern North Atlantic: A Changing Environment, pp. 319–352.
Woodruff, F., S. M. Savin, R. G. Douglas, 1980: Biological fractionation of oxygen and carbon isotopes by recent benthic foraminifera, Marine Micropaleontology, 5, pp. 3-11.
Wüst, G., 1961: On the vertical circulation of the Mediterranean Sea, Journal of Geophysical Research, 66, 3261-3271.

Y

Yu, J. M., H. Elderfield, 2008: Mg/Ca in the benthic foraminifera Cibicidoides wuellerstorfi and Cibicidoides mundulus: Temperature versus carbonate ion saturation, Earth Planet. Sci. Lett., 276, pp. 129–139, doi: 10.1016/j.epsl.2008.09.015.

Z

Zahn, R., J. Schönfeld, H. R. Kudrass, et al., 1997: Thermohaline instability in the North Atlantic during meltwater events: Stable isotopes and detritus records from core SO75-26KL, Portuguese margin, Paleoceanography, 12, pp. 696–710.
Zahn, R., K. Winn, M. Sarnthein, 1986: Benthic Foraminiferal $\delta^{13}C$ and accumulation rates of organic carbon: Uvigerina peregrina group and Cibicidoides wuellerstorfi, Paleoceanography, 1, pp. 27–42.
Zahn, R., Sarnthein, M., and Erlenkeuser, H., 1987: Benthic isotope evidence for changes of the Mediterranean Outflow during the Late Quaternary, Paleoceanography, v. 2, p. 543–559, doi: 10.1029/PA002i006p00543.
Zenk, W., 1975: On the Mediterranean outflow west of Gibraltar: Meteor Forschungen

Ergebnisse, 16, p. 23-34.
Zenk, W., L. Armi, 1990: The complex spreading pattern off the Portuguese continental slope, Deep-Sea Research, 37, pp. 1805–1823.
Ziv, B., H. Saaroni, P. Alpert, 2004: The factors governing the summer regime of the eastern Mediterranean, Int J. Climatol, 24, pp. 1859–1871.

Appendices

Table 4.1. Summary of stable isotope data measured in this study at Site 982

#	HOLE	CORE	SECTION	INTERVAL	DEPTH (mcd)	Cib. $\delta^{18}O$ corr.
1	982A	7	1	0,5–2	63.67	3.45
2	982A	7	1	20–21.5	63.87	3.17
3	982A	7	1	40–41.5	64.07	3.06
4	982A	7	1	60–61.5	64.27	3.30
5	982A	7	1	80–81.5	64.47	3.44
6	982A	7	1	100–101.5	64.67	3.50
7	982A	7	1	120–121.5	64.87	3.21
8	982A	7	1	140–141.5	65.07	3.33
9	982A	7	2	10–11.5	65.27	3.55
10	982A	7	2	30–31.5	65.47	3.46
11	982A	7	2	50–51.5	65.67	3.48
12	982A	7	2	70–71.5	65.87	2.98
13	982A	7	2	90,5–92.5	66.07	3.29
14	982A	7	2	111–113	66.28	3.32
15	982A	7	2	131–133	66.48	3.20
16	982A	7	3	0–1.5	66.67	3.08
17	982A	7	3	20–22	66.87	3.07
18	982A	7	3	41–43	67.08	3.11
19	982A	7	4	26–28	68.58	3.14
20	982A	7	4	38–40	68.70	3.10
21	982A	7	4	54–55,5	68.86	3.17
22	982A	7	4	68–70	6900	3.19

23	982A	7	4	85–87	69.17	3.03
24	982A	7	4	98–100	69.30	3.23
25	982A	7	4	114–116	69.46	3.20
26	982A	7	4	128–130	69.6	3.16
27	982A	7	4	145–147	70.24	3.15
28	982A	7	5	2,5–4	70.29	3.10
29	982A	7	5	10–11,5	70.33	3.12
30	982A	7	5	20–21,5	70.39	3.16
31	982A	7	5	30–31,5	70.59	2.92
32	982A	7	5	40–41,5	70.59	3.13
33	982A	7	5	50–51,5	70.59	3.16
34	982A	7	5	60–61,5	70.60	3.04
35	982A	7	5	70–71,5	70.60	3.20
36	982A	7	5	80–81,5	70.61	3.11
37	982A	7	5	90–91,5	70.61	3.09
38	982A	7	5	100–101,5	70.62	2.99
39	982A	7	5	110–111,5	70.92	3.14
40	982A	7	5	120–121,5	71.02	3.18
41	982A	7	5	130–131,5	71.12	3.15
42	982A	7	5	140–141,5	71.22	3.10
43	982A	7	6	0–1,5	71.32	3.02
44	982A	7	6	10–11,5	71.42	3.13
45	982A	7	6	20,5–22	71.52	3.09
46	982A	7	6	30–31,5	71.62	3.18
47	982A	7	6	40–41,5	71.72	3.10
48	982A	7	6	50–51,5	71.82	3.20

49	982A	7	6	60–61,5	71.92	3.29
50	982A	7	6	70–71,5	72.02	3.00
51	982A	7	6	80–81,5	72.12	3.26
52	982A	7	6	90–91,5	72.22	3.24
53	982A	7	6	100–101,5	72.32	3.22
54	982A	7	6	110–111,5	72.42	3.22
55	982A	7	6	120–121,5	72.52	3.19
56	982A	7	6	130–131,5	72.62	3.27
57	982A	7	6	140–141,5	72.73	3.26
58	982A	8	4	22–24	84.57	3.04
59	982A	8	4	32–34	84.93	3.03
60	982A	8	4	42–44	85.03	2.94
61	982A	8	4	52–54	85.24	2.85
62	982A	8	4	62–64	85.34	2.73
63	982A	8	4	72–74	85.44	2.88
64	982A	8	4	82–84	85.54	2.83
65	982A	8	4	92–94	85.64	2.87
66	982A	8	4	102–104	85.74	2.90
67	982A	8	4	112–114	85.84	2.97
68	982A	8	4	122–124	85.94	3.01
69	982A	8	4	132–134	86.04	2.99
70	982A	8	4	142–144	86.18	3.00

#	HOLE	CORE	SECTION	INTERVAL	DEPTH (mcd)	Cib. $\delta^{18}O$ corr.
1	982B	6	6	100–102	57.51	3.77
2	982B	6	6	110–112	57.61	3.31
3	982B	6	6	120–122	57.71	3.29
4	982B	6	6	130–132	57.81	3.41
5	982B	6	6	140–142	57.91	3.33
6	982B	6	7	0–2	58.01	3.47
7	982B	6	7	10–12	58.11	3.71
8	982B	6	7	20–22	58.21	3.67
9	982B	6	7	30–32	58.31	3.40
10	982B	6	7	40–42	58.41	3.33
11	982B	6	CC	0–2	58.51	3.18
12	982B	6	CC	10–12	58.61	3.00
13	982B	7	1	20–22	58.97	3.19
14	982B	7	1	30–32	59.07	3.20
15	982B	7	1	40–42	59.17	3.14
16	982B	7	1	50–52	59.27	3.46
17	982B	7	1	60–62	59.37	3.28
18	982B	7	1	70–72	59.47	3.39
19	982B	7	1	80–82	59.57	3.76
20	982B	7	1	90–92	59.67	3.75
21	982B	7	6	0–2	66.27	3.38
22	982B	7	6	10–12	66.37	3.46
23	982B	7	6	20–22	66.47	3.52
24	982B	7	6	30–32	66.59	3.28
25	982B	7	6	40–42	66.67	3.31

26	982B	7	6	50–52	66.77	3.07
27	982B	7	6	60–62	66.87	3.11
28	982B	7	6	70–72	66.97	3.10
29	982B	7	6	80–82	67.07	3.16
30	982B	7	6	90–92	67.17	3.19
31	982B	7	6	100–102	67.27	3.20
32	982B	7	6	111–113	67.38	3.06
33	982B	7	6	120–122	67.47	3.09
34	982B	7	6	130–132	67.57	3.21
35	982B	7	6	140–142	67.67	3.32
36	982B	7	7	0–2	67.77	3.33
37	982B	7	7	10–12	67.87	3.34
38	982B	7	7	20–22	67.97	3.51
39	982B	7	7	30–32	68.07	3.40
40	982B	7	7	40–42	68.17	3.51
41	982B	7	CC	0–2	68.26	3.54
42	982B	7	CC	10–12	68.36	3.45
43	982B	8	2	20–22	77.27	3.12
44	982B	8	2	32–34	77.39	3.09
45	982B	8	2	40–42	77.47	3.17
46	982B	8	2	50–52	77.57	2.98
47	982B	8	2	62–64	77.69	3.12
48	982B	8	2	70–72	77.77	3.31
49	982B	8	2	80–82	77.87	3.11
50	982B	8	2	92–94	77.99	3.30
51	982B	8	2	100–102	78.07	3.22

52	982B	8	2	110–112	78.17	3.15
53	982B	8	2	122–124	78.29	3.07
54	982B	8	2	130–132	78.37	3.06
55	982B	8	2	140–142	78.47	2.99
56	982B	8	3	02–04	78.59	3.17
57	982B	8	3	10–12	78.67	3.19
58	982B	8	3	20–22	78.77	3.43
59	982B	8	3	32–34	78.89	3.54
60	982B	8	3	40–42	78.97	3.35
61	982B	8	3	50–52	79.07	3.37
62	982B	8	3	62–64	79.19	3.71
63	982B	8	3	70–72	79.27	3.37
64	982B	8	3	80–82	79.37	3.47
65	982B	8	3	92–94	79.49	3.46
66	982B	8	3	100–102	79.57	3.31
67	982B	8	3	110–112	79.67	3.33
68	982B	8	3	122–124	79.79	3.12
69	982B	8	3	130–132	79.87	3.44
70	982B	8	3	140–142	79.97	2.97
71	982B	8	4	02–04	80.09	3.06
72	982B	8	4	10–12	80.17	2.85
73	982B	8	4	20–22	80.27	2.91
74	982B	8	4	32–34	80.39	3.11
75	982B	8	4	40–42	80.47	3.14
76	982B	8	4	50–52	80.57	3.15
77	982B	8	4	62–64	80.69	3.28

78	982B	8	4	70–72	80.77	3.23
79	982B	8	4	80–82	80.87	3.18
80	982B	8	4	92–94	80.99	3.28
81	982B	8	4	100–102	81.07	3.14
82	982B	8	4	110–112	81.17	3.12
83	982B	8	4	122–124	81.29	3.04
84	982B	8	4	130–132	81.37	3.04
85	982B	8	4	140–142	81.47	3.07
86	982B	8	5	20–22	81.77	2.87
87	982B	8	5	50–52	82.07	2.89
88	982B	8	5	60–62	82.17	3.02
89	982B	8	5	70–72	82.27	2.91
90	982B	8	5	80–82	82.37	3.07
91	982B	8	5	90–92	82.47	2.99
92	982B	8	5	100–102	82.57	3.18
93	982B	8	5	110–112	82.67	3.00
94	982B	8	5	120–122	82.77	2.91
95	982B	8	5	130–132	82.87	2.92
96	982B	8	5	140–142	82.97	2.92
97	982B	8	6	0–2	83.07	2.95
98	982B	8	6	10–12	83.17	2.93
99	982B	8	6	20–22	83.27	3.01
100	982B	8	6	30–32	83.37	3.06
101	982B	8	6	40–42	83.47	3.04
102	982B	8	6	50–52	83.57	3.04
103	982B	8	6	60–62	83.67	2.90

104	982B	8	6	70–72	83.77	2.92
105	982B	8	6	80–82	83.87	2.78
106	982B	8	6	90–92	83.97	2.91
107	982B	8	6	100–102	84.07	2.71
108	982B	8	6	110–112	84.17	2.86
109	982B	8	6	120–122	84.27	2.76
110	982B	8	6	130–132	84.37	2.95
111	982B	8	6	140–142	84.47	2.82
112	982B	8	7	0–2	84.57	2.93
113	982B	8	7	10–12	84.67	2.88
114	982B	8	7	30–32	84.87	2.80
115	982B	8	CC	0–2	84.93	3.13
116	982B	8	CC	10–12	85.03	3.17
117	982B	8	CC	18–20	85.11	2.98
118	982B	9	1	0–2	86.18	2.99
119	982B	9	1	10–12	86.28	2.98
120	982B	9	1	20–22	86.38	2.81
121	982B	9	1	30–32	86.48	2.97
122	982B	9	1	40–42	86.58	2.95
123	982B	9	1	50–52	86.68	2.99
124	982B	9	1	60–62	86.78	2.84
125	982B	9	1	70–72	86.88	2.75
126	982B	9	1	80–82	86.98	2.84
127	982B	9	1	90–92	87.08	2.94
128	982B	9	1	100–102	87.18	2.92
129	982B	9	1	110–112	87.28	3.12

130	982B	9	1	120–122	87.38	3.15
131	982B	9	1	130–132	87.48	3.06
132	982B	9	1	140–142	87.58	2.99
133	982B	9	2	0 - 2	87.68	2.99
134	982B	9	2	10–12	87.78	3.02
135	982B	9	2	20–22	87.88	2.96
136	982B	9	2	30–32	87.98	2.89
137	982B	9	2	40–42	88.08	2.82
138	982B	9	2	60–62	88.28	2.93
139	982B	9	2	70–72	88.38	3.05
140	982B	9	2	80–82	88.48	3.05
141	982B	9	2	90–92	88.58	3.07
142	982B	9	2	100–102	88.68	3.15
143	982B	9	2	110–112	88.78	2.92
144	982B	9	2	120–122	88.88	2.94
145	982B	9	2	130–132	88.98	2.93
146	982B	9	2	140–142	89.08	2.91
147	982B	9	3	0–2	89.18	2.84
148	982B	9	3	10–12	89.28	2.85
149	982B	9	3	20–22	89.38	2.84
150	982B	9	3	30–32	89.48	3.00
151	982B	9	3	40–42	89.58	3.16
152	982B	9	3	50–52	89.68	3.14
153	982B	9	3	60–62	89.78	3.19
154	982B	9	3	70–72	89.88	2.96
155	982B	9	3	80–82	89.98	3.30

156	982B	9	3	90–92	90.08	3.29
157	982B	9	3	100–102	90.18	3.07
158	982B	9	3	110–112	90.28	2.88
159	982B	9	3	120–122	90.38	3.00
160	982B	9	3	130–132	90.48	2.77
161	982B	9	3	140–142	90.58	2.88
162	982B	9	4	0–2	90.68	2.92
163	982B	9	4	10–12	90.78	2.82
164	982B	9	4	20–22	90.88	3.05
165	982B	9	4	30–32	90.98	2.97
166	982B	9	4	40–42	91.08	3.09
167	982B	9	4	50–52	91.18	3.21
168	982B	9	4	60–62	91.28	3.24
169	982B	9	4	70–72	91.38	3.17
170	982B	9	4	80–82	91.48	3.41
171	982B	9	4	90–92	91.58	3.29
172	982B	9	4	100–102	91.68	3.25
173	982B	9	4	110–112	91.78	3.16
174	982B	9	4	120–122	91.88	3.17
175	982B	9	4	130–132	91.98	2.89
176	982B	9	4	140–142	92.08	2.86
177	982B	9	5	0–2	92.18	2.98
178	982B	9	5	10–12	92.28	3.26
179	982B	9	5	20–22	92.38	2.99
180	982B	9	5	30–32	92.48	2.94
181	982B	9	5	40–42	92.58	2.92

182	982B	9	5	50–52	92.68	2.80

#	HOLE	CORE	SECTION	INTERVAL	DEPTH (mcd)	Cib. $\delta^{18}O$ corr.
1	982C	8	1	3–5	66.62	3.63
2	982C	8	1	20–21.5	66.79	2.99
3	982C	8	1	40–41.5	66.99	3.11
4	982C	8	1	60–61.5	67.19	3.15
5	982C	8	1	80–81.5	67.39	3.36
6	982C	8	1	100–101.5	67.59	3.41
7	982C	8	1	120–121.5	67.79	3.49
8	982C	8	1	140–141.5	67.99	3.56
9	982C	8	2	10–11.5	68.19	3.6
10	982C	8	2	30–31.5	68.39	3.14
11	982C	8	2	50–51.5	68.59	3.16
12	982C	8	2	70–71.5	68.79	3.03
13	982C	8	2	90–91.5	68.99	3.09
14	982C	8	2	110–111.5	69.19	3.06
15	982C	8	2	130–131.5	69.39	3.23
16	982C	8	3	1–3	69.6	3.21
17	982C	8	3	20–21.5	69.79	3.13
18	982C	8	3	40–41.5	69.99	3.09
19	982C	8	3	60–61.5	70.19	2.87
20	982C	8	3	80–81.5	70.39	2.92
21	982C	8	3	100–101.5	70.59	2.89
22	982C	8	3	120–121.5	70.79	3.01

23	982C	8	3	140–141.5	70.99	3.14
24	982C	8	4	10–11.5	71.19	2.94
25	982C	8	4	30–31.5	71.39	2.94
26	982C	8	4	50–51.5	71.59	2.97
27	982C	8	4	70–71.5	71.79	3.13
28	982C	8	4	90–91.5	71.99	3.1
29	982C	8	4	110–111.5	72.19	3.14
30	982C	8	4	130–131.5	72.39	3.16
31	982C	8	5	2–4.5	72.61	3.25
32	982C	8	5	20–21.5	72.79	3.35
33	982C	8	5	40–41.5	72.99	3.35
34	982C	8	5	60–61.5	73.19	3.45
35	982C	8	5	80–81.5	73.39	3.48
36	982C	8	5	100–101.5	73.59	3.5
37	982C	8	5	120–121.5	73.79	3.35
38	982C	8	5	140–141.5	73.99	3.28
39	982C	8	6	10–11.5	74.19	3.07
40	982C	8	6	30–32	74.39	in prep.
41	982C	8	6	50–52	74.59	in prep.
42	982C	8	6	70–72	74.79	in prep.
43	982C	8	6	90–92	74.99	in prep.
44	982C	8	6	110–112	75.19	in prep.
45	982C	8	6	130–132	75.39	in prep.
46	982C	8	7	0–2	75.59	in prep.
47	982C	8	7	20–22	75.79	in prep.

48	982C	8	7	40–42	75.99	in prep.
49	982C	8	8 (7CC)	0–2	76.13	in prep.
50	982C	8	8 (7CC)	18–20	76.31	in prep.
51	982C	9	1	10–12	76.22	in prep.
52	982C	9	1	30–32	76.42	in prep.
53	982C	9	1	50–52	76.62	in prep.
54	982C	9	1	90–92	77.02	in prep.
55	982C	9	1	110–112	77.22	in prep.
56	982C	9	1	130–132	77.42	in prep.
57	982C	9	2	0–2	77.62	in prep.
58	982C	9	2	20–22	77.82	in prep.
59	982C	9	2	40–42	78.02	in prep.
60	982C	9	2	60–62	78.22	in prep.
61	982C	9	2	80–82	78.42	in prep.
62	982C	9	2	100–102	78.62	in prep.
63	982C	9	2	120–122	78.82	in prep.
64	982C	9	2	140–142	79.02	in prep.
65	982C	9	3	10–12	79.22	in prep.
66	982C	9	3	30–32	79.42	in prep.
67	982C	9	3	50–52	79.62	in prep.
68	982C	9	3	70–72	79.82	in prep.
69	982C	9	3	90–92	80.02	in prep.
70	982C	9	3	110–112	80.22	in prep.
71	982C	9	3	130–132	80.42	in prep.
72	982C	9	4	0–2	80.62	in prep.

73	982C	9	4	20–22	80.82	in prep.
74	982C	9	4	40–42	81.02	in prep.
75	982C	9	4	60–62	81.22	in prep.
76	982C	9	4	80–82	81.42	in prep.
77	982C	9	4	100–102	81.62	in prep.
78	982C	9	4	120–122	81.82	in prep.
79	982C	9	4	140–142	82.02	in prep.
80	982C	9	5	0–2	82.12	in prep.
81	982C	9	5	10–12	82.22	in prep.
82	982C	9	5	30–32	82.42	in prep.
83	982C	9	5	50–52	82.62	in prep.
84	982C	9	5	70–72	82.82	in prep.
85	982C	9	5	90–92	83.02	in prep.
86	982C	9	5	110–112	83.22	in prep.
87	982C	9	5	130–132	83.42	in prep.
88	982C	9	6	0–2	83.62	in prep.
89	982C	9	6	20–22	83.82	in prep.
90	982C	9	6	40–42	84.02	in prep.
91	982C	9	6	60–62	84.22	in prep.
92	982C	9	6	80–82	84.42	in prep.
93	982C	9	6	100–102	84.62	in prep.
94	982C	9	6	120–122	84.82	in prep.
95	982C	9	6	140–142	85.02	in prep.